Ultrastructural study of extracellular matrix of brown algae
(褐藻の細胞外マトリクスにおける微細構造学的研究)

Makoto Terauchi

Division of Biosphere Science,
Graduate School of Environmental Science,
Hokkaido University

2014

Contents

Acknowledgement

I would like to thank the people mentioned below, and this research could not be gotten along and accomplished without anyone of them.

First of all, I want to express the deepest appreciation to my supervisors, Prof. Taizo Motomura, Associate Prof. Chikako Nagasato and Assistant Prof. Atsuko Tanaka, Muroran Marine Station, Field Science Center for Northern Biosphere, Hokkaido University. They provided me the precious opportunity to study basic biology in this attractive research field and gave me constructive comments and infinite guidance during the experiments. They have been always greatly tolerant and supportive in my study. My heartfelt appreciation goes to Prof. Masaaki Morikawa, Graduate School of Environmental Science, Hokkaido University and Associate Prof. Tomomichi Fujita, Department of Biological Sciences, Faculty of Science, Hokkaido University, for their valuable suggestions and critical reading of this thesis.

I owe a very important debt to Associate Prof. Akira Inoue, School of Fisheries Sciences, Hokkaido University for providing alginate polymers, Mr. Toshiaki Ito, Electron Microscope Laboratory, Research Faculty of Agriculture, Hokkaido University and Dr. Naoko Kajimura, Research Center for Ultra-High Voltage Electron Microscopy, Osaka University for their excellent technical supports in electron tomography. I am deeply grateful to the colleagues in my laboratory, Dr. Gang Fu, Nana Kinoshita and Hiroki Kawamoto for their generous support and warm encouragement.

Special thanks goes to Mr. Teruo Tomioka and Mrs. Saeko Kitabayashi, the staffs of my laboratory, for their all times warm care and helps.

I wish to offer sincere thanks to my parents, Katsumi Terauchi and Tomoka Terauchi, for their infinite support in all my life.

General introduction

Brown algae

Brown algae are photosynthetic eukaryotes possessing multicellularity. Almost all species of the brown algae are the habitat of the marine. They include various sized species microscopic to large ones exceeding tens of meters, namely, giant kelps. Large species form the marine forests in coastal environments, being an ecologically important group for their contributions to marine ecosystems (Schiel and Foster 2006). Some species like *Saccharina* (Kombu), *Undaria* (Wakame) and *Hizikia* (Hiziki), have been widely used for food in Japan. Recently, they are becoming an attractive food source in other countries. Alginic acid and fucoidan which are the main cell wall components of brown algae have been well studied in applied research fields such as medicine (Kusaykin et al. 2008, Lee and Mooney 2012), bioenergy (Wargacki et al. 2012) and chemical industry (Schuster et al. 2014). Basic and applied researches of brown algae are both highly important because they provide many profits to human beings. Brown algae belong to the heterokontophyta together with diatoms by heterogenous two flagellar having hair-like structure, mastigoneme, on the anterior flagellum in swamers (Bouck 1969, Andersen 2004). They are classified as a phylum stramenopiles with other heterotrophic organisms including Oomycetes. Stramenopiles are phylogenetically distant from the Opistokonts including animals and fungi, and to the Archaeplastida including green plants and red algae (Yoon et al. 2004). In other lineages, occurrence of the complex multicellularity is limited to animals, fungi, green plants and red algae. Brown algae independently evolved the complex multicellularity in eukaryotes. In many cases, brown algae have the complicated life histories, and the alternation occurs between isomorphic or heteromorphic generations, sporophyte and gametophyte (Wynne and Loiseaux 1976). The two generations are linked by asexual and sexual reproductions with diverse reproductive modes. Brown algae acquired unique systems enabling such very complex life histories during adaptation to the coastal environment.

Key steps to the occurrence of complex multicellularity

In stramenopiles, some groups have a simple multicellularity. Some species of yellow-green algae form a colony and filamentous thalli (Bold and Wynne 1985). *Schizocladia ischiensis*, a sister group of brown algae, has a uniseriate filamentous thallus (Kawai et al. 2003). The simple multicellularity and the complex one are different in that the former lacks intercellular connections. Brown algae have plasmodesmata as intercellular connections. The other four multicellular groups mentioned above generally have the connections: gap junctions in animals (Makowski et al. 1984, Kumar and Gilula

1996), septal pores in fungi (Marchant 1976), pit plugs in red algae (Pueschel 1977, Ueki et al. 2008) and plasmodesmata in green plants (Ehlers and Kollmann 2001). Some members of them have no intercellular connections. For example, green algae include uniseriate branched filamentous species lacking plasmodesmata (Zygnematales and Klebsormidiales in Charophyceae, Trebouxiophyceae, Ulotrichales, Ulvales and Siphonocladales in Ulvophyceae, Raven 2008). Taken together with *Schizocladia*, intercellular connections may be crucial to establish the more complex multiseriate body with differentiated tissues. In brown algae, laminarialean species (e.g. kelps) have well differentiated tissues. Trumpet-shaped hyphae in medulla behave as sieve elements analogous to ones in land plants. In the trumpet hyphae, dense plasmodesmata (pit field) exist (Marchant 1976), which suggests their involvement in molecular transports.

In multicellular organisms, extracellular matrix (ECM) is highly developed. It is known that ECM participates in various biological processes. In animals, ECM mainly contains collagens and glycosaminoglycans, and functions in cell adhesion and cell-to-cell communication (Rozario and DeSimone 2010). In land plants, ECM is cell wall mainly composed of polysaccharides such as cellulose and hemicellulose forming rigid supermolecular structures. The cell wall provides the strength to support the plant body, and works for sensing of the environmental change and inducing proper responses (Brownlee 2002). Additionally, it is a mechanical system that regulates cell division and cell expansion of plant cells (Zuo et al. 2000, Baskin 2005, Yoshikawa et al. 2013). ECM is the central player for morphogenesis in multicellular organisms and its development is probably key step to the emergence of complex multicellularity. Genome sequencing has been completed in a number of organisms. Recent comparative genomic analysis showed that in the green lineage, some gene families implicated in ECM are more expanded in the genome of *Volvox* and *Arabidopsis* compared with that of *Chlamydomonas* (Prochnik et al. 2010).

As well as in the green lineage, evolution of multicellularity in brown algae is conceivably the consequence of the acquirement of plasmodesmata and development of ECM while their underlying essential system may be unique among eukaryotes. Structural and functional studies of plasmodesmata and cell wall will give us new knowledge of the fundamental morphogenesis of brown algae.

Recent advances on research of multicellularity of brown algae

In brown algae, there have been many morphological studies of cell division (Katsaros and Galatis 1992, Motomura 1994), cytokinesis (Nagasato and Motomura 2002a, b) and cell polarity (Kropf 1994, Katsaros 1995). Brown algal cells have centrioles

as in animal cells and do not have cortical microtubules unlike land plants. Brown algal cells have unique cell division system different from that of animals and land plants (Katsaros et al. 2006). *Ectocarpus siliculosus* is an emerging model brown alga (Charrier et al. 2008). The genome of *E. siliculosus* has been recently fully sequenced (Cock et al. 2010). The novel receptor kinase family proteins are found in the *Ectocarpus* genome by the molecular phylogenetic analysis. Receptor kinases contain plasma membrane proteins responsible for signal transductions. The buildup of intra and intercellular signal transduction system may be a key step toward the invention of multicellularity in brown algae (Cock et al. 2010). In the early developmental mutant (*etoile*), the expression level of genes coding Notch-like receptor proteins reduced, in which the cell-to-cell communication via Notch-like receptor proteins are associated with the early developmental process in *E. siliculosus* (Le Bail et al. 2011). In the sporophyte to gametophyte transition, unispores develop to gametophytes. When unispores are cultured in sporophyte-cultured medium, they develop back to sporophytes. This phenomenon demonstrates that the diffusing factor that induce unispores to develop to sporophytes exists (Arun et al. 2013). After unispores form the cell wall, they are not affected by the factor. It might be difference in cell wall between sporophyte and gametophyte, which concerns the permeability of the factor (Arun et al. 2013). In the study, well developed gametophytes are stained by congo red, while those of sporophytes are not. It implies that the cell wall is structurally or chemically different between sporophyte and gametophyte.

Structural bases of plasmodesmata for cell-to-cell communication and the cell wall are still poorly understood despite the advances described above. The morphological characterization of plasmodesmata and cell wall is of great importance in order to shed light on the multicellular system of brown algae. In the following sections, detail information of plasmodesmata and cell wall is introduced.

Plasmodesmata

Plasmodesmata in green plants

The intercellular connections in land plants and green algae are called plasmodesmata (Maule 2008). Plasmodesmata directly connect plasma membranes of adjacent cells forming membranous tubular channels with a diameter of tens of nanometers. They are structurally unlike gap junctions (Makowski et al. 1984, Kumar and Gilula 1996), septum pores in fungi (Marchant 1976, Müller et al. 2000) and pit plugs in red algae (Pueschel 1977, Ueki et al. 2008). Plasmodesmata have been observed

in Charales and Coleochaetales (Charophyceae), Oedogoniales and Chaetophorales (Chlorophyceae), Trentepohliales (Ulvophyceae) (Raven 2008). Extensive studies of plasmodesmata in land plants, ultrastructure (Ding et al. 1992), formation process (Hepler 1982), molecular components (Salmon and Bayer 2012) and biological processes (Benitez-Alfonso 2014), were performed.

Ultrastructure of plasmodesmata

The ultrastructure of plasmodesmata has been investigated in land plants and charophycean algae by transmission electron microscopy (TEM) (Robards 1968, Ding et al. 1992, Botha et al. 1993, Cook et al. 1997). Within the membranous tubular structure of plasmodesmata, additional structures have been reported. Endoplasmic reticulum (ER) pass through each plasmodesma, which is called desmotubule (Robards 1968). The molecular traffic generally occurs through the space between plasmodesmata membrane and desmotubule. The space contains other structures both on the inner surface of plasmodesmata membrane and desmotubule: particulate and spoke-like structures (Ding et al. 1992, Botha et al. 1993, 2000). They supposedly select molecules that pass through plasmodesmata according to their molecular weight although the component of them are not identified yet. To observe structure of plasmodesmata and their formation process by TEM, samples have been often prepared by chemical fixation. In these fixation methods, plasma membrane and plasmodesmata membrane are wavy and substructures are difficult to observe (Robards 1968). In the samples prepared by cryofixation and freeze substitution method, plasma membrane and plasmodesmata membrane are smooth and substructures are well preserved (Ding et al. 1992). The cryofixation would be a suitable technique to interpret precisely the structure of plasmodesmata.

Formation of plasmodesmata

Studies of land plants and some green algae propose that there are two types of plasmodesmata concerning the timing of their formation or morphology (Hepler 1982, Franceschi et al. 1994, Ehlers and Kollmann 2001, Faulkner et al. 2008): primary plasmodesmata are formed during cytokinesis, secondary plasmodesmata are produced after cytokinesis. In land plants, expansion of the cell plate is driven by the cell division machinery, phragmoplast which consists of microtubules, actins and Golgi-derived vesicles (Samuels et al. 1995, Seguí-Simarro et al. 2004). TEM observations hypothesize that ER gotten into the growing cell plate patches creates the pores of the plasmodesmata (Hepler 1982, Staehelin and Hepler 1996). Primary plasmodesmata are unbranched membranous tubules called simple plasmodesmata. Secondary

plasmodesmata are generated by the modification of primary plasmodesmata or by post-cytokinetic *de novo* formation and often appear as multiple branched, complex plasmodesmata (Ehlers and Kollmann 2001). Secondary plasmodesmata formation are accompanied with the degradation of cell wall and the protrusion of plasma membrane by the turgor pressure. Afterwards, ER is incorporated into the secondary plasmodesmata. During the secondary plasmodesmata formation, the arrangement of plasmodesmata is restricted in the specific area of the cell wall to create the pit field (Faulkner et al. 2008). The secondary plasmodesmata are inserted into the vicinity of the primary plasmodesmata. Pre-existing plasmodesmata can be removed from the cell wall during developmental process. For example, it is well known that cell walls in guard cells lose plasmodesmata during maturation (Wille and Lucas 1984). The distribution of plasmodesmata is highly regulated during morphogenesis in plants. In *Arabidopsis*, epidermal cells and underlying mesophyll cells are connected by simple plasmodesmata. The number of the branched complex plasmodesmata increases during the maturation of the leaf, the sink-source transition after removing of the leaf from the plant, salicylic acid treatment and osmotic shock by mannitol treatment (Fitzgibbon et al. 2013). These reports infer that the plasmodesmata distribution is controlled by variety of endogenous and exogenous cues, and the very important factor for the plant morphogenesis.

Molecular components of plasmodesmata

The plasmodesmata-associated proteins have been identified by the subcellular localization analysis using antibodies or green fluorescent protein (GFP) fusion proteins and proteomic analysis. In the analysis (Epel et al. 1996, Thomas et al. 2008), the localization of the target protein in plasmodesmata is evaluated at the light microscopic level by combining the callose (β1,3-glucan) staining as the positional marker of plasmodesmata with the labelling of the target protein. At the electron microscopic level, the specific antibody against the target protein is used. Plasmodesmata contain cytoskeletal elements (e.g. actin) shown by immunoelectron microscopy using the anti-actin antibody (Blackman and Overall 1998). In proteomic analysis, plasmodesmata-rich fraction was isolated from the cell wall fraction and plasmodesmata-associated proteins were searched by mass spectrometry. The subsequent analysis of some proteins confirmed their localization in plasmodesmata using GFP fusion proteins (Fernandez-Calvino et al. 2011). Plasmodesmata located proteins (PDLPs) are type I membrane receptors controlling the plasmodesmata conductance (Thomas et al. 2008). Plasmodesmata callose binding proteins (PDCBs) are glycosylphosphatidylinositol (GPI)-anchor proteins located in the neck region of plasmodesmata and contribute to the

callose-dependent regulation of molecular traffic (Simpson et al. 2009). Receptor kinases are present in plasmodesmata membrane mediating signal transduction via plasmodesmata (Jo et al. 2011). These studies intimate that variety of proteins are integrated in plasmodesmata membrane and function in concert for cell-to-cell communication.

Biological function of plasmodesmata

The biological function of plasmodesmata is the cell-to-cell communication, and they provide the route for the intercellular molecular transport. The cargo molecules pass through plasmodesmata freely or selectively. Various micro- and macromolecules, such as inorganic ions, metabolic products, proteins, RNAs and viral RNA complex, are transported via plasmodesmata in green plants (Kim 2005). The regulatory mechanism of the molecular traffic via plasmodesmata has been analysed by movement of GFP or different sized fluorescent probes (Zambryski 2004, Christensen et al. 2009). Plasmodesmata have the selective transportation system by molecular weight (Size Exclusion Limit, SEL). The SEL is affected by the structure of plasmodesmata, endogenous (e.g. developmental process) and exogenous (e.g. pathogen infection and cell injury) factors. The formation of complex plasmodesmata is correlated with a decrease in plasmodesmata conductance (Oparka et al. 1999). The molecular mechanisms of SEL transition include degradation and synthesis of callose at the neck region of plasmodesmata (Zavaliev et al. 2011). When the cell is damaged or receives several stimuli, callose deposits at the neck region of plasmodesmata, resulting in the decrease of the diameter of plasmodesmata and SEL. The degradation of the callose deposition recovers SEL. This process is adjusted by β1,3-glucanase. The localization of β1,3-glucanase in plasmodesmata was proved by proteomic analysis and analysis of GFP fusion protein (Levy et al. 2007). The molecular traffic via plasmodesmata utilizes the cytoskeletal system (e.g. actin-myosin machinery for SEL regulation) (White and Barton 2011). The alternation of plasmodesmata permeability takes place at single cell and cell group level during plant morphogenesis. Studies using *Arabidopsis* embryo expressing 1x GFP (27 kiloDalton) and 2 x GFP (54 kiloDalton) have shown that the movement of 2 x GFP was limited to some part of the embryo while 1x GFP moved entirely in the embryo (Kim et al. 2004). The local grouping of cells by SEL of plasmodesmata is the fundamental mechanism in creating the positional information, and achieving cell and tissue differentiation.

Plasmodesmata of brown algae

Brown algal plasmodesmata have been studied since 1970s. They mainly focused on plasmodesmata of sieve elements in kelps (Laminariales). The long-distance transport of photosynthetic products occurs through sieve elemnts verified by the trace experiments with ^{14}C (Schmitz and Srivastava 1979). Studies in the member of Fucales also support that (Diouris 1989). Numerous plasmodesmata are observed in the end walls of sieve elements (sieve plates) by TEM. In Laminariales, callose is present in the sieve plate (Schmitz 1990) but the functional relationship between callose and molecular transport remains unclear. The existence of callose in plasmodesmata of epidermal and cortex cells has not been reported. The inner diameter of plasmodesmata of cortex cells of *Laminaria* is about 20 nm (Schmitz and Kuhn 1982). Although brown algal plasmodesmata are functionally analogous to those of green plants, detail information about the structure and function of brown algal plasmodesmata are largely unknown. The molecular components of brown algal plasmodesmata are completely unknown. In *Ectocarpus* genome, the homologous proteins to plasmodesmata-associated proteins in land plants such as PDLPs (Thomas et al. 2008) and PDCBs (Simpson et al. 2009) are not found. Some plasmodesmata-associated proteins in *Arabidopsis* can be seen in the genome of moss, *Physcomitrella patens* (Lee 2014) and the list of ones in charophycean algae (Faulkner et al. 2005). This means that part of them and the molecular transport system is conserved in the green lineage. The similarity of molecular components might be low between brown algal plasmodesmata and those of green plants although they are partially common.

Cell wall

Cell wall in green plants

ECM of plant cells is called cell wall which mainly consists of polysaccharides constructing the rigid supermolecular structure. Cell wall is distributed in diverse organisms such as fungi, protists and bacteria. Its components are varied in organisms but similar between phylogenetically related groups (Popper et al. 2011). The cell wall has been extensively studied in land plants. There are numerous information of its structure, synthetic mechanism and biological processes.

Structure and molecular components of cell wall

The cell wall of land plants is divided into the two phases: structural phase and apoplastic fluid phase (Sakurai 1998). The structural phase consists of polysaccharides, structural proteins, phenolic compounds (lignin) and inorganic compounds. The

polysaccharides contain skeletal and matrix polysaccharides. The former includes cellulose microfibril which is common in all green plants (Sarkar et al. 2009). The cellulose microfibril has a highly crystalized organization of laterally arranged β1, 4-glucan chains. It is cylindrical or ribbon shaped with a diameter ranged from 2 to 30 nm depending on organisms illustrated by TEM observations of negative stained samples (Tsekos 1999). The cellulose microfibrils are bridged by hemicellulose such as xyloglucan and xylan. Hemicellulose strongly binds to cellulose microfibrils by hydrogen bonds since they are extracted from cellulose microfibrils using alkali solutions (Scheller and Ulvskov 2010). Their diameter is ~3.2 nm and they are tightly packed with hemicellulose and lignin visualized by the electron tomographic analysis of cell walls of radiata pine early wood (Xu et al. 2007). The xyloglucan fibrils are about 30 nm-long and about 6 nm-wide between cellulose microfibrils demonstrated by rapid freeze deep edging technique (Fujino et al. 2000). Xyloglucan fibrils determine the intervals of cellulose microfibrils in one lamella and between adjacent lamellae. The cellulose-xyloglucan network influences the mechanical strength of the cell wall. The matrix phase includes pectin. It is acidic complex polysaccharide, and contains galacturonic acids which are generally composed of three domains, homogalacturonan, rhamnogalacturonan I and II (Carpita and Gibeaut 1993). Cell wall polysaccharides are often localized in some part of the cell wall revealed by metachromatic staining and specific antibodies (Lee et al. 2011). Homogalacturonan has the two types: methyl esterised and de-methyl esterised types. The latter type forms the gel in the presence of calcium ions (Morris et al. 2009). The analysis using the monoclonal antibody against the de-methyl esterised type makes clear that it is localized in the middle lamella of the cell wall and takes part in the cell adhesion (Knox et al. 1990). Pectin is observed under TEM as the electron staining-positive fibrous structures (Wells et al. 1994). In atomic force microscopy, pectin forms branched fibrous gel structures (Morris et al. 2009). Pectin also affects the mechanical property of the cell wall as the pectin fibrous gel network independent of the cellulose-xyloglucan network (Hongo et al. 2012). The two networks are not completely independent each other. Their interaction is detected by nuclear magnetic resonance (NMR) analysis (Dick-Pérez et al. 2011). The cell wall polysaccharides are pivotal for the physicochemical characters of the cell wall. They interact each other by intermolecular force, ionic bond, hydrogen bond and covalent bond (Carpita and Gibeaut 1993, Scheller and Ulvskov 2010).

The cell wall of land plants is categorized into primary and secondary cell wall. The actively dividing cells like meristem cells have primary cell walls. The primary cell wall consists of cellulose (15-40 %), hemicellulose (20-30 %) and pectin (30-50 %) (Fry 2004, Cosgrove and Jarvis 2012). The secondary cell wall is formed under the primary

cell wall of differentiated cells (e.g. xylem). Xyloglucan and pectin are replaced with xylan and glucomannan in the secondary cell wall and the cellulose content greatly increases (Cosgrove and Jarvis 2012). Lignin deposits and binds to cellulose microfibrils strengthening the cell wall (Salmén 2004). The cell wall has small amount of proteins (a few % of the dry weight). The cell wall proteins encompass the polysaccharide-binding structural ones, enzymes and non-enzymatic ones which travel the apoplast. They govern the maintenance, modification and degradation of the polysaccharides (Jamet et al. 2006). The well-known structural proteins belong to hydoxyproline-rich glycoprotein (HRGP) family (e.g. extensin) (Showalter et al. 2010). Extensin forms intramolecular and intermolecular covalent bonds and reinforces the cell wall organization in the pathogenic response (Lamport et al. 2011). Enzymes that modify and degrade polysaccharides are glycoside hydrolases (GHs) family, carbohydrate esterases (CEs) family, glycosyl transferases (GTs) family and polysaccharide lyases (PLs) family (Lombard et al. 2014). Xyloglucan endotransglucosylase/hydrolase degrades the xyloglucan chain and exchange the link to another xyloglucan chains for the modification of the cellulose-xyloglucan network (Rose et al. 2002). Cellulase (GH family 9) hydrolyzes the cellulose and reduces the crystallinity of cellulose microfibril for regulating the organization of the cellulose-xyloglucan network (Gilbert 2010). Representative non-enzymatic proteins are members of the expansin family. The expansin non-enzymatically excises hydrogen bonds between cellulose microfibril and xyloglucan, to increase the flexibility of the cell wall (Cosgrove 2000). Proteomic studies have been identifying many other cell wall proteins (Jamet et al. 2006). It is predicted that the plant genome encodes the numerous unidentified cell wall proteins.

Cell wall synthesis and biological function

Cell wall synthesis is strictly regulated during the developmental processes and response to the environmental changes. The most essential role of the cell wall is to control the cell morphology and the mode of cell expansion (Baskin 2005). The cell expansion of plant cells includes radial growth, elongation growth, diffusional growth and tip growth. Since the turgor pressure is constant in any directions, the pattern of cell expansion is influenced by mechanical characters of the cell wall. Epidermal cells of the hypocotyl and the root hair exhibit the strong elongation growth. In these cells, arrangement of cellulose microfibrils are perpendicular to the direction of the elongation growth and parallel to the underlying cytoplasmic cortical microtubules (Smith and Oppenheimer 2005). The arrangement of cellulose microfibrils regulates the direction of the cell expansion. Cellulose microfibrils are synthesized by the cellulose synthesizing

enzymes (CES) complex on plasma membrane (Richmond and Somerville 2000). The freeze fracture and immunolabeling of CES ensure that the CES complex of land plants resides on the plasma membrane and takes rosette form (Kimura et al. 1999). The live cell imaging of GFP fusion proteins of CES and tubulin verifies that the CES complex is linked to the cortical microtubules via adapter proteins and moves along the cortical microtubules (Li et al. 2012). The CES complex inserts the cellulose micofibril into the cell wall by traveling on the cortical microtubules. During the cell elongation, the extent of the cell elongation coincides with the extensibility of the cell wall. The cell wall extensibility is regulated by the linking polysaccharides among cellulose microfibrils (Scheller and Ulvskov 2010). In the study using rapid freeze deep edging, the linker structures of xyloglucan between cellulose microfibrils are more frequently observed after the cell elongation than elongating cells (Fujino et al. 2000). Plant cells achieve the cell expansion by alternating the cell wall extensibility through the modification of the architecture of the polysaccharide network. Xyloglucan, pectin and other polysaccharides are synthesized in Golgi body and transported into the cell wall via vesicle transport in the proper timing and place for plant morphogenesis (Lerouxel et al. 2006, Zhong and Ye 2007).

Cell wall in brown algae

Structure and molecular components of cell wall

The previous studies of brown algal cell wall cover biochemical, morphological and molecular biological analyses. The cell wall of brown algae consists of polysaccharides, phenolic compounds (phlorotannin) and halogenated compounds and proteins (Kloareg and Quatrano 1988, Schoenwaelder and Clayton 1999, La Barre et al. 2010). The composition of the cell wall of brown algae is very unique among plants. The main polysaccharides are alginate, cellulose and sulfated polysaccharides. Alginate comprises over 50 % of the dry weight of the cell wall. Alginate is the unbranched carboxylic β1, 4-glycan consisting of mannuronic acids (M) and guluronic acids (G) (Kloareg and Quatrano 1988). The two units are optical isomers each other. The MG ratio differs in species, generations and the seasons. The MG sequence in the alginate chain is highly diverse. Bacterial alginates are often modified such as acetylation (Davidson et al. 1977). The acetylation and other modifications have not been reported in brown algae. Alginate is found in the heterokont organisms phylogenetically related to brown algae such as yellow-green algae (Chi et al. 1999), some red algae (Okazaki and Tazawa 1989, Bilan and Usov 2001) and some bacteria (Ramsey and Wozniak 2005). *Fucus* zygotes

(*Fucus vesiculosus* Linnaeus, *F. distichus* Linnaeus, *F. inflatus* Linnaeus) contain about 20 % of cellulose of the dry weight of the cell wall (Quatrano and Stevens 1976). The cellulose content in brown algal cell wall is generally from one to a few % (Cronshaw et al. 1958). It is much lower than that of land plants. The negative staining of cellulose microfibrils presents that brown algae have the ribbon-shaped cellulose microfibril. In *Sphacelaria rigidula* Kützing, the width of the cellulose microfibril is 2.6-30 nm and its longitudinal length is from hundreds of nm to one μm (Tamura et al. 1996). In the polarized microscopic observation of fucoid zygotes, crystalized materials are detected in the cell wall of the zygotes at several hours after fertilization (Bisgrove and Kropf 2001). Sulfated polysaccharides in brown algae are heteropolysaccharides with high amount of sulfated fucose residues. In *Fucus* zygotes, the content of sulfated polysaccharides is about 20 % of the dry weight of the cell wall (Quatrano and Stevens 1976). They have other monosaccharides such as xylose, galactose, mannose, glucose and rhamnose. The content of each monosaccharides are varied in each sulfated polysaccharide such as xylo-fuco-glucuronan (glucan), galacto-fucan, homofucan (fucoidan). The position and degree of sulfation of fucose depends on species (Quatrano and Stevens 1976, Ponce et al. 2003, Kusaykin et al. 2008). The cell wall of brown algae is dissimilar from that of land plants in that acidic polysaccharides such as alginate and sulfated polysaccharides are major components of the cell wall. The cell wall of land plants lacks sulfated polysaccharides. Xyloglucan, xylan, mannan and pectin are absent in brown algae (Popper et al. 2011). The model of the cell wall architecture in brown algae is presented on the physicochemical nature of the cell wall polysaccharides and TEM observations (Kloareg and Quatrano 1988). In the model, cellulose microfibrils are embedded in the amorphous matrix. The model has not been updated so far. There is still gap between the model and the morphological information. The cell wall architecture of brown algae is yet unclear and its detail analysis remains to be conducted.

Cell wall synthesis and biological function

The *de novo* synthesis of cell wall has been studied using the fucoid algal zygotes at cellular level (Quatrano and Stevens 1976, Vreugdenhil et al. 1976, Callow et al. 1978a, Bisgrove and Kropf 2001, Nagasato et al. 2010). The chemical analysis of the monosaccharide composition detects alginate and cellulose in zygotes after 30 min from fertilization (Quatrano and Stevens 1976). The sulfated polysaccharide (xyloguco-glucan) is produced after one hour from fertilization. Fucoidan shows uneven distribution in emerging rhizoid about 12 hours after fertilization. The zygotes synthesize each cell wall polysaccharides under the strict schedule. This is supported by

the histochemical analysis using metachromatic staining (Bisgrove and Kropf 2001). It is thought that alginate and sulfated polysaccharides are synthesized in Golgi body and transported to the cell wall according to the results of autoradiography and pharmacological experiments (Callow et al. 1978a, Bisgrove and Kropf 2001). In zygotes of *Silvetia babingtonii* (J. Agardh) E. Serrão, T. O. Cho, S. M. Boo and Brawley, fucoidan is transported to the newly formed cell partition membrane via vesicle transport demonstrated by immunoelectron microscopy using anti-fucoidan antibody (Nagasato et al. 2010). Bacterial alginate is first synthesized as mannuronan (poly mannuronic acids) by mannuroran synthase on plasma membrane and secreted into the periplasmic space (Ramsey and Wozniak 2005). Some mannuronic acid residues of the mannuronan chain are epimerized into guluronic acids by mannuronan C5-epimerase (MEP). This process creates the specific MG blocks. In *Laminaria digitata* (Hudson) J.V. Lamouroux, cDNAs encoding bacterial MEP homologue were first isolated (Nyvall et al. 2003). MEPs are probably secreted into the cell wall and modify the cell wall architecture. In the freeze fracture studies of several species in the Ectocarpales, Fucales, Sphacelariales and Syringodermatales, cellulose microfibril is synthesized at plasma membrane as well as in land plants (Peng and Jaffe 1976, Reiss et al. 1996, Tamura et al. 1996, Schüβler et al. 2003). Brown algae presumably have the linearly arranged CES complex although there is no morphological evidence that it is bona fide CES complex. It is observed in Golgi vesicles, suggesting that the cellulose synthesis may start before reaching plasma membrane (Reiss et al. 1996).

Biological functions of brown algal cell wall are unknown. Although the cell wall may play mechanical roles for constructing the plant body as in land plants, its regulatory mechanism and physiological functions are almost unclear.

Insights from *Ectocarpus* genome

There have been several comparative genomic analyses for cell wall-related genes using *Ectocarpus* genome (Cock et al. 2010, Michel et al. 2010a, b). These analyses predict that brown algae have the unique carbohydrate metabolism much different from that of animals and land plants. *Ectocarpus* genome encodes several alginate synthesis-related genes, homologous to the bacterial counterparts: 28 MEP genes form the largest family in the *Ectocarpus* genome. The high redundancy of the MEP family suggests that the regulation of the MG sequence of alginate is the important biological process in brown algae. *Ectocarpus* genome seems to lack cellulase and alginate lyase for the alginate degradation (Michel et al. 2010a). *Ectocarpus* genome has unsaturated glucuronic acid hydrolases. The unsaturated uronic acid hydrolases generally hydrolyse

the substrates produced by polysaccharides lyases. The unidentified novel PL family protein possibly exists in *Ectocarpus* genome. The cell wall proteins in land plants such as HRGP and expansin are absent in *Ectocarpus* genome. The brown algal cell wall probably has alternative proteins. Recently, *in vitro* analysis of recombinant guanosine diphosphate (GDP)-mannose dehydrogenase confirmed its enzyme activity for the production of GDP-mannuronic acid, a subunit of alginate (Tenhaken et al. 2011) and type III polyketide synthase for the synthesis of phloroglucinol, a precursor of phlorotannin (Meslet-Cladière et al. 2013). Other putative cell wall-related genes remain to be experimentally characterized.

The objective and approach in the present study

The present study carried out the detail ultrastructural analysis of plasmodesmata and cell wall using TEM in order to clarify the structural base of ECM in brown algae. The present study adapted the conventional TEM observations of ultrathin sections and electron tomography. Electron tomography is computer tomography (CT) technique that has been recently used in many research fields (Haas and Otegui 2007, Urban et al. 2010). Images are acquired by tilting the specimen at interval of 1° or 2° and tilt-series of two dimensional images are obtained. Then, the three dimensional structure is reconstructed from the two dimensional tilt-series using the computer. The technique can be used for the analysis of nano-scale tiny cell structures such as plasmodesmata and cell walls. In sample preparations, the present study made use of rapid freezing/freeze substitution method. The cryofixation can preserve the intact cell structures much better than the conventional chemical fixation.

In chapter 1, plasmodesmata of the brown alga *Dictyota dichotoma* (Hudson) J.V. Lamouroux were firstly observed in order to reveal ultrastructure of plasmodesmata and process of plasmodesmata formation during cytokinesis. In the apical region of *D. dichotoma* thallus, cell divisions actively take place. According to the previous studies, it was predicted that plasmodesmata were formed during cytokinesis (La Claire 1981, Katsaros et al. 2009). *D. dichotoma* was the good sample for investigating the relationship between plasmodesmata formation and cytokinesis. Second, the comparative analysis was applied using several brown algal species on ultrastructure of plasmodesmata, distribution of plasmodesmata in the cell wall and relationship between plasmodesmata and body plan. Finally, the common features of brown algal plasmodesmata and the difference between brown algal plasmodesmata and green plant ones were discussed.

In chapter 2, the model brown alga *Ectocarpus siliculosus* (Dillwyn) Lyngbye

(Charrier et al. 2008) was chosen in order to reveal ultrastructure of the cell wall. In electron tomography, the qualitative and quantitative analyses on the cell wall architecture were performed. The present study examined the distribution of cell wall polysaccharides by indirect immunofluorescence microscopy and labeling experiments under TEM. The analysis focused on the diversity of the molecular structure of alginate and discussed the distribution of MG blocks of alginate in the cell wall. This study conclusively proposed the updated cell wall model of brown algae.

Chapter 1 Ultrastructural study of plasmodesmata of brown algae

Introduction

There have been studies that revealed structural and functional aspects of plasmodesmata in land plants. On the other hand, information of the structure of plasmodesmata in brown algae is still limited (Marchant 1976). The long-distance translocation of substances through plasmodesmata and pores of sieve elements in some species of kelps, *Laminaria groenlandica* Rosenv., *Alaria marginata* Postels and Ruprecht, *Nereocystis luetkeana* (K. Mertens) Postels and Ruprecht, *Laminaria hyperborea* (Gunnerus) Foslie and *Laminaria saccharina* (Linnaeus) Lamouroux (Schmitz and Srivastava 1974, 1975, 1976, Schmitz and Kuhn 1982) has been investigated by ultrastructural analyses (Schmitz 1981, 1990). In these studies, and those on other species in Fucales, Cutleriales and Dictyotales (Bisalputra 1966, La Claire 1981, Katsaros and Galatis 1988), the plasmodesmata in brown algae do not have a desmotubule, although one of the published figures from *L. groenlandica* may include ER (Fig. 18 of Schmitz and Srivastava 1974). The pores on the cross wall of sieve elements in lamenarialean species have a larger diameter, 100-400 nm in *N. luetkeana* (Schmitz and Srivastava 1976), compared to plasmodesmata in land plants. These large pores are considered to be specialized structures for the translocation of substances through sieve elements of large kelps (Schmitz 1990). It is hypothesized that these pores are formed by the enzymatic digestion of segments of the walls that contain plasmodesmata (Marchant 1976). In the brown alga, *Cutleria cylindrica* Okamura, plasmodesmata-like structures were observed in the cell partition membrane during cytokinesis (La Claire 1981). A recent ultrastructural study of cytokinesis in several other brown algae also found plasmodesmata-like structures on the nascent cell partition membrane (Katsaros et al. 2009). These reports imply that brown algae have primary plasmodesmata. Detailed ultrastructural studies of cytokinesis in brown algae have also been conducted using rapid freezing/freeze substitution (Nagasato and Motomura 2002b, 2009, Katsaros et al. 2009, Nagasato et al. 2010, 2014). Novel membranous structures, called “flat cisternae”, together with Golgi vesicles contribute to the formation of the partition membrane during cytokinesis in a manner different from that of the phragmoplast-cell plate system in land plants (Schopfer and Hepler 1991, Samuels et al. 1995). Primary plasmodesmata in brown algae are perhaps formed through a different process to that of green plants. In this chapter, first, electron tomography was applied in combination with conventional electron microscopy to characterize the plasmodesmata of the brown alga *Dictyota dichotoma* (Hudson) J.V. Lamouroux. Then, the comparative analysis of structure and distribution of plasmodesmata in vegetative cells was carried

out against several brown algal species in order to provide insights into the relationship between plasmodesmata and morphogenesis in brown algae.

Materials and methods

Culture

Sporophytes of *D. dichotoma* were collected by Dr. Kei Kimura (National Research Institute of Fisheries and Environment of Inland Sea, Fisheries Research Agency, Hiroshima, Japan) at Charatsunai, Muroran, Japan (42°19'N, 140°590'E). Culture of the apical parts began in October, 2007, using half-strength PES medium (Provasoli 1968) at 20 °C under long day conditions (14 h light, 10 h dark, 20 μmol m^{-2} s^{-1}, photon flux density). Male gametophytes of *Sphacelaria rigidula* Kützing and sporophytes of *Halopteris paniculata* (Suhr) Prud'homme van Reine were cultured under the same condition. Sporophytes of *Ectocarpus siliculosus* (Dillwyn) Lyngbye (32-m sporophyte strains) were cultured in half-strength PES medium at 15 °C under long day conditions (14 h light, 10 h dark, 30-40 μmol m^{-2} s^{-1}, photon flux density). Male gametophytes of *Saccharina japonica* (Areschoug) C.E. Lane, C. Mayes, Druehl and G.W. Saunders were cultured in Fe-free $ASP_{12}NTA$ medium at 10 °C under long day conditions (14 h light, 10 h dark) (Motomura and Sakai 1984).

Rapid freezing/freeze substitution for electron microscopy

Samples of *D. dichotoma* were obtained from the cultures after 2-3 h from the end of the light period and used for cryofixation. Samples of *S. rigidula*, *H. paniculata, E. siliculosus* and *S. japonica* were fixed during the light period. The cryofixation and embedding methods were adapted from previous reports (Nagasato and Motomura 2002b, Ueki et al. 2008). For *D. dichotoma*, the apical parts of thalli (up to 3 mm from the apex) were cut by the razor (5-10 mm in diameter). For *S. rigidula*, *H. paniculata, E. siliculosus* and *S. japonica,* tufts of the filamentous thalli were cut by the razor into smaller pieces. They were placed on formvar-coated gold loops and rapidly frozen by transferring into liquid propane pre-cooled to -180 °C by liquid nitrogen, and then immediately transferred to liquid nitrogen. The samples were subsequently transferred into cooled acetone (-80 °C) containing 4 % osmium tetroxide and stored at -80 °C for 2 days. Next, the samples were gradually brought to room temperature according to the following schedule: -20 °C for 2 h; 4 °C for 2 h; and room temperature for 1 h. They were washed several times with acetone at room temperature. Samples of *D. dichotoma* were stained *en bloc* with 2 % uranyl acetate in a 1:2 mixture of methanol and acetone in an ice bath for 1 h. After staining, the tissues were washed several times with a 1:2 mixture of methanol and acetone and then with acetone. In other samples, the *en bloc* staining was omitted. Infiltration of Spurr's epoxy resin into samples was performed at room temperature according to the following schedule: 20 % resin in acetone for 12 h; 30 %

resin for 5 h; 40 % for 5 h; 50 % for 12 h; 70 % for 5 h; 80 % for 5 h; 100 % for 2 days. *S. japonica* sample was infiltrated with Spurr low-viscosity embedding media (Polyscience Inc, Eppelheim, Germany) using the same schedule for Spurr's epoxy resin. The final two steps of infiltration were carried out in desiccators. Samples were put on dishes of aluminum foil and polymerized at 70 °C, overnight. Ultrathin sections (80-100 nm) were cut using a diamond knife (Diatome, Hatfield, PA, USA) on an ULTRACUT ultramicrotome (Reichert-Jung, Depew, NY, USA) and mounted on formvar-coated copper slot grids. Sections were stained with 4 % uranyl acetate and Reynolds' lead citrate (Reynolds 1963) and observed with a JEM-1011 electron microscope (Jeol, Tokyo, Japan).

Chemical fixation for electron microscopy

Alaria crassifolia Kjellman (sporophytes), *Costaria costata* (C.Agardh) De A. Saunders (sporophytes), *Saccharina japonica* (Areschoug) C.E. Lane, C. Mayes, Druehl and G.W. Saunders (sporophytes) in Laminariales, *Desmarestia ligulata* (Stackhouse) J.V. Lamouroux (sporophytes), *Desmarestia viridis* (O.F. Müller) J.V. Lamouroux (sporophytes) in Desmarestiales, *Scytosiphon lomentaria* (Lyngbye) Link (gametophytes), *Colpomenia bullosa* (D.A. Saunders) Yamada (gametophytes) in Scytosiphonales, *Analipus japonicus* (Harvey) M.J. Wynne (sporophytes) in Ralfsiales, *Fucus distichus* Linnaeus (sporophytes), *Sargassum thunbergii* (Mertens ex Roth) Kuntze (sporophytes) in Fucales, *Dictyopteris divaricata* (Okamura) Okamura (sporophytes) in Dictyotales were collected at Charatsunai, Muroran, Hokkaido, Japan, on June from April in 2010 and 2011. They were washed with filtrated seawater and cut into small pieces (1-2 mm^3). Samples were fixed with 1:1 mixture of seawater and fixative: 2% glutaraldehyde, 2% NaCl, 0.1% $CaCl_2$, and 1% caffeine in 0.1 M cacodylate buffer (pH 7.2) for 1 h on ice bath, and further fixed with the new fixative for 1h at room temperature. They were washed with 0.1 M cacodylate buffer containing 2% NaCl and 0.1% $CaCl_2$, and post-fixed with 2% OsO_4 in the same buffer composition for 1 h on ice bath and for 1 h at room temperature. The buffer was substituted with H_2O. Samples were dehydrated in a graded series of acetone and embedded in Spurr's epoxy resin. Ultrathin sections (80-100 nm) were cut using a diamond knife on an ULTRACUT ultramicrotome and mounted on formvar-coated copper slot grids. Sections were stained with 4 % uranyl acetate and Reynolds' lead citrate and observed with a JEM-1011 electron microscope.

Sample preparation for electron tomography

Two hundred to 300-nm sections were prepared for analysis using a 300 kV H9500 electron microscope (Hitachi, Tokyo, Japan). The sections were mounted on formvar-coated slot grids and stained with 4 % uranyl acetate at 70 °C for 1 h and lead citrate at room temperature for 10 min. After staining, the side of the grid carrying the sample was coated with formvar to sandwich the section. Then, 15 nm colloidal gold particles were attached to both sides of the grids to be used as fiducial markers to align the series of tilted images. Five hundred to 700-nm-thick sections were prepared for analysis using a 2,000 kV H3000 electron microscope (Hitachi, Tokyo, Japan). The sections were floated on hot distilled water in order to remove any wrinkles. They were then mounted on formvar-coated slot grids and stained with 2 % uranyl acetate in 70 % methanol in microwave for 30 s. The sections were kept on the dark for 20 min, and then stained with Sato's lead citrate (Sato 1968) in the microwave for 30 s. The sections were sandwiched with formvar, and 20 nm colloidal gold particles were attached to both sides. Then, the grids were coated with carbon on both sides.

Image acquisition and tomographic analysis

In this study, single- and dual-axis electron tomography were conducted. The 200-300 nm sections were placed on a tilt-rotate specimen holder and observed using the H-9500 electron microscope with a 300 kV acceleration voltage. Images were captured using an F224HD CCD camera (TVIPS, Gauting, Germany) at either x 12,000 or x 20,000 magnification from -60° to +60° at 1° intervals with a resolution of 2,048 x 2,048 pixels and a pixel size of 1.54 and 0.92 nm, respectively. Dual-axis electron tomography was performed around two orthogonal axes in order to obtain high resolution images and to reduce the "missing wedge" artifact (Mastronarde 1997). Similarly, sections were placed on the tilt-rotate specimen holder and viewed using the H-3000 electron microscope with a 2,000 kV acceleration voltage. Images were captured with an F486BK CCD camera (Hitachi) at a magnification of either x 10,000 or x 15,000 from -60° to +60° at 1° intervals with a resolution of 4,096 x 4,096 pixels and a pixel size of 3.45 and 2.23 nm, respectively. The frame of each image was reduced to 4,028 x 3,774 pixels using Photoshop software (Adobe system Inc., San, Jose, CA, USA). The size of images was further binned into half (2,014 x 1,887 pixels) by bicubic interpolation. All images were taken at the Research Center for Ultra-High Voltage Electron Microscopy (Osaka University, Osaka, Japan). Tomograms were reconstructed by aligning each set of tilted images using gold particles as fiducial markers. All tomograms were analyzed using IMOD software (Kremer et al. 1996). "SLICER", a program packaged in IMOD, was used to extract slices by setting the rotation angles about the x, y and z axes. Three-dimensional models were drawn by

tracing membranous structures using “3DMOD” which is the graphics component of IMOD, or “ISOSURFACE” which is an automatic drawing program packaged in IMOD. The volumes of objects were calculated using object meshes and “IMODINFO”, a program packaged in IMOD. The frequency of tubular membranous structures in proximity to thin and thick cell wall regions was analyzed by calculating their volumes in boxes of 0.924 x 0.200 x 0.154 μm^3 extracted along the cell wall, including the thin and thick cell wall regions. The values were averaged from three parts with the standard deviation and the frequency of occurrence was shown as the volumes of membranous structures per 0.028 μm^3 box. The frequency in the thin cell wall regions was compared with that in the thick cell wall regions using Student’s t-test. Student’s t-test was performed after F-tests for evaluating whether the variances were equivalent.

Immunoelectron microscopy and cellulase-gold labeling

Cryofixation was performed as described above. Cryofixed tissues were transferred into cooled ethanol (-80 °C) containing 0.2 % glutaraldehyde, and stored at -80 °C for 2 days. The samples were brought to room temperature as follows: -20 °C for 2 h, 4 °C for 2 h and room temperature for 30 min. After several washes with ethanol at room temperature, the samples were infiltrated with Lowicryl HM20 resin (Polysciences Inc, Warrington, PA) at -30 °C as follows: 10 % resin in ethanol for 5 h, 20 % for 12 h, 30 % for 5 h, 50 % for 5 h, 70 % for 12 h, 80 % for 5 h and 100 % for 2 days. The samples were embedded in TAAB Embedding Capsules (TAAB Laboratories Equipment Ltd, Berks, England) using UV polymerizer (DOSAKA EM Co. Ltd, Kyoto, Japan) under UV light for 2 days at -30 °C and for 1 day at room temperature. Ultrathin sections (80-100 nm) were cut with a diamond knife on an ULTRACUT ultramicrotome and mounted on formvar-coated nickel slot grids. Sections on formvar-coated nickel grids were floated on a 10 µL drop of phosphate buffered saline (PBS) (137 mM NaCl, 2.7 mM KCl, 4.9 mM Na_2HPO_4, 1.5 mM KH_2PO_4, pH 7.4) for 10 min at room temperature, followed by incubation on blocking solution (2.5 % skim milk, 5 % normal goat serum and 0.05 % NaN_3 in PBS) for 30 min or 1 h at 37 °C. They were then treated with a rabbit polyclonal anti-alginate antibody (Chi et al. 1999, Nagasato et al. 2010), diluted 1:1,000 with PBS, overnight at 20 °C in the dark. For the control experiments, the primary antibody was omitted or was pre-incubated with 1 mg mL^{-1} alginate (sodium salt, Sigma, Saint Louis, MO, USA) in PBS for 1 h at 37 °C. After washing with PBS for 10 min at room temperature, the specimens were treated with the secondary antibody, a goat anti-rabbit IgG conjugated with 15 nm colloidal gold particles (BBInternational, Cardiff, UK) for 1 h at 37 °C. After washing with distilled water for 10 min at room temperature, the grids

were stained with 4 % uranyl acetate. Cellulase from *Trichoderma reesei* (Sigma) was conjugated to colloidal gold particles using a slight modification of the method described by Samuels et al. (1995) and Nagasato et al. (2010). The 10 nm colloidal gold solution (BBInternational) was adjusted to pH 4.9 with HCl. Five microliters of 2 mg mL^{-1} cellulase in distilled water was added to 500 μL of 10 nm colloidal gold and incubated in an ice bath for 5 min with stirring. Then, 25 μL of 1 % polyethylene glycol (PEG 4000, Merck, Darmstadt, Germany) was added for stability. The cellulase gold conjugates were centrifuged at 15,000g (Kokusan RM-190, Tokyo, Japan) for 90 min at 4 °C. The resultant mobile pellet was transferred into a new microtube and 0.05 M citrate buffer (pH 4.9) was added up to 500 μL, followed by centrifugation at 15,000g for 90 min at 4 °C. The mobile pellet was transferred into a new microtube as the concentrated solution, and was diluted 1:10 with 0.05 M citrate buffer to form the working solution. Sections on formvar-coated nickel grids were floated on a 10 μL drop of 5 % H_2O_2 for 10 min at room temperature, followed by blocking solution for 20 min at room temperature. After washing with distilled water for 5 min at room temperature, they were rinsed with 0.05 M citrate buffer for 10 min at room temperature. Then, they were incubated with the cellulase gold conjugate for 30 min at 37 °C. After washing with citrate buffer for 5 min and distilled water for 5 min at room temperature, they were stained with 4 % uranyl acetate.

Analysis of pit field

Quantitative properties of pit fields were analyzed by Image J 1.47t (Abramoff et al. 2004). For all analysis, images showing transverse view of plasmodesmata were used. The plasmodesmata frequency was measured by counting the number of plasmodesmata per 1 μm^2. The 1 μm^2 square (1 μm x 1 μm) was drawn using the rectangle drawing tool in Image J and put on the pit field. Then, the number of plasmodesmata in the square was counted. When the pit field was smaller than 1 μm^2, smaller squares (0.25 μm x 0.25 μm, 0.4 μm x 0.4 μm, 0.5 μm x 0.5 μm) were applied. Then, the result was converted to the number of plasmodesmata per 1 μm^2. For the distance between plasmodesmata, the length between the center of the canal of one plasmodesma and that of the adjacent one was measured. For the area of the pit field, outermost plasmodesmata in the pit field were outlined using the circle drawing tool and the area was measured.

Results

Cell morphology of *D. dichotoma*

D. dichotoma has a macroscopic thallus and undergoes the isomorphic alternation of generations. The thallus had the multiseriate system (Plate 1a). At the tip of the apex, one large dome-shaped cell (arrowhead in inset of Plate 1b) was followed by much smaller epidermal cells (Plate 1b). Epidermal cells took rectangle or square-like shape and their size in longitudinal direction of the thallus was generally larger than that in transverse direction of the thallus. In the apical part, the size of epidermal cells in transverse and the longitudinal directions of the thallus was 5-16 μm, 10-25 μm, respectively. Discoid chloroplasts were arranged in the peripheral part of the cell (Plate 1b, c). In this part, cell division actively took place both in longitudinal and transverse directions of the thallus. In the middle part of the thallus, epidermal cells were bigger than those in apical part. Well-elongated cells in the longitudinal direction of the thallus were often observed (Plate 1c). The size of epidermal cells in transverse direction of the thallus was 7-23 μm while 13-46 μm in longitudinal direction of the thallus. This was due to the cell expansion. The one cell wall interface of a cell crossed with that of the other cell to form the three-way junction (arrowheads in Plate 1d). One cell had multiple three-way junctions and shared cell wall interfaces with 5-7 cells. In the middle part of the thallus, some epidermal cells formed hair cells (asterisks in Plate 1e). The hair cells were formed by division and elongation (inset in Plate 1f), which had uniseriate filamentous form (Plate 1f). In the following sections, observations were focused on the epidermal cells in the apical part of the thallus in order to clarify the structure and formation process of plasmodesmata.

Observation of plasmodesmata using conventional TEM

The mature cell walls of epidermal cells in *D. dichotoma* were up to 1 μm in thickness (Plate 2a). Simple, unbranched plasmodesmata were observed in the cell walls ~0.1 μm thick (Plate 2b, c). In addition to occurring in walls between epidermal cells, plasmodesmata were also observed between epidermal and medullary cells. Electron-dense cell wall materials were tightly packed in the thin cell wall region in which plasmodesmata formed a pit field (Plate 2b-e). There was the transparent part between the plasmodesmata and the surrounding electron-dense cell wall (Plate 2d, e). The plasma membrane was continuous through the lumen of plasmodesmata and formed a link between the cytoplasm in adjacent cells. In contrast to land plants, ER (desmotubule) was not observed in the plasmodesmata of *D. dichotoma* (Plate 2f). Tubular and other membranous structures in the cytoplasm were located close to the pit

field (Plate 2b). On a transverse view of the plasmodesmata, the inner diameter of the canal ranged from 10 to 20 nm (Plate 2g). Tiny electron-dense internal bridges were often observed (Plate 2g). They appeared to extend from the inner plasma membrane to the central region of the plasmodesmata. In the sleeves around the plasmodesmata, electron-dense spokes were observed to run from the plasma membrane to the surrounding cell wall (arrowhead in Plate 2g).

Observation of plasmodesmata using electron tomography

Pit fields were analysed by electron tomography (Plates 3, 4). When longitudinal sections of pit fields were used (Plate 3a), numerous membranous structures were observed adjacent to the pit fields (Plate 3b). These structures were not vesicles but were tubular and sometimes branched (arrowheads in Plate 3c, d). In order to evaluate the close association of these structures to the pit fields, the frequencies of membranous structures in pit fields and non-pit field regions were compared quantitatively. The volumes of the modeled membranous structures and the cross wall were calculated using 0.028 μm^3 box in thin (I, III, V in Plate 3a) and thicker (II, IV, VI in Plate 3a) cell wall regions. The frequency of the membranous structures was expressed as the volume of those structures per 0.028 μm^3. The volumes of membranous structures and cross walls were 0.00146 ± 0.00012 and 0.00530 ± 0.00035 μm^3, respectively, in regions with thin cell walls, compared to 0.00053 ± 0.00020 and 0.01249 ± 0.00075 μm^3, respectively, in the thicker cell wall regions (Plate 3e). The volume of membranous structures in regions with thin cell walls is significantly higher than that in the thicker cell wall regions ($P < 0.01$). These results indicated that localization of membranous structures was closely related to the pit fields. Some membranous structures were fused to the plasma membrane (Plate 4a, arrow in Plate 4b). Analysis of glancing sections of pit fields (Plate 4c) confirmed that the membranous structures formed a complex network (Plate 4d-f). In SLICER-tilted images, there were electron-dense internal bridges within the plasmodesmata (arrowheads in Plate 4g-i).

Plasmodesmata formation during the early stages of cytokinesis

Cytokinesis was investigated in *D. dichotoma* in order to clarify the process of plasmodesmata formation. At the beginning of cytokinesis, flat cisternae and Golgi vesicles were arranged along the cytokinetic plane (Plate 5a, b). Patches of membranous sacs were formed by fusion of flat cisternae and Golgi vesicles. Plasmodesmata-like perforations with a diameter of about 20 nm appeared in the membranous sacs (arrows in Plate 5b). It is assumed that these tubular microcanals are the precursor structures

for plasmodesmata, i.e., pre-plasmodesmata (PPD). Observation of serial sections of membranous sacs (Plate 5c-g) illustrated the presence of funnel-shaped protrusions from the membranes (Plate 5d-f). It was predicted that these protrusions would further proceed and penetrate the membranous sac to become PPD. Although ER membranes could be observed near the cytokinetic plane, they were never entrapped in the membranous sac regions, in contrast to land plants. The structure of developing membranous sacs was analyzed by electron tomography (Plate 5h). Flat cisternae and Golgi vesicles were seen near the membranous sacs, which appears to be at the same stage of cytokinesis to that of Plate 5b. By slicer-tilted images showing a transverse view of a membranous sac, it was revealed that the PPD were not simply membrane gaps in the nascent cell partition membrane, but tubular microcanals with an inner diameter of about 20 nm (arrowheads in Plate 5i). Many PPD were formed in a restricted region of the membranous sacs to create PPD-rich and PPD-free regions. In longitudinal view, electron-dense deposits could be observed on the outer surface of the central region of some PPD (Plate 5h, inset).

The thallus of *D. dichotoma* consists of three layers of the cells: two outer epidermal cell layers and inner medullary cells (Plate 6a). In transverse sections of thallus (Plate 6b), pit fields were located in the part of the cell walls of epidermal cells corresponding to the inner side of the thallus. PPD were preferentially formed in the restricted region of the cell wall as the mature pit field (Plate 6c). This observation suggested that the PPD distribution was regulated during cytokinesis in epidermal cells (Plate 6d).

Involvement of plasmodesmata in the initial development of the cell wall during cytokinesis

As cytokinesis proceeds, a new cell partition membrane is formed and contains numerous PPD (Plate 7a). The average thickness of this cell partition membrane was about 70 nm, and thus substantially thinner than a mature cell wall. Tomographic observations demonstrated that electron-dense material accumulated on the central portion of the outer surface of PPD, from which thin-layered electron-dense structures began to extend along the middle space of the cell partition membrane (Plate 7b). Tomographic slices that grazed the cell partition membrane showed a distinct differentiation of PPD-rich and PPD-free regions (Plate 7c). Slices extracted from the middle of the cell partition membrane visualized that these electron-dense structures originating from one PPD fused to those of neighboring PPD and finally extended over the PPD-rich region (Plate 7d). At the same time, they spread out to PPD-free regions.

The thin-layered electron-dense structure will be a nascent cell wall component. These electron-dense structures extended further into the cell partition membrane (Plate 7e). Notably, the thickness of the new cell wall in the PPD-rich region increased (average 110 nm) and was similar to that of a mature cell wall in pit field areas (Plate 2a-c, 7f). There was no such thickening in the PPD-free regions (average 80 nm, Plate 7g). Three-dimensional models made from the sections affirmed that cell wall synthesis was more advanced in the PPD-rich region (Plate 7h) compared to the PPD-free region (Plate 7i).

Localization of alginate and cellulose

The distribution of alginate and cellulose was examined using immunoelectron microscopy and specific enzyme-binding colloidal gold labeling, respectively. Gold particles were frequently detected on the thick cell walls when the anti-alginate antibody was used (Plate 8a). A control experiment with pre-incubation of the primary antibody with alginate yielded few or no gold particles on the cell wall (Plate 8b). The distribution of alginate was also tested during cytokinesis. Alginate could be detected in the membranous sacs (Plate 8c) and in the thickening pit field at later stages (Plate 8d, e). The colloidal gold-conjugated cellulase probe resulted in strong labeling of thick cell walls, suggesting the presence of cellulose (Plate 8f). Cellulose was not detected during the early stages of development of the cell partition membrane (Plate 8g, h), but did exhibit a gradually increased labeling of the cell wall as the cell partition membrane developed (Plate 8i).

Survey of plasmodesmata in other brown algal species

Plasmodesmata of *Saccharina japonica*

The ultrastructural survey of plasmodesmata was carried out against several other brown algal species. Sporophyte of *Saccharina japonica* has the more complex multiseriate thallus than *D. dichotoma* (Plate 9a). In the outer surface of the thallus, epidermal cells were observed. The lower part contained several layers of round-shaped cortex cells. Cortex cells were highly vacuolated and much bigger than epidermal cells. These cells were surrounded by the electron-dense cell wall. In the deeper part, medullary cells were observed. Cell wall was expanded between medullary cells. Similar to *D. dichotoma*, simple and unbranched plasmodesmata traversed the cell wall at places with a reduced cell wall thickness of about 0.1 μm (Plate 9b). Pit fields were observed as *D. dichotoma.* Desmotubule was not observed in the plasmodesmata. Tubular and other membranous structures in the cytoplasm were closely associated with the pit field. Transverse sections of the thallus gave the cross view of plasmodesmata between cortex

cells (Plate 9c, d). Multiple pit fields were located in the central part of the cell wall (arrowheads in Plate 9d). Some cells had pit fields in their peripheral region. The inner diameter of plasmodesmata was 10-20 nm (Plate 9e). The similar features of plasmodesmata were obtained in other laminarialean species (sporophytes of *Alaria crassifolia* and *Costaria costata*). Pit fields were round-shaped and their average area was 0.3 μm^2 (Table 1). The plasmodesmata frequency of the pit field in the cell wall was 226 ± 41 / μm^2 which was lower than that of *D. dichotoma* (332 ± 38 / μm^2). Based on the average area of the pit field (0.3 μm^2) and average plasmodesmata frequency (226 / μm^2), the number of plasmodesmata per pit field was calculated to be about 70 plasmodesmata per pit field (Table 1). Since one cell wall interface contained multiple pit fields in *S. japonica*, the number of plasmodesmata per cell wall interface was estimated to be more than 140 plasmodesmata per cell wall. The distance between plasmodesmata was 71 ± 13 nm indicating that plasmodesmata were distributed at almost regular intervals. The gametophyte of *S. japonica* has a uniseriate filamentous thallus (Plate 9f). In the gametophyte, the plasmodesmata frequency was quite low and the gametophyte of *S. japonica* lacked the pit field (Plate 9g). A few plasmodesmata were often located close together (arrowheads in Plate 9g).

Plasmodesmata of *Fucus distichus*

F. distichus has the complex multiseriate thallus as *S. japonica* (Plate 10a). The round-shaped cortex cells had their own cell wall and additional electron-dense cell wall in the outer intercellular space (arrowheads in Plate 10a). Plasmodesmata of these cells created one large pit field in the central part of the cell wall (arrowheads in Plate 10b). Pit fields were round-shape and their average area was 9.8 μm^2 which was the highest among species examined (Table 1). Plasmodesmata of *F. distichus* were observed in the thick cell wall (arrowhead in Plate 10c). In transverse views of plasmodesmata, the inner diameter of plasmodesmata was ranged from 10 to 24 nm (Plate 10d). Some plasmodesmata lumens had high electron density (arrowheads in Plate 10d inset). The plasmodesmata frequency of the pit field in the cell wall was 90 ± 10 / μm^2 which was lower than that of *D. dichotoma* and *S. japonica*. This was probably due to the distance between plasmodesmata (81 ± 12 nm) which was longer than that of *D. dichotoma* and *S. japonica*. The similar plasmodesmata distribution was observed in the other member of Fucales (Sporophyte of *Sargassum thunbergii*).

Plasmodesmata of Sphacelariales species

The male gametophyte of *Sphacelaria rigidula* has the simple multiseriate

filamentous thallus (Plate 11a). In the longitudinal direction of the thallus, cells were separated by the quite thick cell wall up to 1 μm. Those cell walls contained very long plasmodesmata (arrowheads in Plate 11b). The longitudinal length of the canal was highest among that of species examined. The transverse section of plasmodesmata gave the similar appearance to those of *D. dichotoma*, Fucales and Laminariales (Plate 11c). The inner diameter of plasmodesmata was about 20 nm. *S. rigidula* lacked the pit field (arrowheads in Plate 11d) and plasmodesmata frequency in the cell wall was quite low and the distance between plasmodesmata was 265 ± 151 nm. The other member of Sphacelariales, *Halopteris paniculata*, had the similar plasmodesmata distribution in the cell wall (arrowheads in Plate 11e). Although plasmodesmata were dispersed in the cell wall, the slight clustering was observed.

Plasmodesmata of *Ectocarpus siliculosus*

The male sporophyte of *E. siliculosus* has the branched uniseriate filamentous thallus (Plate 12a). In the longitudinal view, the septum contained simple plasmodesmata (arrowheads in Plate 12b). In the transverse view, the inner diameter of plasmodesmata was ranged from 10-20 nm similar to those of other species examined (arrowheads in Plate 12c). In serial transverse sections of the thallus, plasmodesmata were dispersed in the central part of the septum (Plate 12d, e) as well as in the peripheral part (Plate 12f, g). This ascertained that plasmodesmata were distributed in the whole region of the septum. The plasmodesmata frequency was 13 ± 5 / μm^2 (Table 1) which was much lower than that of other species. Plasmodesmata were also observed at the basal cell wall of branches and between vegetative cells and reproductive cells (plurilocular sporangium, unilocular sporangium).

Discussion

Ultrastructure of plasmodesmata in brown algae

The detailed analysis of plasmodesmata ultrastructure in the present study revealed that *D. dichotoma* possesses an ER-free and simple plasmodesmata with an inner diameter of 10-20 nm. The continuity of the plasma membrane along the entire canal indicated that plasmodesmata provided the functional cytoplasmic connections for cell-to-cell communication. Moreover, this study has identified substructures, internal bridges, in the plasmodesmata of *D. dichotoma*. In land plants, there have been many reports of plasmodesmatal internal components (Ding et al. 1992, Botha and Cross 2000), i.e., a desmotubule that passes through the entire canal (Robards and Lucas 1990), particular structures both on the inner plasma membrane and the outer membrane of the desmotubule, and spoke-like extensions. In green algae, globular structures filled in the inner space of the plasmodesmata (Fraster and Gunning 1969). In *D. dichotoma*, the observation of transverse ultrathin sections found that electron-dense internal bridges linked between the plasma membrane and the central point of the plasmodesmata. These structures were confirmed by the electron tomographic analysis. Given the pixel size used in the tomogram (1.54 nm), we conclude that the internal bridges are not a "superimposed" structure but an actual internal structure. However, it is still unclear whether they are present throughout the entire canal, because the present tomographic analysis could not obtain a clear image of the central region of plasmodesmata. This difficulty may be the result of the central region of the plasmodesmata being surrounded by electron-dense cell wall material. In ultrathin sections, internal bridges were not always observed in the plasmodesmata. This may suggest that they do not fill the whole canal, unlike the plasmodesmatal substructures of land plants (Ding et al. 1992). The internal bridges might have a similar function for the intercellular traffic of a variety of molecules. By bridging the plasma membrane of the canal, they can physically limit the size of the cytoplasmic space through which the molecules can freely move. In green plants, it has been reported that there is a relationship between the size of the cytoplasmic space and the size exclusion limit on the maximum molecular weight able to pass through the plasmodesmata (Citovsky 1993, Lucas and wolf 1993, Cook et al. 1997). At present, it is still unknown how and what molecules can actually be transported through the plasmodesmata of brown algae. Further analyses are required, particularly into the molecular components of the plasmodesmata of brown algae. In *D. dichotoma*, well-developed tubular membranous structures were located near the plasma membrane at pit fields, as also described in laminarialean plants (Schmitz and Kuhn 1982). These membranous structures exhibited a similar electron density and thickness

as the plasma membrane. Both conventional TEM observations and electron tomography clearly verified that some parts of the structures were fused to the plasma membrane. The close position of this complex membranous network to pit fields, where the cell walls were relatively thin, hints that they also participate in cell-to-cell traffic via the plasmodesmata.

Brown algae have primary plasmodesmata

Plasmodesmata are categorized into two groups according to the timing of their formation: primary plasmodesmata produced during cytokinesis, secondary plasmodesmata formed post-cytokinesis (Maule 2008). The process of formation of plasmodesmata has been studied in green plants. The generally accepted model in land plants is that ER membranes are entrapped during cell plate formation and these physical inclusions give rise to plasmodesmatal perforations in the cell plate (Hepler 1982). ER traverses the developing cell plate in some charophycean algae (Pickett-Heaps 1967, Cook et al. 1997). In contrast to land plants, there is limited information of appearance of plasmodesmata in brown algae. The present study has ensured that the formation of plasmodesmata in vegetative cells of *D. dichotoma* takes place on the membranous sac during cytokinesis. On the early stages of cytokinesis, structures termed here as pre-plasmodesmata (PPD) appeared and had the following features: (1) they were tubular microcanals with almost the same size (20 nm) as mature plasmodesmata, (2) they were evenly distributed in specific areas of the membranous sacs and persisted after completion of the cell partition membrane, and (3) they were formed at the sites of "future" pit fields. Perforations in the cell partition membrane have been described in *C. cylindrica*, *Halopteris congesta*, *S. rigidula* and *D. dichotoma* (La Claire 1981, Katsaros and Galatis 1985, Katsaros et al. 2009). Nagasato and Motomura (2002) and Nagasato et al. (2010) reported that the formation of plasmodesmata was not detected during the first cytokinesis in zygotes of the brown algae *Scytosiphon lomentaria* and *Silvetia babingtonii*. Plasmodesmata were clustered in the cell walls of more developed thalli of *S. lomentaria* and *Fucus distichus*. From these observations, apart from the primary plasmodesmata formation in the present study, plasmodesmata may form secondarily in development of reproductive cells of brown algae. Plasmodesmata are gathered in the pit fields located at distinct sites in the cell wall of *D. dichotoma*. Pit fields are similarly arranged in the periphery of cortical cells of *L. hyperborea* and *L. saccharina* (Schmitz and Kuhn 1982). From the findings in the present study, it is speculated that PPD formation and subsequent pit field formation occur during cytokinesis in brown algae and the positions of pit fields are controlled.

Indeed, the position of nascent pit fields, with a dense accumulation of PPD on the inner side of *Dictyota* epidermal cells, almost corresponded to the position of the "mature" pit fields in epidermal cells.

Plasmodesmata are involved in the initial cell wall development

In the present study, it was observed that during cytokinesis, an electron-dense material was accumulated on the outer surface of the midpoint of the PPD, and from which thin-layered electron-dense structures extended further from PPD-rich to PPD-free regions, and finally formed the initial cell wall in the cell partition membrane. While the thin section observation was hard to confirm the accurate location of the material in the cell partition membrane due to its superimposed image, electron tomographic analysis clearly demonstrated that the electron-dense material did indeed accumulate on the middle surface of PPD. The material was both amorphous and fibrous in tomographic slices of the cell partition membrane. In brown algae, main components of the cell wall are cellulose, acidic polysaccharides such as alginate and sulfated fucans, phenolic compounds and proteins (Kloareg and Quatrano1988, Schoenwaelder and Clayton 1999). The candidate of the observed material is either cellulose or alginate, because sulfated fucans exist as amorphous state in the cell wall (Kloareg and Quatrano 1988). In the present study, cellulose was detected after the completion of the cell partition membrane. This is supported by the previous study of the cytokinesis of *Silvetia* zygotes (Nagasato et al. 2010) demonstrating that Golgi vesicles containing fucoidan (sulfated fucan) first fused to flat cisternae and then developed into expanded flat cisternae, a membranous network and membranous sacs. The membranous sacs containing fucoidan exhibited amorphous appearance with the low electron density. Alginate was detected in the membranous sacs, although few plasmodesmata were present in the septum of *Silvetia* zygotes. The cell wall of *Dictyota* contains ascophyllan (xylofucoglucuronan) and glucuronofucogalactan as sulfated fucans, instead of fucoidan (Kloareg and Quatrano 1988). Likewise, in this study, these sulfated fucans could not be detected during cytokinesis of *D. dichotoma* using a monoclonal anti-fucoidan antibody. Considering the amorphous properties of sulfated fucans, the thin-layered electron-dense cell wall materials elongating from the middle part of PPD in membranous sacs during cytokinesis may be alginate. This suggestion is supported by the results of the immunoelectron microscopy using an anti-alginate antibody. Thus, formation of plasmodesmata might be linked to alginate synthesis during cytokinesis in *D. dichotoma*.

Common feature of plasmodesmata in brown algae

In the present study, vegetative cells of all species examined had ER-free simple plasmodesmata with an inner diameter ranged from 10 to 20 nm. The branched complex plasmodesmata were never observed in contrast to land plants. The longitudinal length of plasmodesmata were varied depending on the thickness of surrounding cell wall. In *D. dichotoma*, the longitudinal length of mature plasmodesmata was longer than that of PPD. Therefore, the longitudinal length of plasmodesmata of brown algae is likely to be remodified during cytokinesis and subsequent cell wall development. The survey of brown algal plasmodesmata in the present study infers that the ultrastructure of individual plasmodesma of vegetative cells is almost conserved from simple uniseriate to complex multiseriate species. Previous studies of plasmodesmata of brown algae mainly have focused on sieve elements in species of Laminariales (Schmitz and Srivastava 1974, 1975, 1976, Schmitz 1981, 1990). Those studies reported that the thickness of sieve plates was ranged from 200 to 650 nm. The longitudinal length of pores (=plasmodesmata) also corresponds to the range. The range of the longitudinal length of plasmodesmata of vegetative cells obtained in this study is comparable with that of sieve elements. The longitudinal length of plasmodesmata of *S. rigidula* exceeds that of sieve elements. It is not the marked difference between plasmodesmata of vegetative cells and those of sieve elements. The diameter of pores in sieve plates was ranged from 37.5 nm to 2.6 μm (Schmitz 1990). Plasmodesmata of vegetative cells and those of sieve elements significantly differ in their diameter. Sieve elements are highly differentiated and specialized for the long-distance transport in brown algae (Schmitz and Srivastava 1979). Taken together, the diameter of plasmodesmata may be regulated in brown algae as the main determinant for molecular transport conductance as well as green plants. It is yet unclear whether there is the temporal regulation of diameter of plasmodesmata in brown algae. The monitoring of molecular transport in living cells is needed to elucidate it.

Considering the narrow variation of diameter of plasmodesmata of vegetative cells, other factors should be implicated in the molecular traffic conductance between vegetative cells. The plasmodesmata frequency and their distribution are probably the other main determinants for the molecular transport conductance across the cell wall. In the present study, the clustering of plasmodesmata in the cell wall termed “pit field” was observed in many species examined (Dictyotales, Laminariales, Fucales, Desmarestiales, Scytosiphonales). Plasmodesmata were exclusively present in the thin cell wall rather than the thick one in Dictyotales, Laminariales and Fucales. The clustering of plasmodesmata was observed in the relatively uniform cell wall in other species (Desmarestiales and Scytosiphonales). The definition of pit field should be just a clustering of plasmodesmata in the cell wall regardless of the thickness of the cell wall.

The plasmodesmata frequency in the cell wall was varied in species (Table 1). The plasmodesmata frequency between cortex cells in *Laminaria saccharina* was 100-200 / μm^2 (Schmitz and Kuhn 1982). In the paper, the authors calculated the plasmodesmata frequency from published micrographs of other brown algae, 168 / μm^2 for *Himanthalia lorea* (Fucales), 132 and 172 / μm^2 for *Egregia menziesii* (Laminariales). The plasmodesmata frequency in *S. japonica* calculated in this study (Table 1) corresponds well with those calculated plasmodesmata frequencies. According to the previous studies, in end walls of sieve elements (sieve plates), the pore frequency was 0.03-100 / μm^2 for Laminariales (Schmitz and Srivastava 1974, 1975, 1976, Schmitz 1981, 1990), 50-60 / μm^2 for Fucales and 2000-3000 / μm^2 for *Dictyopteris membranacea* (Dictyotales, Katsaros and Galatis 1988). It seems that the pore frequency greatly depends on their diameter. The inner diameter of plasmodesmata in vegetative cells was ranged from 10 to 20 nm in all species examined. The variation of the plasmodesmata frequency in the present study is correlated with the distance between plasmodesmata. Longer the distance of plasmodesmata, lower the plasmodesmata frequency. The measurement of the distance between plasmodesmata in the pit field validated that they were arranged at almost regular intervals. The even distribution of plasmodesmata was described in the sieve plate of *Fucus vesiculosus* (Fielding et al. 1987). Additionally, the sieve plate of *D. membranacea* presented by Katsaros and Galatis (1988) also had the even distribution of plasmodesmata. The even plasmodesmata arrangement is likely to be the common feature of pit fields and sieve plates in brown algae. In *D. dichotoma*, plasmodesmata formation took place during cytokinesis. The distance between PPD in the newly formed cell partition membrane was 81 ± 17 nm before, and 74 ± 11 nm after the initial cell wall development (Table 1). This means that PPD are also arranged at almost regular intervals in the cell partition membrane and the distance between PPD is comparable with that between plasmodesmata of the mature pit field. Moreover, the distance between PPD corresponds well to that between plasmodesmata of the pit field in *F. distichus* and *S. japonica*. In vegetative cells of brown algae, PPD are inserted into the cell partition membrane at regular intervals and they form the precursor structure of the pit field during cytokinesis. The process of pit field formation in land plants is different from that of brown algae. In the meristem of the root of fern, *Dryopteris filix-mas*, primary plasmodesmata are randomly distributed in the newly formed cell wall (Burgess 1971). In four plant species including corn, the comparison of plasmodesmata distribution in the root meristem cells with that in the elongating cells provided the evidence that the clustering of plasmodesmata and secondary plasmodesmata formation took place during cell wall expansion. As the result of wall expansion, there was a general

shift from dispersed to clustered plasmodesmata (Seagull 1983). Due to the secondary plasmodesmata formation, the plasmodesmata frequency was maintained even after the cell wall expansion. During leaf development, the observation of plasmodesmata in the basal cell walls of trichomes proved that there was a shift from randomly distributed simple plasmodesmata to pit field containing many paired plasmodesmata during the cell wall expansion (Faulkner et al. 2008). Land plants possess the system that inserts secondary plasmodesmata into the vicinity of primary plasmodesmata giving rise to pit fields. The pit field of land plants has a post-cytokinetic origin and the arrangement of plasmodesmata can be changed during the cell wall expansion. The pit field of brown algae and land plants are much different in 1) the timing and process of its formation, 2) the presence or absence of branched complex plasmodesmata, 3) the arrangement of plasmodesmata within the pit field. As mentioned above, the existence of secondary plasmodesmata in brown algae remained obscure. If they exist, they are probably also simple plasmodesmata that are inserted around primary plasmodesmata at the regular interval, resulting in the expansion of the pit field. In the brown algae having pit fields, the plasmodesmata frequency and distance between plasmodesmata were almost constant in each organism. It is speculated that during the cell wall expansion, the structure of the cell wall containing the pit field may be maintained while that of the pit field-free cell wall region may be altered. If this is correct, the number, area and position of the pit field would affect the morphogenesis of brown algal cells.

Plasmodesmata distribution may be related to body plan in brown algae

In the present study, the pit field was hardly observed in gametophyte of *S. japonica* (Plate 9), Sphacelariales species (Plate 11) and *E. siliculosus* (Plate 12). Plasmodesmata were dispersed over the cell wall in those species. Gametophytes of *S. japonica* and *E. siliculosus* are uniseriate filamentous organisms. Sphacelariales species have a simple multiseriate filamentous thallus. From this, the occurrence of the pit field may be associated with the complex multiseriate system. How do pit fields participate in the establishment of the complex multiseriate system? One possibility might be that since the pit field contains a number of plasmodesmata (Table 1), the increase of the total number of plasmodesmata per cell wall interface could lead to the higher flux rate of the molecular transport and active cell-to-cell communication. The plasmodesmata frequency in the septum of gametophyte of *S. japonica* was quite low. In *E. siliculosus*, while the plasmodesmata frequency was relatively much lower than that of other multiseriate species, the total number of plasmodesmata in the septum was quite high. The area of the septum will be about 300 μm^2 when the diameter of the cylindrical cell is

20 μm. Since plasmodesmata of *E. siliculosus* are dispersed over the septum (average 13 plasmodesmata / μm^2), the total number of plasmodesmata in the septum will be about 4000 plasmodesmata. This number is much higher than that of any other species examined. Therefore, the total number of plasmodesmata between cells is not definitive, but rather requirement for constructing the complex multiseriate thallus. The area, number and position of pit fields may comprehensively influence the pattern of the molecular transport. This idea is supported by the report of laminarialean species that those properties of the pit field are different between anticlinal and periclinal cell walls of epidermal and cortex cells, which makes the transport pattern of photosynthetic products from epidermis toward medulla (sieve elements) (Schmitz and Kuhn 1982). In the present study, the membranous structures near pit fields were obvious in *D. dichotoma* (Plates 3, 4), sporophyte of *S. japonica* (Plate 9) and *S. lomentaria*. The pit field may be functionally coupled with the endomembrane system in brown algae. One hypothesis for the significance of pit fields is that those membranous structures and pit fields cooperatively contribute to the controlled molecular traffic via plasmodesmata: the molecular transport through a group of plasmodesmata is possibly adjusted together. If the mechanism exsists, they could give rise to the diverse patterns of the intercellular molecular flow and create the more advantageous domain for the transport regulation than dispersed plasmodesmata do. Another hypothesis is that the occurrence of the pit field enables other plasmodesmata-free cell wall to expand and differentiate. In the species having the pit field and the complex multiseriate system (e.g. *Fucus* and *Saccharina*), intercellular space (ECM) is well developed (Plates 9, 10). The pit field might be the better adaptive solution to achieve both the regulated cell-to-cell communication and large multicellular body. These hypotheses need to be validated in the future.

Chapter 2 Ultrastructural study of cell wall of *Ectocarpus siliculosus*

Introduction

The plant cell wall plays crucial roles in fundamental biological processes such as cell division and cell expansion by its mechanical properties. The study of the architecture of the cell wall is a key step to understand the morphogenetic system of brown algae. Studies of brown algal cell wall have been focusing on 1) chemical analysis of extracted cell wall polysaccharides (Quatrano and Stevens 1976), 2) TEM observation of the cell wall (Mariani et al. 1985), 3) histochemical analysis of distribution of cell wall polysaccharides using metachromatic staining (Evans and Holligan 1972).

The model of the cell wall architecture of brown algae was presented decades ago (Kloareg and Quatrano 1988). In this model, cellulose microfibrils are embedded in the matrix composed of alginate and sulfated polysaccharides. The intermolecular network is estimated to be constructed by hydrogen bonds and interactions via unknown linker proteins. However, this model harbors some problems. The biggest problem is that the model is largely on the basis of the molecular structure and the chemical properties of cell wall polysaccharides. The structural information of the intact cell wall is limited. It has been reported that the brown algal cell wall has multiple layers consisting of differently arranged fibrous structures and amorphous materials (Evans and Holligan 1972, Novotny and Forman 1975, Vreugdenh et al. 1976, Callow et al. 1978a, Mariani et al. 1985, Bisgrove and Kropf 2001). These observations come from the thin sectioning (thickness of sections was 100-150 nm). The fibrous structures are nano-scale tiny structures. It is quite difficult to understand accurately their three-dimensional arrangement in the cell wall. Previous TEM observations were performed by the conventional chemical fixation (Evans and Holligan 1972). The chemical fixation often results in serious alternations of cell structures especially on the soluble polysaccharides like alginate. It is still unclear how alginate, cellulose and sulfated polysaccharides construct the cell wall.

In land plants, each cell wall polysaccharide has its own distribution pattern in the cell wall (Lee et al. 2011). The localization of the cell wall polysaccharides is an important factor in plant morphogenesis because it affects the mechanical and physicochemical properties of the cell wall. In brown algae, histochemical analysis using toluidine blue, alcian blue and periodic acid/Schiff (PAS) staining disclosed that the multilayered architecture of the cell wall was built up by the different polysaccharide composition in each layer (Evans and Holligan 1972, Vreugdenh et al. 1976, Callow et al. 1978a, Burns et al. 1982, Mariani et al. 1985). Since toluidine blue stains acidic polysaccharides, it is generally used for detecting alginate and sulfated polysaccharides

under the neutral pH condition or sulfated polysaccharides under the acidic pH conditions (Novotny and Forman 1974, 1975). Still, it has drawbacks such as difficult evaluation of the staining pattern, low detection sensitivity and specificity. Toluidine blue staining was hard to distinguish alginate and sulfated polysaccharides at different pH conditions (Burns et al. 1982). PAS staining detects both cellulose and alginate. Other many polysaccharides including sulfated fucans can be PAS-positive (Leblond et al. 1957, Burns et al. 1982). In the analysis of distributions of cell wall polysaccharides in brown algae, examinations using toluidine blue and PAS staining are not enough, and alternative methods that are easier and have the high specificity are required. The fluorescent dye, calcofluore, has been widely used for the cell wall staining *in vivo* in brown algae (Callow et al. 1978b) and land plants (Lee et al. 2011). Since calcofluore stains both alginate and cellulose (Wood 1980), it cannot be used for the accurate evaluation of the distribution of alginate and cellulose. In land plants, a variety of probes including specific antibodies have been used for the localization analysis of cell wall polysaccharides. Those studies unmasked that each cell wall polysaccharide has its specific distribution pattern at cellular and tissue level (Knox 2008). In brown algae, monoclonal (Vreeland et al. 1984) and polyclonal (Chi et al. 1999) anti-alginate antibodies and monoclonal anti-fucoidan antibody (Mizuno et al. 2009) are available at present, enabling the localization analysis with the high specificity.

The present study describes the results from the conventional TEM observations and electron tomographic analysis of the cell wall in the brown alga *Ectocarpus siliculosus* (Dillwyn) Lyngby with rapid freezing/freeze substitutions and distribution analysis of cell wall polysaccharides using specific probes. *E. siliculosus* has the relatively simple uniseriate filamentous thallus making easier considering the relationships between the cell wall architecture and cell morphology. *E. siliculosus* is the emerging model brown alga of which genome has been fully sequenced (Charrier et al. 2008, Le Bail et al. 2008, Cock et al. 2010). It is suitable for studying the brown algal cell wall. In this chapter, the cell wall architecture of *E. siliculosus* and brown algae are discussed.

Materials and methods

Culture

Sporophytes of *E. siliculosus* (32-m strains) were cultured in half-strength PES medium (Provasoli 1968) under cool white fluorescent lamps (30-40 μmol photons m^{-2} s^{-1}) at 15 °C in long day conditions (14-h light, 10-h dark). Cultures were maintained by transferring zoospores from plurilocular zoidangia into the new medium in plastic dishes. The zoospores were settle down within 1 day and germinated 1 or 2 days after settlement. Under these conditions, erect thallus was formed around 10 days after settlement and further grown. Plurilocular zoidangia were produced on the erect thallus 20-30 days after settlement and zoospores were released again from the plurilocular zoidangia. They were transferred into the new medium in plastic dishes to restart the culture cycle. The medium was renewed in every 1 week.

Electron microscopy

The cryofixation and embedding methods were adapted from previous reports (Nagasato and Motomura 2002b, Ueki et al. 2008). The maturing erect thalli were placed on formvar-coated gold loops (5-10 mm in diameter) or gel support film (ATTO Co. Tokyo, Japan), rapidly frozen by transfer into liquid propane pre-cooled to -180 °C by liquid nitrogen, and then immediately transferred to liquid nitrogen. The samples were subsequently transferred into cooled acetone (-80 °C) containing 4 % osmium tetroxide and stored at -80 °C for 2 days. Next, the samples were gradually brought to room temperature according to the following schedule: -20 °C for 2 h, 4 °C for 2 h, and room temperature for 1 h. They were washed several times with acetone at room temperature and infiltrated with Spurr's epoxy resin at room temperature using the following schedule: 20 % resin in acetone for 12 h, 30 % resin for 5 h, 40 % for 5 h, 50 % for 12 h, 70 % for 5 h, 80 % for 5 h, 100 % for 2 days. The final two steps of infiltration were carried out in desiccators. Samples were finally embedded in Spurr resin on dishes of aluminum foil at 70 °C, overnight. Ultrathin sections (80-100 nm) were cut using a diamond knife (Micro star, Micro star tech, TX, USA) on an ULTRACUT ultramicrotome (Reichert-Jung, Depew, NY, USA) and mounted on formvar-coated copper slot grids. Sections were stained with 4 % uranyl acetate and Reynolds' lead citrate (Reynolds 1963) or Reynolds' lead citrate only and observed with a JEM-1011 electron microscope (Jeol, Tokyo, Japan).

Sample preparation for electron tomography

Eighty to 100 nm sections were cut for analysis using a 200 kV JEM-2100 electron microscope (JEOL, Tokyo, Japan) and 120 to 200 nm thick sections for a 300 kV

JEM-3200FS electron microscope (JEOL, Tokyo Japan). The sections were mounted on formvar-coated slot grids and stained with 4 % uranyl acetate and Reynolds' lead citrate (Reynolds 1963) or Reynolds' lead citrate only. After staining, the side of the grid carrying the sample was coated with formvar to sandwich the section. Then, 10 or 15 nm colloidal gold particles were attached to both sides of the grid. Finally, the grids were carbon coated on both sides. These samples were used to obtain tilted images for tomographic analysis.

Image acquisition and tomogram reconstruction

Sections were placed on a tilt-rotate specimen holder and were viewed using the 200 kV JEM-2100 electron microscope and the 300 kV JEM-3200FS electron microscope. Images were captured using a Veleta digital camera (Olympus Soft Imaging Solutions, Munster, Germany) at 60 k, 80 k, 100 k, 120 k, 150 k x magnification for 200 kV JEM-2100 electron microscope and 15 k, 25 k, 30 k x magnification for 300 kV JEM-3200FS electron microscope from -60° to +60° at 1° intervals with a resolution of 2,048 x 2,048 pixels and a pixel size of 1.045 nm for 60 k, 0.784 nm for 80 k, 0.627 nm for 100 k, 0.522 nm for 120 k, 0.418 nm for 150 k in the 200 kV JEM-2100 electron microscope, 0.868 nm for 15 k, 0.521 nm for 25 k, 0.434 nm for 30 k in the 300 kV JEM-3200FS electron microscope. Dual-axis electron tomography was performed around two orthogonal axes in order to obtain high resolution images and to reduce the "missing wedge" artifact (Mastronarde 1997). All images were taken at the Electron Microscope Laboratory, Research Faculty of Agriculture, Hokkaido University, Sapporo, Japan. Tomograms were reconstructed by aligning each set of tilted images using gold particles as fiducial markers. Filtering was treated for each axis in order to remove noises: 2-D filter (radius: 0.35, falloff 0.05) and radial filter (radius: 0.1-0.35, falloff: 0.05). Generally, the lower radius (0.1-0.25) in the radial filter gave the better result. The tomogram of each axis that got the best result was used for the tomogram combination. All tomograms were reconstructed by R-weighted back-projection algorithm and analyzed using IMOD software (Kremer et al. 1996). "SLICER", a program packaged in IMOD, was used to extract slices by setting the rotation angles about the x, y and z axes. Generated tomograms were numbered Tomogram-1 to -5 (indicated in Plates 15, 16).

Quantification of fibrous structures

The amount of the electron staining-positive fibrous structures per unit area was measured. In the analysis, the two independent tomograms containing both the inner and outer layers of the cell wall were used (Tomogram-1 and -5). Tomographic slices

showing the vertical and horizontal views of the cell wall were extracted from the tomograms using SLICER as tiff images. In the SLICER mode, the vertical and horizontal views of the cell wall were shown by setting the rotation angles about the x and z axes. The gray value of pixels comprising the fibrous structures of the test tiff images was measured using Image J 1.47t (Abramoff et al. 2004). By the line drawing tool, the central part of the fibrous structures in the image was lined and the gray value of pixels on the line was measured. In each measurement, the maximum and minimum values were recorded. The measurement was done for 100 points (50 points for the inner (L1) and outer (L2) layers, respectively) in the vertical and horizontal directions. The pixels comprising the non-fibrous region was measured in the same way. The maximum and the minimum values were averaged, respectively, and the distribution of the gray value (mean ± SD) was obtained. There was no significant difference of the gray value distribution between the inner (L1) and outer (L2) layers. The results for the inner and outer layers were combined. The gray value distribution was expressed as mean ± SD of maximum and minimum gray value for the fibrous structures and non-fibrous region in the vertical and horizontal directions of the cell wall. The thresholding gray value to distinguish fibrous structures and non-fibrous region was defined according to the lower limit of the gray value distribution of non-fibrous region in order to prevent the contaminant (false positive) of pixels comprising non-fibrous region: 160 for Tomogram-1 and 150 for Tomogram-5 in vertical direction, 120 for Tomogram-1 and 130 for Tomogram-5 in horizontal direction. The pixels with the gray value lower than the thresholding gray value were regarded as those comprising the fibrous structures. For the quantification of the fibrous structures, the sampling area was defined as the rectangle of 1200 nm x 50 nm (0.06 μm^2). The sampling area was drawn on the test image using the rectangle drawing tool in Image J. The histogram of the gray value of pixels in the sampling area was obtained and the number of pixels with the gray value lower than the thresholding gray value, namely the fibrous structures, was recorded. Then, the ratio (%) of the number of those pixels to the total number of pixels in the sampling area was calculated. The quantification was performed on 10 areas (images) in vertical and horizontal directions of the inner (L1) and outer (L2) layers of the cell wall. The final result was expressed as mean ± SD (%) calculated from the results of two independent tomograms (20 areas for the vertical and horizontal directions, respectively).

Quantification of the number of junctions

The number of junctions of fibrous structures per unit volume was counted in the cell wall. In the analysis, the two independent tomograms containing both the inner

(L1) and outer (L2) layers of the cell wall were used (Tomogram-1 and -5). Tomographic slices showing the vertical and horizontal views of the cell wall were extracted from the tomograms using SLICER as tiff images. The traced images were drawn using the free hand line drawing tool in Image J so that the line went through the center of the fibrous structures in the the sampling area. The sampling area was defined as the rectangle of 1200 nm x 50 nm (0.06 μm^2). The branched points of the fibrous structures were regarded as the junctions. Ten traced images from ten consecutive tiff images were merged to make one master traced image. The master traced image was drawn using the free hand line drawing tool in Image J so that the line covered the overlapped lines from ten traced images. Since the pixel size of Tomogram-1 and -5 was 0.78 nm, the thickness corresponding to ten traced images was 7.8 nm, the unit volume was 1200 nm x 50 nm x 7.8 nm (0.00047 μm^3). Finally, the number of junctions on the master traced image was counted in the inner (L1) and outer (L2) layers of the cell wall. In each tomogram, three sampling areas were analysed for vertical direction and five to eight sampling areas were analysed for horizontal direction. The final result was expressed as mean ± SD of junctions per unit volume calculated from the results of two independent tomograms (six areas for the vertical direction and 13 areas for horizontal direction).

Immunoelectron microscopy

Samples were prepared as described above. The subsequent steps of immunoelectron microscopy using anti-alginate antibody are indicated in "Materials and methods" in chapter 1. The samples on grids were stained with Reynolds' lead citrate. The labeling frequency was analysed by counting the number of gold particles per 1 μm^2 (2.5 μm x 0.4 μm) in the inner (L1) and outer (L2) layers of the lateral cell wall. The result was expressed as mean ± SD of gold particles per 1 μm^2 from three independent cell walls. The labeling frequency for L1 of the lateral cell wall was compared with that of L2 using Student's t-test.

Preparation of cellulase-gold probe and labeling

The cellulase gold probe was prepared as described in "Materials and methods" in chapter 1. The final mobile pellet was diluted 1:4 with 0.05 M citrate buffer to form the working solution. The subsequent labeling steps are indicated in "Materials and methods" in chapter 1. The samples on grids were stained with Reynolds' lead citrate.

Preparation of alginate lyase-gold probe and labeling

Alginate lyase from flavobacterium (Sigma) was conjugated to colloidal gold

particles using a slight modification of the method for preparation of cellulase-gold probe described above. The 10 nm colloidal gold solution (BBInternational) was adjusted to pH 7.0 with HCl. Five microliters of 2 mg mL^{-1} alginate lyase in distilled water was added to 500 μL of 10 nm colloidal gold and incubated in an ice bath for 5 min with stirring. Then, 25 μL of 1 % polyethylene glycol (PEG 4000, Merck, Darmstadt, Germany) was added for stability. The alginate lyase-gold conjugates were centrifuged at 15,000g (Kokusan RM-190, Tokyo, Japan) for 90 min at 4 °C. 100 μL of the resultant mobile pellet was transferred into a new microtube and 400 μL of 0.05 M PIPES buffer (pH 7.0) was added up to 500 μL, followed by centrifugation at 15,000g for 60 min at 4 °C. This cycle was repeated again. 100 μL of the mobile pellet was transferred into a new microtube as the concentrated solution, and was diluted 1:5 with 0.05 M PIPES buffer to form the working solution. Sections on formvar-coated nickel grids were floated on a 20 μL drop of blocking solution (2.5 % skim milk, 5 % normal goat serum and 0.05 % NaN_3 in PBS) for 30 min at 37 °C in the moisture chamber. After washing with distilled water for 5 min at room temperature, they were rinsed with 0.05 M PIPES buffer for 10 min at room temperature. Then, they were incubated with the alginate lyase-gold conjugate for 30 min at 37 °C. After washing with 0.05 M PIPES buffer for 5 min and distilled water for 5 min at room temperature, they were stained with Reynolds' lead citrate. Statistical analysis of the labeling frequency was performed as described above (see the method of "Immunoelectron microscopy"). The result was expressed as mean ± SD of the number of gold particles per 1 μm^2 from eight independent cell walls. The labeling frequency for the inner layer (L1) of the lateral cell wall was compared with that of the outer layer (L2) using Student's t-test.

Preparation of alginate-calcium gel

450 μL of 5 mg mL^{-1} alginate (sodium salt, Sigma, Saint Louis, MO, USA) in H_2O was mixed with 50 μL of 1 M $CaCl_2$ (to 100 mM) and incubated for 10 min at room temperature to form the gel. After centrifugation, the supernatant was removed. The precipitation (gel) was cut into small pieces and placed on gel support film (ATTO Co. Tokyo, Japan), rapidly frozen. The subsequent freeze-substitution and embedding was described above. Ultrathin sections (80-100 nm) were cut using a diamond knife on an ULTRACUT ultramicrotome and mounted on formvar-coated copper slot grids. Sections were stained with Reynolds' lead citrate or TI blue (Nisshin EM Corporation, Tokyo, Japan).

Dot blot assay

The original (x1) solution of 5 mg mL^{-1} alginate (sodium salt, Sigma, Saint Louis, MO, USA) in tris-buffered saline (TBS) (137 mM NaCl, 20 mM Tris, pH 7.6) was diluted 1:10, 1:100, 1:1000 and 1:10000 with TBS to form 500, 50, 5, 0.5 μg mL^{-1} solution. The solutions of polymannuronate block (poly M), random block (poly MG) and polyguluronate block (poly G) were kindly gifted from Dr. Akira Inoue (School of Fisheries Sciences, Hokkaido University, Hakodate, Japan). These alginate blocks were prepared by partial acid hydrolysis of the commercial alginate according to Gacesa and Wusteman (1990). The stock (x1) solution of 5 mg mL^{-1} poly M, poly MG and poly G in 10 mM sodium phosphase buffer (pH 7.0) was diluted with TBS as the commercial alginate. The PVDF membrane (ATTO Co. Tokyo, Japan) was treated with methanol for 1 min at room temperature and then with TBS for 5 min at room temperature. The 10 μL of each solution (commercial alginate, poly M, poly MG and poly G) was spotted on the membrane and dried at room temperature. For the control, TBS was spotted instead of the alginate solution. The membrane was incubated with blocking solution (5 % skim milk, 1 % BSA, 0.1 % Tween 20 in TBS) for 30 min at room temperature. After three times of washing (5 min each) with T-TBS (0.1 % Tween 20 in TBS), the membrane was treated with a rabbit polyclonal anti-alginate antibody, diluted 1:2000 with T-TBS, for 1 h at room temperature. After three times of washing (5 min each) with T-TBS, the membrane was labeled with an alkaline phosphatase conjugated anti-rabbit antibody (Promega, Madison, WI, U.S.A), diluted 1:5000 with T-TBS, for 30 min at room temperature. After three times of washing (5 min each) with T-TBS, the membrane was reacted with the substrate for alkaline phosphatase (Promega, Madison, WI, U.S.A) for 10 min at room temperature.

Comparison of gelation ability of alginates having different MG blocks

Eighty μL of each alginate solution (5 mg mL^{-1} poly M, poly MG and poly G in 10 mM phosphate buffer, pH 7.0) was mixed with 20 μL of 100 mM $CaCl_2$ (to 20 mM) in the microtube and incubated for 10 min at room temperature. After centrifugation, the supernatant was removed and the wet weight of the precipitated gel was measured. The mean weight of the gel and standard deviation (mean ± SD) was calculated from the results of three independent experiments.

Indirect immunofluorescence microscopy

The procedure of freezing of samples was adapted from the method described by Arun et al. (2013) with a modification. Erect thalli on gel support film were frozen by transferring the film into liquid nitrogen. They were immediately transferred into PBS

and then attached to poly L-lysine coated coverslips. Samples were incubated with blocking solution (2.5 % skim milk, 5 % normal goat serum and 0.05 % NaN_3 in PBS) for 30 min at 37 °C. Then, they were reacted with polyHistidine-tagged carbohydrate-binding module (CBM3a) to crystalline cellulose (PlantProbes, Leeds, UK), which was diluted 1:100 with PBS, 1 h at 20 °C in the dark. For the control experiments, CBM3a was omitted. After three times of washing with PBS, they were treated with a mixture of a mouse monoclonal anti-polyHistidine antibody (Sigma) diluted 1:200 with PBS and a rabbit polyclonal anti-alginate antibody (Chi et al. 1999, Nagasato et al. 2010), diluted 1:500 with PBS, 4 h at 20 °C in the dark. For the control experiments, the anti-alginate antibody was omitted. After three times washing with PBS, they were stained with a mixture of fluorescein isothiocyanate (FITC) labeled goat anti-mouse IgG (Sigma) diluted 1:50 with PBS and TRITC labeled goat anti-rabbit IgG (Sigma) diluted 1:50 with PBS, 1 h at 20 °C in the dark. After three times of washing with PBS, they were mounted with Mowiol 4-88 mounting medium (Osborn and Weber 1982) containing 0.2 % *p*-phenylene diamine. Samples were observed with an epifluorescence microscope (BX50-FLA, OLYMPUS, Tokyo, Japan). Photographs were taken with a CCD camera (AxioCam MRm, Carl Zeiss, Jena, Germany) and Axio Vision 4.6 (Carl Zeiss).

Statistical analysis

All statistical analyses in this study were carried out against data pair using Student's t-test after F-test for evaluating whether the variances were equivalent.

Results

Multilayered architecture of the lateral cell wall and electron staining-positive fibrous structures

In the present study, the maturing cell wall of sporophyte of *E. siliculosus* was analysed by TEM. *E. siliculosus* is a uniseriate filamentous brown alga. Under 15 °C, long day condition and 1/2 PES medium, settled zoospores germinated at 1-2 Day after the settlement and formed primary filament and secondary filament. Then, prostrate filaments were formed as the basal structure. After about 10 days, erect filaments were grown from the basal structure. The erect filament consisted of lineary arranged cylindrical cells (Plate 13a). In the early stage, cells of the erect filament were about 10 μm-wide and 20 μm-long. Both radial (~ 2 μm / day) and elongation (~ 5 μm / day) growths were observed. After the maturation (Day 30 ~), the maximum width of the cells was about 40 μm and the maximum length of the cells was about 70 μm. Each cell was surround by the septum and the lateral cell walls. Cells were connected by plasmodesmata in the septum cell wall (see chapter 1). Cell division was observed in almost entire parts of the erect thallus. The erect thallus was grown by the increase of the number and volume of the cells. Branches emerged from some cells of the erect thallus and grew as the main filament. By 20 to 30 days after settlement, plurilocular and unilocular sporangia were produced and matured resulting in the release of zoospores and unispores, respectively.

In TEM observations, the maturing thalli were fixed by rapid freezing/freeze substitution. The observations focused on the lateral and septum cell walls. In thin sectioning, longitudinal and cross sections of the erect thallus were prepared (Plate 13b). The cross view of the erect thallus was observed as the cylindrical shape of the cells (Plate 13c). Cells contained large vacuoles and the cytoplasm with chloroplasts and mitochondria was located in the cell periphery. In the longitudinal sections (Plate13d-h), the lateral cell wall consisted of the electron staining-positive fibrous structures. In the longitudinal views, the cell wall exhibited the different appearances depending on the angle of the section to the cell wall and plasma membrane. The unit membrane structure of plasma membrane was recognizable and it indicated that the section plane was almost vertical to the plasma membrane and the cell wall (Plate 13d). In these sections, the thickness of the lateral cell wall was from 0.8 to 1 μm. In the following observations, the interpretation took into account the angle of sections to the cell wall and plasma membranes. In Plate 13d, the cell wall seemed to contain at least two layers. In the layer just over the plasma membrane (solid line), electron-dense fibrous structures (arrow) were arranged parallel or at an acute angle to plasma membrane (horizontal direction of

the wall). In the outer layer (dashed line), fibrous structures were randomly arranged and amorphous materials were present. When the section plane was at an oblique angle to the plasma membrane and the cell wall (Plate 13e), the unit membrane structure of plasma membrane is unrecognizable (arrow). In these sections, each layer showed the different appearance from the vertical sections (Plate 13d). While the inner layer had the packed net arrangement (solid line), the outer layer retained relatively loose one. Many lateral cell walls took the additional layer (Plate 13f). It contained the innermost (L1), the outer (L2) and the outermost (L3) layers. L1 held fibrous structures parallel or at an acute angle to plasma membrane (arrowhead) and rod- or wedge-shaped structures lying on the multiple fibrous structures (white arrow). L2 was composed of randomly arranged fibrous structures. In L3, there was fibrous structures parallel or at an acute angle to plasma membrane as L1 (black arrow) while the rod- or wedge-shaped structures were hardly seen. More loosely arranged fibrous structures were observed in L3 than L1 and L2. It was predicted that the spatial density of the fibrous structures in L3 was relatively lower than that of L1 and L2. When the section plane was almost parallel to the plasma membrane and the cell wall, the clear net arrangement of L1 consisting of fibrous structures was observed (arrowhead in Plate 13g). The width of the fibrous structures was 4.0 ± 1.0 nm (n=100). The net arrangement included relatively regular pores. The tubular membranous structures were sometimes observed in the space between plasma membrane and cell wall (arrow in Plate 13g). L2 appeared to have a relatively irregular net arrangement compared with L1 (Plate 13h). The width of the fibrous structures of L2 was almost same as those of L1.

Electron staining-negative fibrous structures

Some parts of the lateral cell wall had the high electron density. In the longitudinal view, the region was located in the outer side of the lateral cell wall (white arrow in Plate 14a). In the tangential view of the lateral cell wall (Plate 14b), the material accumulated in the region internal to L3 (black arrow) and widely distributed in L2 (white arrow). In the region, many white lines were observed (arrow in Plate 14c). These were linear fibrous structures (arrows in Plate 14c, d), distinguished from the electron staining-positive fibrous structures (arrowhead in Plate 14d). These structures were visible only in the electron-dense region, but invisible in other regions (Plate 14d). The electron-dense materials visualized the linear fibrous structures by the negative contrast. The width of the fibrous structures was 12.6 ± 4.9 nm (n=72) and the longitudinal length was 420 ± 200 nm (n=51). In the labeling of the thin section using colloidal gold-conjugated cellulase, the region containing the fibrous structures was

detected (Plate 14e, f). The cell wall-rich fraction was isolated from the thallus and observed by negative staining. The linear fibrous structures were observed (arrow in Plate 14g). The width of the structures was 14.8 ± 5.8 nm (n=65) and the longitudinal length was 660 ± 350 nm (n=30). The size well corresponded to white lines observed in sections, suggesting that they were identical structures. They were labeled by cellulase-gold (Plate 14h).

Electron tomographic analysis

In order to describe the detail spatial arrangement of the cell wall, the present study adopted electron tomography.

Plate 15 explains the relationship between the projection image and tomographic slice in Tomogram-5. When the vertical section to the cell wall and plasma membrane was used for acquisition of the tilt series, the unit membrane structure of plasma membrane is obvious in the projection image of tilt series at an angle of 0° (Plate 15a). In L1 and L2, many electron staining-positive fibrous structures were arranged in the horizontal direction of the cell wall. In the projection images of tilt series at a higher angle, the unit membrane structure of plasma membrane became obscure and the cell wall presented the complex net arrangement different from the projection image at an angle of 0° (Plate 15b, c). The appearance of the region indicated by asterisk in Plate 15c was very similar to Plate 13e, 14a. It was evident that the image of the cell wall depended on the view angle of the cell wall and plasma membrane. In tomographic slices, the internal structure of the cell wall was extracted (Plate 15d).

Plate 16 represents the overview of the reconstructed tomograms. As mentioned above, the interpretation of the spatial arrangement of the structure of interest took account of the angle of the tomographic slice plane to the cell wall and plasma membrane. The vertical slice of whole thickness of cell wall and plasma membrane (Plate 16a) noted that the cell wall consisted of L1, L2 and L3 as observed in the ultrathin sections. Since the tomographic slice was the 0.78 nm-thick, the net arrangement in the vertical direction of the cell wall was present in L1, L2 and L3. L1 was composed of fibrous structures parallel or at an acute angle to plasma membrane (arrow in Plate 16b) and rod- or wedge-shaped and lump-like structures (arrowheads in Plate 16b). The width of the fibrous structures was 4.3 ± 1.4 nm (n=100), almost the same as the result in ultrathin sections. When the oblique section of the cell wall was used, L2 comprised the net arrangement on the plane oblique to the cell wall (Plate 16c). The width of the fibrous structures was 3.9 ± 1.0 nm (n=100). L3 contained fibrous structures parallel or at an acute angle to the horizontal direction of the cell wall (arrow in Plate 16c). The region as

observed in Plate 14 contained electron staining-positive fibrous structures (arrow in Plate 16d), electron staining-negative fibrous structures (arrowheads in Plate 16d) and electron-dense amorphous materials (asterisk). The amorphous materials filled the space between the electron staining-positive structures and around the electron staining-negative fibrous structures.

In tomograms, the slices in any planes can be obtained. Plate 17 is the tomographic analysis of L1 in Tomogram-2. The direction parallel to plasma membrane was x-axis. The direction vertical to plasma membrane was y-axis. The slice plane was set with the rotation degree about x-axis and y-axis (Plate 17a). In the slice vertical (0°) to plasma membrane (Plate 17b), fibrous structures parallel or at an acute angle to plasma membrane were observed (arrowhead). The rod- or wedge-shaped and lump-like structures were connected to the fibrous structures (white arrows). Keeping the slicing center as Plate 17b (marked by diamond) and tilted at 45° (Plate 17c), it indicated that the net arrangement was present on the plane oblique to the cell wall. When tilted at 90° (Plate 17d), the fibrous structures were arranged in the direction parallel to plasma membrane (=horizontal direction of the cell wall). They were randomly arranged and form the net arrangement as observed in the ultrathin sections (Plate 13). They were frequently branched from the junctions (arrowheads in Plate 17d). The space between the cell wall and plasma membrane did not contain the net arrangement of the fibrous structures (Plate 17e). When the rod- or wedge-shaped and lump-like structures were observed from several angles, they were bridged to the surrounding network in multiple directions (arrowheads in Plate 17f-j). It was interpreted that the fibrous structures had branches and the rod- or wedge-shaped and lump-like parts, creating the net arrangement.

Quantitative analysis of the cell wall architecture

Amount of fibrous structures

The quantitative evaluation of the cell wall architecture was carried out. First, the amount of the fibrous structures per area was measured. In the analysis, the tomograms containing both L1 and L2 were used (Tomogram-1, Plate 18a). In the qualitative view, it was predicted that the amount of the fibrous structures per unit area (1200 nm x 50 nm rectangle, Plate 18b) in L1 was higher than that in L2 in both the vertical (Plate 18c, d) and the horizontal directions of the cell wall (Plate 18e, f). The amount of the fibrous structures was measured by calculating the ratio of the number of pixels comprising the fibrous structures to the total number of pixels of the sampling

area. The most important point was to objectively determine the gray value to distinguish pixels comprising the fibrous structures from those comprising the non-fibrous region. As a preliminary measurement, the range of gray value of pixels comprising the fibrous structures was determined by measuring the gray value of pixels comprising the fibrous structures and ones comprising the non-fibrous region (Plate 18g). For the gray value of pixels comprising the fibrous structures, 50 points each in L1 and L2 were measured (n=100). For the gray value of pixels comprising the non-fibrous region, 50 points each in L1 and L2 were measured (n=100). In the measurement of each point, the maximum and minimum gray values of the pixels were obtained. The total result gave mean ± SD of the maximum gray values and the minimum gray ones of all points. The preliminary measurement was done in both vertical and horizontal directions of the cell wall. Gray value of the pixel was ranged from 0 (black) to 255 (white). The gray value of electron-dense fibrous structures was near to 0. In both vertical and horizontal directions of the cell wall, the gray value of pixels comprising the fibrous structures was ranged in the "black" side (45-159, 26-142, respectively), the gray value of pixels comprising the non-fibrous region was ranged in the "white" side (165-248, 124-227, respectively). In both vertical and horizontal directions, there was no difference of the gray value range between L1 and L2. In the horizontal direction, the gray value range of both fibrous structures and non-fibrous region were shifted to the "black" side compared to those in vertical direction. Thus, the analysis needed to be made in vertical and horizontal directions separately. The thresholding gray value to distinguish fibrous structures and non-fibrous region was defined from the upper limit of the gray value of the fibrous structures and lower limit of the gray value of non-fibrous region. In order to prevent the contaminant (false positive) of pixels comprising non-fibrous region, the thresholding gray value was defined as the one lower than the lower limit of the range of the gray value of pixels comprising non-fibrous region. In vertical direction, the thresholding gray value was defined as 160. In horizontal direction, it was defined as 120. In the other tomogram (Tomogram-5), the preliminary measurement and the quantification were taken as described above (Plate 18h). The pixels comprising the fibrous structures were defined as those having the gray value lower than the thresholding gray value. The measurement was conducted on 10 areas per tomogram in both vertical and horizontal directions of L1 and L2. The final result was expressed as mean ± SD calculated from the result of two tomograms. In the vertical direction of the cell wall, the amount of the fibrous structures in L1 was 50.8 ± 6.4 % while that in L2 was 44.6 ± 5.0 %. The amount of the fibrous structures per unit area in L1 was higher than that in L2 ($P < 0.01$). In the horizontal direction, the amount of the fibrous

structures in L1 was 28.1 ± 5.7 % while that in L2 was 21.8 ± 6.6 %. The amount of the fibrous structures per unit area in L1 was higher than that in L2 ($P < 0.01$). In each L1 and L2, the amount of the fibrous structures per unit area in the vertical direction was higher than that in the horizontal direction ($P < 0.001$).

The number of junctions

In the qualitative analysis of the cell wall, it was presumed that the complexity of each cell wall layer (L1 and L2), which means the frequency of the net arrangement, was different between L1 and L2, between vertical and horizontal directions. The quantitative analysis of the fibrous structures suggested that the difference was related to the spatial density of the fibrous structures (Plate 18). In principle, the complex net arrangement has many junctions. The analysis of the number of junctions and their distributions enables us to quantitatively evaluate the complexity of cell wall architecture. The distribution of junctions was quantitatively analysed in L1 and L2 of vertical and horizontal directions of the cell wall. The analysis counted the number of junctions per unit volume. In the analysis, the tomograms containing both L1 and L2 were used (Tomogram-5, Plate 19a). In the qualitative view, the complexity of the net arrangement per unit volume (1200 nm x 50 nm rectangle, Plate 19b) in L1 was higher than that in L2 in both the vertical (Plate 19c, d) and the horizontal directions of the cell wall (Plate 19e, f). First, the fibrous structures were traced (Plate 19g, h). The branched points were regarded as the junctions. In the tracing, ten traced images of ten serial slices were merged into one master traced image. This process tolerated the migration of the fibrous structures from the analysed plane and made easier to recognize them. Finally, the number of junctions on the master traced image was counted (Plate 19i). The final result was expressed as mean ± SD of junctions per volume of 1200 nm x 50 nm x 7.8 nm calculated from the result of two tomograms (Tomogram-1 and -5). In the vertical direction of the cell wall, the number of junctions in L1 was 141 ± 26 while that in L2 was 105 ± 11. The number of junctions per unit volume in L1 was higher than that in L2 ($P < 0.05$). In the horizontal direction, the number of junctions in L1 was 66 ± 21 while that in L2 was 35 ± 19. The number of junctions per unit volume in L1 was higher than that in L2 ($P < 0.001$). In each L1 and L2, the number of junctions per unit volume in vertical direction was significantly higher than that in horizontal direction ($P < 0.05$ for L1 vertical vs L1 horizontal, $P < 0.01$ for L2 vertical vs L2 horizontal).

Immunohistochemical analysis of alginate and cellulose

The fibrous structures mostly consist of cell wall polysaccharides. In order to

resolve the distribution of cell wall polysaccharides, immunohistochemical analyses was undertaken at light microscope and TEM. Plate 20 is indirect immunofluorescence microscopy using CBM3a and anti-alginate antibody. CBM3a has been widely used for detecting crystalline cellulose (Blake et al. 2006). In CBM3a (Plate 20a), the lateral cell walls were strongly stained (arrowhead). The septum cell walls had weak fluorescence (arrow). In the control in which CBM3a treatment was skipped (Plate 20b), there was no fluorescence. Anti-alginate antibody stained both the lateral and septum cell walls (arrows and arrowheads in Plate 20c). The fluorescence was also observed in the broundary of the lateral and septum cell walls. In the control in which anti-alginate antibody treatment was skipped (Plate 20d), there was no fluorescence. These results made clear that in almost all cells, the lateral cell wall contained crystalline cellulose and alginate.

On the immunoelectron microscopy using anti-alginate antibody, binding of gold particles to the cell wall was observed (Plate 21). The antibody labeled the inner layer (L1) of the lateral cell wall (i) while not the outer layer (L2) (o) (Plate 21a). In the control in which the antibody was pre-incubated with alginate before use (Plate 21c), the labeling was greatly reduced. There was the possibility that the labeling pattern was caused by the technical problems that the epitopes were not exposed to the surface of the section in L2 of the lateral cell wall. In order to validate the possibility, colloidal gold-conjugated alginate lyase was used (Plate 21c). The probe evenly labeled the lateral cell wall. In the control in which the probe was boiled before use (Plate 21d), the labeling was greatly reduced. These results denoted that alginate existed in L2 of the lateral cell wall as well and the epitopes of anti-alginate antibody were characteristically localized in L1. The labeling efficiency of anti-alginate antibody and alginate lyase-gold was each compared between L1 and L2 of the lateral cell wall (Table 2). For anti-alginate antibody, the number of gold particles per unit area (1 μm^2 (2.5 μm x 0.4 μm)) in L1 of the lateral cell wall was higher than that in L2 ($P < 0.05$). For alginate lyase-gold, there was no difference between the two layers. It bacame statistically clear that the specific epitopes of the anti-alginate antibody were localized in L1 of the lateral cell wall while targets of alginate lyase-gold were evenly spread in the lateral cell wall.

In order to validate what caused the biased recognition pattern by anti-alginate antibody, the dot blot assay was applied using several alginate polymers having different MG blocks (Plate 22). When the commercial alginate (Sigma) which was the antigen of the anti-alginate antibody was used, the signal was detected in all concentrations (5 mg mL^{-1}-0.5 μg mL^{-1}, lane 1-5). In lane 1 (5 mg mL^{-1}), the spot was reversed due to the too high concentration of alginate. When only TBS was used, the signal was not detected. In

poly M, the signal was not detected in all concentrations. In poly MG, the signal was detected even in 5 μg mL^{-1} (lane 4). In poly G, the signal was detected in 500 μg mL^{-1} (lane 2) while not in the lower concentrations (lane 3-5). This result connoted that the anti-alginate antibody well recognized poly MG and secondly poly G while poly M was difficult to be recognized. The localization of epitopes of the anti-alginate antibody matched the biased recongnizability of the antibody for different MG blocks. Inversely, it was deduced that alginates having different MG blocks were distributed in the lateral cell wall.

Septum cell walls

The septum cell walls were also observed (Plate 23). The highly electron-dense cell wall is laid down between adjacent cells (Plate 23a). The thickness of the septum was about 200 nm. The layer with relatively lower density was sometime observed in the middle of the septum cell wall (asterisk in Plate 23a). The transverse section displayed that the septum cell wall entirely consisted of electron staining-positive fibrous structures (arrowhead in Plate 23b), which was quite similar to the transverse view of L1 (Plate 13g). The width of the fibrous structures was 4.9 ± 1.4 nm (n=30). L1 was continuous to the septum cell wall (arrowhead and arrow in Plate 23c). Anti-alginate antibody strongly labeled the septum cell wall (arrowhead in Plate 23d). In the control in which the antibody was pre-incubated with alginate before use (Plate 23e), the labeling was greatly reduced. Alginate lyase-gold also labeled the septum cell wall (arrowhead in Plate 23f). In the control in which the probe was boiled before use (Plate 23g), the labeling was greatly reduced. These results were consistent with the result of indirect immunofluorescence microscopy (Plate 20). It was inferred that the septum cell wall held alginates having the same properties to those of L1.

Alginate-calcium gel

Alginates form the gel (alginate-calcium gel) in the presence of calcium. Since sea water contains calcium, alginates in the cell wall most likely form the alginate-calcium gel. In order to check the structure of the alginate-calcium gel, the commercial alginate (Sigma) and calcium chloride were mixed *in vitro* to form the gel. The gel was fixed by rapid freezing/freeze substitution as conducted in the cell wall observation and the ultrathin sections were observed (Plate 24). When stained using lead citrate, the net arrangement was observed consisting of electron staining-positive fibrous structures. The width of the fibrous structures was 4.9 ± 1.6 nm (n=50). They had the irregular appearance (Plate 24a). The other position of the same section showed the different

appearance (Plate 24b, c). When stained using TI blue, electron staining-positive fibrous structures were observed although the contrast of TI blue-stained samples was much lower than that of lead citrate stained samples (Plate 24d). Since the gel contained only alginate and calcium chloride, the observed fibrous structures were alginate. Therefore, the alginate-calcium gel had the net arrangement consisting of electron staining-positive fibrous structures.

The gelation of alginate with calcium generally occurs by the formation of intermolecular and intramolecular linkages via calcium in the poly G block. As mentioned above, the alginate-calcium gel had the fibrous structures. Are the fibrous structures composed of poly G polymers? The gelation ability of poly M, poly MG and poly G was compared in the presence of calcium (Plate 25). Each alginate solution (poly M, poly MG and poly G) was mixed with calcium chloride (final concentration: 20 mM) to form the gel. After centrifugation, the wet weight of the gel was measured. Poly M, poly MG and poly G formed the gel suggesting that all have the ability. The weight of the gel was lowest in poly M which was significantly lower than that of poly MG and poly G. The mean weight of the gel of poly MG was almost the same to that of poly G. It is likely that all MG blocks can form the fibrous structures.

Discussion

Multilayered architecture of brown algal cell wall

The present study revealed ultrastructure of the cell wall of the model brown alga *E. siliculosus* using the conventional TEM observation, electron tomography and immunohistochemical analysis on the distribution of cell wall polysaccharides. In the observation of ultrathin sections, the cell wall of *E. siliculosus* generally had the net arrangement of 4 nm-wide electron staining-positive fibrous structures (Plate 13). In previous studies of the cell wall of fucoid zygotes (Novotny and Forman 1975, Vreugdenh et al. 1976, Callow et al. 1978a, Bisgrove and Kropf 2001) and thallus (Mariani et al. 1985), tip cell of *Sphacelaria* (Tamura et al. 1996), and *Dictyota* (Evans and Holligan 1972), the cell wall contained the electron staining-positive fibrous structures. In these reports, the cell wall was composed of 2-4 layers, 1) the layer having the parallel arrangement of the fibrous structures, 2) the layer having loosely arranged fibrous structures, 3) the layer having amorphous materials (Evans and Holligan 1972, Callow et al. 1978a, Mariani et al. 1985). In fucoid zygotes after several hours from fertilization, the cell wall had only one layer composed of the fibrous structures arranged parallel to each other. At the later stage, the cell wall of zygotes took the additional inner layer composed of loosely arranged fibrous structures (Vreugdenhil et al. 1976, Bisgrove and Kropf 2001). In the outer cell wall of epidermal cells of the thallus of *Fucus* and *Dictyota*, the parallel arrangement of the fibrous structures was observed in the innermost layer. Loosely arranged ones and osmiophilic materials constituted the outer layer, and the electron-dense amorphous material covered the whole surface of the thallus (Evans and Holligan 1972, Mariani et al. 1985). In conventional TEM observations of previous studies, the cell wall displayed various appearances. This may be because the cell wall was sectioned at various angles in these studies. The interpretation of the images needed to take into account the angle of the section to the cell wall (Plates 13, 14). The lateral cell wall of *E. siliculosus* had 2-3 layers. In the vertical section of the cell wall, L1 had fibrous structures arranged parallel or at an acute angle to plasma membrane. L2 had loosely arranged fibrous structures. In the oblique sections of the cell wall, each layer represented the net arrangement but the different architecture. This is probably due to the different three-dimensional arrangement since the width and electron density of the fibrous structures are almost the same between layers. The conventional thin sectioning (ca 100 nm thickness) is quite difficult to understand accurately the architecture of the cell wall. It was analysed qualitatively and quantitatively by electron tomography (Plates 15-19). In the network of fibrous structures in the cell wall, many lump-like structures were observed (Plates 16, 17). In ultrathin section observations of the cell wall

of *Pelvetia* zygote, it was described that the fibrous structures arranged parallel each other were interconnected by the "feathery" structure (Bisgrove and Kropf 2001). In the present tomographic analysis, the lump-like structures were often a part of the fibrous structures arranged in the horizontal direction of the cell wall. These structures had branches in many directions, being connected to the surrounding network (Plate 17). Although the lump-like structures were larger than fibrous structures (diameter: around 7 nm), it may be better to regard them as the parts of the fibrous structures. The horizontal slices of the cell wall confirmed the presence of the fibrous structures arranged in the horizontal direction of L1. They were observed more frequently in L1 than L2 (Plates 17-19). The quantitative analysis discovered that in the horizontal direction of the cell wall, the amount of fibrous structures per unit area (Plate 18) and the number of junctions per unit volume (Plate 19) in L1 was higher than that in L2, respectively. In the net arrangement, as the amount of fibrous structures gets higher, the number of junctions increases. The results of the quantitative analysis demonstrate that L1 has the relatively complex net arrangement in the horizontal direction than L2 does. In the vertical direction, the similar trends are seen (Plate 17-19). It is concluded that the local alternation of the three-dimensional arrangement of the fibrous structures creates the multilayered architecture of the cell wall.

Alginate-calcium fibrous gel structures

Considering the previous studies and the present study, it is speculated that the fibrous structure is mainly composed of alginate. In previous studies, the content of cell wall polysaccharides of brown algae (alginate, cellulose and sulfated polysaccharides) was examined by chemical analysis. In *Fucus* zygotes, the content of alginate, cellulose and sulfated polysaccharide was 60 %, 20 %, 20 %, respectively of the total cell wall polysaccharides (Quatrano and Stevens 1976). In species of Fucales and Laminariales, the content of cellulose was ranged from one to 20 % of the dry weight of the thallus (Cronshaw et al. 1958). In brown algae, it is common that alginate is the major (> 50 %) cell wall polysaccharide. In the indirect immunofluorescence microscopy, alginate was detected in the lateral and septum cell walls (Plate 20). The labeling using anti-alginate antibody and alginate lyase-gold gave the same result at TEM level (Plates 21, 23). These results are consistent with the high content of alginate in the cell wall. The alginate molecule has the linear strand of mannuronic acid and guluronic acid with β1, 4 configuration (Kloareg and Quatrano 1988). The mannuronic acid-rich region forms the ribbon-like structure as cellulose (Rees 1972). Alginates may be assembled to form the fibrous structure as cellulose. In lands plants, non-cellulosic polysaccharides form

fibrous structures. In tomato suspension cultured cells treated with cellulose synthesis inhibitor (2,6-dichlorobenzonitrile, DCB), the pectin network was observed as electron staining-positive fibrous structures in cell wall by TEM (Wells et al. 1994). In the presence of DCB, the content of cellulose was severely reduced compared with non-treated cells. Despite that, there was no difference of the cell wall appearance between DCB-treated and non-treated cells under thin sections observation. Immunoelectron microscopy using anti-pectin antibody affirmed that the fibrous structures were pectins. Pectin is an acidic polysaccharide containing galacturonic acids and forms the gel in the presence of calcium. In atomic force microscopy (AFM) observation of pectin, fibrous structures occurred during the gelation of pectin with calcium (Morris et al. 2009). In the present study, the thin sections observation of alginate-calcium gel proved that alginate-calcium gel formed the electron staining-positive fibrous structures (Plate 24). From the physicochemical point of view, alginates are probably present in the cell wall as fibrous gel structures (alginate fibrils) that are electron staining-positive under TEM.

Indirect immunofluorescence microscopy using carbohydrate binding module (CBM3a) certified that crystalline cellulose existed in almost all lateral cell walls (Plate 20). The cell wall observed under TEM should have contained crystalline cellulose. In the previous studies in brown algae, TEM observations of Pt-Au shadowed replica of the extracted cell wall fraction from species of Fucales and Laminariales found cellulose-like microfibrils with width of 10-25 nm (Cronshaw et al. 1958). In the freeze fracture study of the tip cell of *Syringoderma*, the mean width of cellulose-like microfibrils was 19 nm (Schüβler et al. 2003). In the negative staining of the extracted cellulose-like microfibrils, they were ribbon-shaped and the mean width was 14.7 nm and the mean thickness was 1.8 nm (Schüβler et al. 2003). In the case of the brown alga, *Sphacelaria*, the mean width was 14 nm and the thickness was constant (2.6 nm) (Tamura et al. 1996). The longitudinal length of the fibrils is from hundreds nm or more from the published images. These microfibrils were confirmed to be cellulose microfibrils by the positive labeling using colloidal gold-conjugated Cellobiohydrolase I against samples for negative staining (Tamura et al. 1996). The electron staining-positive fibrous structures, namely alginate fibrils, observed in the present study are different from these cellulose microfibrils in that 1) the width is 4.2 ± 0.3 nm (n=445, total result from measurements of L1-L3 in both thin section observation and electron tomography), 2) irregular shape, 3) they contain the lump-parts. In the present study, conventional TEM observation and electron tomography ascertained the presence of electron staining-negative fibrous structures (Plates 14, 16). The width of the fibrous structures was 12.0 ± 5.0 nm (n=82) and longitudinal length was 420 ± 200 nm (n=51). They well correspond to the characters of

cellulose microfibrils (Tamura et al. 1996, Schüβler et al. 2003). In the labeling experiment using cellulase-gold against thin sections, the region containing the electron staining-negative fibrous structures was positively detected (Plate 14). The fibrous structures which were extracted from the cell wall were labeled by the cellulase-gold probe (Plate 14). Their width was 14.8 ± 5.8 nm (n=65) and longitudinal length was 660 ± 350 nm (n=30). In conclusion, the electron staining-negative fibrous structures in ultrathin sections and the fibrous structures in negative staining are cellulose microfibrils. This is consistent with previous reports in land plants that cellulose microfibrils are electron staining-negative due to their high crystallinity (Wells et al. 1994, Nakashima et al. 1997, Xu et al. 2007).

In brown algae, sulfated polysaccharides are sulfated fucans containing other monosaccharides. The monoclonal antibody against fucoidan of *Saccharina japonica* was prepared and indirect immunofluorescence microscopy using the antibody noticed that fucoidan was localized in the cell wall of epidermal cells of the thallus (Mizuno et al. 2009). The antibody was applied to analysis of the process of cell wall deposition during cytokinesis in *Silvetia* zygotes (Nagasato et al. 2010). In the present study, however, it could not detect the cell wall of *E. siliculosus* (data not shown). The molecular structure of sulfated fucan is varied depending on species. The antibody did not crossreact with the cell wall of *Undaria pinatifida* (Mizuno et al. 2009). The cell wall of *E. siliculosus* probably contains yet unknown sulfated fucan that is not detected by the antibody. The ultrastructure and distribution of sulfated fucans in the cell wall remain to be elucidated.

Structural anisotropy of the lateral cell wall

Electron tomographic analysis illustrated that the network consisted of alginate-calcium fibrous gel structure. In the network, three-dimensional arrangement was different between L1 and L2. What causes the difference between layers? The clues were obtained by the labeling experiment using anti-alginate and alginate lyase-gold (Plate 21, Table 2). The antibody strongly labeled L1 and alginate lyase-gold evenly labeled the cell wall. This result intimates that the epitopes of the anti-alginate antibody are localized in L1 and the target of alginate lyase is evenly distributed in the cell wall. This idea was supported by the dot blot assay using the antibody and alginate polymers (Plate 22). In the assay, the antibody strongly recognized poly MG block but not poly M block. The alginate molecule mainly consists of poly M, poly MG and poly G blocks (Gacesa and Wusteman 1990). The labeling experiment and dot blot assay complementally argue that the lateral cell wall will be composed of heterogenous MG blocks of alginate. The structural difference between L1 and L2 may be related to the

heterogeneity. The gelation properties of alginates in the presence of calcium depend on the relative proportion of poly G blocks (Haug et al. 1974). Although poly M, poly MG and poly G all formed the gel in the presence of calcium, their gelation properties were different (Plate 25). The distribution of MG blocks probably varies the spatial arrangement of alginate fibrils in L1 and L2, resulting in the alternation of three-dimensional arrangement of the network.

In L1 and L2, there was the difference of the complexity of the net arrangement of alginate fibrils between vertical and horizontal directions (Plates 18, 19). The more complex net arrangement was present in the vertical direction than in the horizontal direction of the cell wall. This means that the cell wall has a structural anisotropy. In land plants, the network of fibrous structures would dominate the mechanical property of the cell wall that governs the cell expansion. Cellulose microfibrils are linked by hemicellulose reinforcing the cell wall. Since the cellulose-hemicellulose networks are arranged in the horizontal direction of the cell wall, the cell wall has the resistance to the stress in the vertical direction (Baskin 2005, Scheller and Ulvskov 2010). During the elongation of cells of root hairs and hypocotyl epidermis, cellulose microfibrils are arranged perpendicular to the growth axis, regulating the direction of the growth (Baskin 2005). In cylindrical cells of the erect thallus of *E. siliculosus*, the cell expansion was observed along entire thallus. The cell expansion occurred in both short and long axes of the thallus. Although the growth rate is low, that in the longitudinal direction is relatively higher than that in the radial direction. The anisotropy of the cell wall of *E. siliculosus* might be related to the growth pattern. Considering the presence of the more complex net arrangement of alginate fibrils in the vertical direction than in the horizontal one of the lateral cell wall, it is hypothesized that the lateral cell wall can be transformed more easily in the horizontal direction than in the vertical one. In *E. siliculosus*, L1 contained alginate fibrils parallel to plasma membrane. Many crystalline cellulose microfibrils were contained in the cell wall (Plates 14, 16, 20). They were randomly arranged in L2 (Plates 14, 16), although their arrangement in L1 was yet unclear. In *Choristocarpus tenellus*, *D. dichotoma* and *S. rigidula*, it was reported that random and transverse arrangements of cellulose microfibrils to the growth axis were observed and the latter arrangement were controlled by that of cortical actin filaments (Karyophyllis et al. 2000, Katsaros et al. 2002). Katsaros et al. (2002) described that the cortical actin filaments was also present in *E. siliculosus*. *E. siliculosus* possibly has the transverse arrangement of cellulose microfibrils, and they may cooperatively regulate the mechanical property of the cell wall with the network of alginate fibrils.

Update of the cell wall model of brown algae

The maturing lateral cell wall of erect thallus of *E. siliculosus* has 2-3 layers containing the different network of electron staining-positive alginate fibrils. The septum cell wall also consisted of electron staining-positive alginate fibrils (Plate 23). The septum cell wall is continuous to L1 of two adjacent cells (Plate 23). This is supported by the presence of the net arrangement of alginate fibrils similar to L1 in the horizontal direction of the septum cell wall and positive labeling as L1 using anti-alginate antibody and alginate lyase-gold (Plate 23). Although the thickness is different, the layer similar to L1 was observed in *Fucus* zygotes just after fertilization (Bisgrove and Kropf 2001) and epidermal cells of the thallus of *Fucus* (Mariani et al. 1985). L1 is possibly one of fundamental architecture of the brown algal cell wall. The outer layer of the cell wall had loosely arranged fibrous structures or amorphous materials in epidermis of multiseriate species (Evans and Holligan 1972, Mariani et al. 1985). In the histochemical analysis, the multilayered architecture was hypothesized to derive from the localization of alginate, cellulose and sulfated polysaccharides. The present study suggested that the localization of MG blocks of alginate may be related to structural difference of the network in each layer. The acidic polysaccharide-rich multilayered architecture is associated with the physiological function adapted to the high salt environment of sea water (Mariani et al. 1985). In addition to the structural function of the cell wall, alginate may play some roles in modulating the physiological conditions around cells.

As discussed above, the majority of the electron staining-positive fibrous structures are alginate fibrils. The size of polymannuronic acids in the planar direction is about 0.8 nm and about 0.4 nm in the equatorial direction. The size of polyguluronic acids in planar direction is about 0.4 nm and about 0.4 nm in the equatorial direction (Aithal et al. 2012). Considering the pixel size in the present electron tomographic analysis (0.418-1.045 nm), one alginate molecule cannot be visualized. Multiple alginate chains are probably assembled to form one alginate fibril. Cellulose microfibril is formed by the highly organized assembly of cellulose chains. The fibrous structures of xyloglucan were observed by deep edging with an average width of 6.7 nm (Fujino et al. 2000). In the study, it was estimated that the width of one xyloglucan chain was 1.1 nm and one fibrous structure consisted of 4-5 xyloglucan chains.

In the present study, in addition to the fibrous structures, electron-dense, non-fibrous, amorphous materials were observed (Plates 14, 16). This amorphous materials co-existed with the electron staining-positive fibrous structures (alginate fibrils) and electron staining-negative fibrous structures (cellulose microfibrils) (Plates 14, 16). The amorphous materials were present in the space of the network of alginate fibrils (Plate

16). In the TEM observation of isolated cell walls of zygotes of *Hormosira banksii*, similar electron-dense amorphous materials were reported (Schoenwaelder and Clayton 1999). In the study, the histochemical analysis identified the materials as phenolic compounds, phlorotannin. There is possibility that the amorphous materials observed in the present study are phenolic compounds. The amorphous materials visualized the cellulose microfibrils arranged through the network of alginate fibrils (Plate 16). It is unclear whether there are linker structures between cellulose microfibrils. In land plants, one linker structure corresponds to one hemicellulose fibril (composed of several hemicellulose chains, Fujino et al. 2000). In the present study, it is hypothesized that cellulose microfibrils locally interact with the alginate fibrils constructing the structural part of the cell wall. Sulfated polysaccharides may be loosely or tightly contained in the structural part. The space in the structural part is probably the fluid part where proteins and other materials can migrate. The amorphous materials may also move through the space and be locally accumulated (Plate 14). The *Ectocarpus* genome encodes many putative secreated cell wall proteins and cell wall synthesis-associated proteins (Cock et al. 2010). For example, mannuronan C5-epimerase family proteins may be involved in the formation of the multilayered architecture through the modification of MG blocks of alginate. Their expression was controlled by many environmental conditions (Tonon et al. 2008, Cosse et al. 2009). The cell wall-related proteins probably function in correct timing and place during life and cell cycle to maintain or modify the cell wall architecture discussed above. It is expected that detail contributions of the cell wall to the morphogenesis of brown algae will be unraveled in the future on the basis of the updated cell wall model and functional characterization of cell wall-related genes.

Summary

In chapter 1, ultrastructural analysis of plasmodesmata was carried out in several brown algal species. In *D. dichotoma*, the observation of ultrathin sections in meristem cells showed that plasmodesmata were membranous tubular structures with a diameter ranged from 10 to 20 nm and clustered to create the pit fied in about 100 nm-thick cell wall. Plasmodesmata were continuous from plasma membrane of adjacent cells indicating that they were functional intercellular symplastic connections. In land plants, ER (desmotubule) passes through the plasmodesmata lumen connecting ER of adjacent cells. The desmotubule was not observed in *D. dichotoma.* On the other hand, plasmodesmata of *D. dichotoma* contained electron-dense structures. In the electron tomographic analysis of the pit field, the network of membranous structures was observed near the pit field. In the quantitative analysis, it was assured that those structures were well localized in the vicinity of the pit field than other pit filed-free cell wall. Plasmodesmata-like tubular structures (PPD) appeared in the developing cell partition membrane at the early stage of cytokinesis. PPD were clustered in the cell partition membrane and created the precursor structure of the pit field at the later stage of cytokinesis. Additionally, electron-dense materials were first accumulated on the outer surface of PPD and expanded in the cell partition membrane. It was concluded that brown algae had primary plasmodesmata that were formed during cytokinesis and PPD took part in the initial cell wall development.

In other brown algal species, the observation of ultrathin sections of vegitative cells affirmed that plasmodesmata were ER-free membranous tubular structures with a diameter ranged from 10 to 20 nm. The longitudinal length of plasmodesmata was varied in species ranging from 0.1 to 1 μm. In land plants, simple plasmodesmata with no branch and branched complex plasmodesmata are known. The latter ones were not observed in brown algae. It was assumed that brown algae had only simple plasmodesmata. In species having the multiseriate thallus including *Saccharina japonica* and *Fucus distichus*, the pit field was observed. In one cell wall interface, one or multiple pit fields were present. The area of the pit field was different between species. The plasmodesmata frequency of the pit field was 50-300 plasmodesmata / μm^2 depending on species. The distance between plasmodesmata of the pit field was almost constant in each organism (60-120 nm) and arranged at a constant interval. In *D. dichotoma*, PPD also had the same arrangement. The pit field of brown algae had the cytokinetic origin. In species having the uniseriate filamentous thallus (e.g. *Ectocarpus siliculosus*) and simple multiseriate one (e.g. *Sphacelaria rigidula*), the pit field was not observed. In *E. siliculosus*, plasmodesmata were dispersed in the septum cell wall. The

average plasmodesmata frequency was 13 plasmodesmata / μm^2 which was lower than that of the pit field. However, the total number of plasmodesmata of one cell wall interface was estimated to be higher than that of multiseriate species. It was speculated that in brown algae, the occurrence of the pit field was correlated to the development of the complex multiseriate system and the arrangement of plasmodesmata in the cell wall played more important roles in cell-to-cell communication than the structure and total number of plasmodesmata per one cell wall interface.

In chapter 2, ultrastructural analysis of cell wall was conducted in the brown alga *E. siliculosus* by the conventional TEM and electron tomography. The lateral cell wall had the multilayered architecture consisting of about 4 nm-wide electron staining-positive fibrous structures, the innermost layer (L1), outer layer (L2) and the outermost layer (L3). The qualitative and quantitative tomographic analyses of the network of the fibrous structures demonstrated that L1 and L2 had the different density of fibrous structures per unit area (indicator of the spatial density of fibrous structures) and number of junctions per unit volume (indicator of the complexity of the net arrangement). These factors were likely to be correlated with the variance of three-dimensional arrangement. It was found that L1 contained the well developed net arrangement in the horizontal direction of the cell wall (=parallel to plasma membrane). The immunohistochemical analysis and the observation of the alginate-calcium gel made *in vitro* supported that the electron staining-positive fibrous structures were mainly composed of alginate-calcium fibrous gel structures (alginate fibrils). The cell wall labeling experiment using anti-alginate antibody and gold-conjugated alginate lyase and dot blot assay remarked the localization of alginates having different molecular structures in the vertical direction of the lateral cell wall (between L1 and L2). This distribution pattern of alginates may coincide with the multilayered architecture of the lateral cell wall. The observation of the septum cell wall and immunohistochemical analyses testified that the septum cell wall had the similar structural and chemical properties to L1 of the lateral cell wall. This implied that cells were entirely surrounded by L1. The network of alginate fibrils retained the structural anisotropy between the vertical and horizontal directions of the cell wall. The anisotropy hypothetically influences the mechanical properties of the cell wall. Electron staining-negative fibrous structures were also observed. It was concluded that they were crystalline cellulose microfibrils based on indirect immunofluorescence microscopy using carbohydrate binding module, negative staining of the isolated cell wall fraction, labeling experiment using cellulase-gold and comparison of their structure with that of cellulose microfibril in previous studies. These results constructed the updated model of brown algal cell wall

that crystalline cellulose was arranged through the three-dimensional network of alginate fibrils.

References

Abramoff, M.D., Magalhaes, P.J. and Ram, S. J. (2004) Image processing with Image J. *Biophotonics international*, **11**, 36-42.

Aithal, A., Sharma, A., Joshi, S., Raghava, G.P.S. and Varshney, G.C. (2012) PolysacDB: a database of microbial polysaccharide antigens and their antibodies. *PLoS ONE*, **7** (4), e34613. doi:10.1371/journal.pone.0034613.

Andersen, R.A. (2004) Biology and systematics of heterokont and haptophyte algae. *Am. J. Bot.*, **91**, 1508-1522.

Arun, A., Peters, N.T., Scornet, D., Peters, A.F., Cock, J.M. and Coelho, S.M. (2013) Non-cell autonomous regulation of life cycle transitions in the model brown alga *Ectocarpus*. *New Phytol.*, **197**, 503-510.

Baskin, T.I. (2005) Anisotropic expansion of the plant cell wall. *Annu. Rev. Cell Dev. Biol.*, **21**, 203-222.

Benitez-Alfonso, Y. (2014) Symplastic intercellular transport from a developmental perspective. *J. Exp. Bot.*, doi:10.1093/jxb/eru067.

Bilan, M.I. and Usov, A.I. (2001) Polysaccharides of calcareous algae and their effect on the calcification process. *Russian Journal of Bioorganic Chemistry*, **27**, 2-16.

Bisalputra, T. (1966) Electron microscopic study of the protoplasmic continuity in certain brown algae. *Can. J. Bot.*, **44**, 89-93.

Bisgrove, S.R. and Kropf, D.L. (2001) Cell wall deposition during morphogenesis in Fucoid algae. *Planta*, **212**, 648-658.

Blackman, L.M. and Overall, R.L. (1998) Immunolocalization of the cytoskeleton to plasmodesmata in *Chara corallina*. *Plant J.*, **14** (6), 733-741.

Blake, A.W., McCartney, L., Flint, J.E., Bolam, D.N., Boraston, A.B., Gilbert, H.J. and Knox, J.P. (2006) Understanding the biological rationale for the diversity of cellulose-directed carbohydrate-binding modules in prokaryotic enzymes. *J. Biological*

Chemistry, **281**, 29321-29329.

Bold, H.C. and Wynne, M.J. (1985) Introduction to the algae: structure and reproduction (2nd edn) *Prentice-Hall, Englewood Cliffs, New Jersey*, pp 430-436.

Botha, C.E.J. and Cross, R.H.M. (2000) Towards reconciliation of structure with function in plasmodesmata-who is the gatekeeper? *Micron*, **31**, 713-721.

Botha, C.E.J., Hartley, B.J. and Cross, R.H.M. (1993) The ultrastructure and computer-enhanced digital image analysis of plasmodesmata at the kranz mesophyll-bundle sheath interface of *Themeda triandra* var. imberbis (Retz) A. Camus in conventionally-fixed blades. *Ann. Bot.*, **72**, 255-261.

Bouck, G.B. (1969) Extracellular microtubules. The origin, structure, and attachment of flagellar hairs in *Fucus* and *Ascophyllum* antherozoids. *J. Cell Biol.*, **40**, 446-460.

Brownlee, C. (2002) Role of the extracellular matrix in cell-cell signalling: paracrine paradigms. *Curr. Opin. Plant Biol.*, **5**, 396-401.

Burgess, J. (1971) Observations on structure and differentiation in plasmodesmata. *Protoplasma*, **73**, 83-95.

Burns, A.R., Oliveira, L. and Bisalputra, T. (1982) A histochemical study of bud initiation in the brown alga *Sphacelaria furcigera*. *New Phytol.*, **92**, 297-307.

Callow, M.E., Coughlan, S.J. and Evans, L.V. (1978a) The role of Golgi bodies in polysaccharide sulphation in *Fucus* zygotes. *J. Cell Sci.*, **32**, 337-356.

Callow, M.E., Evans, L.V., Bolwell, G.P. and Callow, J.A. (1978b) Fertilization in brown algae. I. SEM and other observations on *Fucus serratus. J. Cell Sci.*, **32**, 45-54.

Carpita, N.C. and Gibeaut, D.M. (1993) Structural models of primary cell walls in flowering plants: consistency of molecular structure with the physical properties of the walls during growth. *Plant J.*, **3** (1), 1-30.

Charrier, B., Coelho, S.M., Le Bail, A., Tonon, T., Michel, G., Potin, P., Kloareg, B., Boyen, C., Peters, A.F. and Cock, J.M. (2008) Development and physiology of the brown alga *Ectocarpus siliculosus*: two centuries of research. *New Phytol.*, **177**, 319-332.

Chi, E-S., Henry, E.C., Kawai, H. and Okuda, K. (1999) Immunogold-labeling analysis of alginate distributions in the cell walls of chromophyte algae. *Phycol. Res.*, **47**, 53-60.

Christensen, N.M., Faulkner, C. and Oparka, K. (2009) Evidence for unidirectional flow through plasmodesmata. *Plant Physiol.*, **150**, 96-104.

Citovsky, V. (1993) Probing plasmodesmatal transport with plant viruses. *Plant Physiol.*, **102**, 1071-1076.

Cock, J.M., Sterck, L., Rouze, P., Scornet, D., Allen, A.E., Amoutzias, G., Anthouard, V., Artiguenave, F., Aury, J.M. and Badger, J.H. et al. (2010) The *Ectocarpus* genome and the independent evolution of multicellularity in the brown algae. *Nature*, **465**, 617-621.

Cook, M.E., Graham, L.E., Botha, C.E.J. and Lavin, C.A. (1997) Comparative ultrastructure of plasmodesmata of *Chara* and selected bryophytes: toward an elucidation of the evolutionary origin of plant plasmodesmata. *Am. J. Bot.*, **84**, 1169-1178.

Cosgrove, D.J. (2000) Loosening of plant cell walls by expansins. *Nature*, **407**, 321-326.

Cosgrove, D.J. and Jarvis, M.C. (2012) Comparative structure and biomechanics of plant primary and secondary cell walls. *Front. Plant Sci.*, doi: 10.3389/fpls.2012.00204.

Cosse, A., Potin, P. and Leblanc, C. (2009) Patterns of gene expression induced by oligoguluronates reveal conserved and environment-specific molecular defense responses in the brown alga *Laminaria digitata*. *New Phytol.*, **182**, 239-250.

Cronshaw, J., Myers, A. and Preston, R.D. (1958). A chemical and physical

investigation of the cell walls of some marine algae. *Biochimica. Biophysica. Acta.*, **27**, 89-103.

Davidson, I.W., Sutherland, I. W. and Lawson, C.J. (1977) Localization of O-acetyl groups of bacterial alginate. *J. Gen. Microbiol.*, **98**, 603-606.

Dick-Pérez, M., Zhang, Y., Hayes, J., Salazar, A., Zabotina, O.A. and Hong, M. (2011) Structure and interactions of plant cell-wall polysaccharides by two- and three-dimensional magic-angle-spinning solid-state NMR. *Biochemistry*, **50**, 989-1000.

Ding, B., Turgeon, R. and Parthasarathy, M.V. (1992) Substructure of freeze-substituted plasmodesmata. *Protoplasma*, **169**, 28-41.

Diouris, M. (1989) Long-distance transport of ^{14}C-labelled assimilates in the Fucales: nature of translocated substances in *Fucus serratus*. *Phycologia*, **28** (4), 504-511.

Ehlers, K. and Kollmann, R. (2001) Primary and secondary plasmodesmata: structure, origin, and functioning. *Protoplasma*, **216**, 1-30.

Epel, B.L., Padgett, H.S., Heinlein, M. and Beachy, R.N. (1996) Plant virus dynamics probed with GFP-protein fusion. *Gene*, **173**, 75-79.

Evans, L.V. and Holligan, M.S. (1972) Correlated light and electron microscope studies on brown algae I. Localization of alginic acid and sulfated polysaccharides in *Dictyota*. *New phytol.*, **71**, 1161-1172.

Faulkner, C., Akman, O.E., Bell, K., Jefree, C. and Oparka, K.J. (2008) Peeking into pit fields: a multiple twinning model of secondary plasmodesmata formation. *Plant Cell*, **20**, 1504-1508.

Faulkner, C.R., Blackman, L.M., Cordwell, S.J. and Overall, R.L. (2005) Proteomic identification of putative plasmodesmatal proteins from *Chara corallina*. *Proteomics*, **5**, 2866-2875.

Fernandez-Calvino, L., Faulkner, C., Walshaw, J., Saalbach, G., Bayer, E. and Benitez-Alfonso, Y. et al. (2011) *Arabidopsis* plasmodesmal proteome. *PLoS ONE*, **6**, e18880.

doi: 10.1371/journal.pone.0018880.

Fielding A.H., Carter, P.L. and Smith, C.A. (1987) Sieve plates in *Fucus*: a reappraisal of size and pore distribution. *Phycologia*, **26**: 501-504.

Fitzgibbon, J., Beck, M., Zhou, J., Faulkner, C., Robatzek, S. and Oparka, K. (2013) A developmental framework for complex plasmodesmata formation revealed by large-scale imaging of the *Arabidopsis* leaf epidermis. *Plant Cell*, **25**, 57-70.

Franceschi, V.R., Ding, B. and Lucas, W.J. (1994) Mechanism of plasmodesmata formation in characean algae in relation to evolution of intercellular communication in higher plants. *Planta*, **192**, 347-358.

Fraster, T.W. and Gunning, B.E.S. (1969) The ultrastructure of plasmodesmata in the filamentous green alga, *Bulbochaete hiloensis* (Nordst.) Tiffany. *Planta*, **88**, 244-254.

Fry, S.C. (2004) Primary cell wall metabolism: tracking the careers of wall polymers in living plant cells. *New Phytol.*, **161**, 641-675.

Fujino, T., Sone, Y., Mitsuishi, Y. and Itoh, T. (2000) Characterization of cross-links between cellulose microfibrils, and their occurrence during elongation growth in Pea epicotyl. *Plant Cell Physiol.*, **41** (4), 486-494.

Gacesa, P. and Wusteman, F.S. (1990) Plate assay for simultaneous detection of alginate lyases and determination of substrate specificity. *Applied and Environmental Microbiology*, **56**, 2265-2267.

Gilbert, H. (2010) The biochemistry and structural biology of plant cell wall deconstruction. *Plant Physiol.*, **153**, 444-455.

Haas, T.J. and Otegui, M.S. (2007) Electron tomography in plant cell biology. *J. Integrative Plant Biology*, **49** (8), 1091-1099.

Haug, A., Larsen, B. and Smidsrød, O. (1974) Uronic acid sequence in alginate from different sources. *Carbohydrate Res.*, **32**, 217-225.

Hepler, P.K. (1982) Endoplasmic reticulum in formation of the cell plate and plasmodesmata. *Protoplasma*, **111**, 121-123.

Hongo, S., Sato, K., Yokoyama, R. and Nishitani, K. (2012) Demethylesterification of the primary wall by PECTIN METHYLESTERASE35 provides mechanical support to the *Arabidopsis* Stem. *Plant Cell*, **24**, 2624-2634.

Jamet, E., Canut, H., Boudart, G. and Pont-Lezica, R.F. (2006) Cell wall proteins: a new insight through proteomics. *TRENDS in Plant Sci.*, **11**, 33-39.

Jo, Y., Cho, W. K., Rim, Y., Moon, J., Chen, X. Y. and Chu, H., et al. (2011) Plasmodesmal receptor-like kinases identified through analysis of rice cell wall extracted proteins. *Protoplasma*, **248**, 191-203.

Karyophyllis, D., Katsaros, C. and Galatis, B. (2000) F-actin involvement in apical cell morphogenesis of *Sphacelaria rigidula* (Phaeophyceae): mutual alignment between cortical actin filaments and cellulose microfibrils. *Eur. J. Phycol.*, **35**, 195-203.

Katsaros, C. (1995) Apical cells of brown algae, with particular reference to Sphacelariales, Dictyotales, and Fucales. *Phycol. Res.*, **43**, 43-59.

Katsaros, C. and Galatis, B. (1985) Ultrastructural studies on thallus development in *Dictyota dichotoma* (Phaeophyta, Dictyotales). *Eur. J. Phycol.*, **20**, 263-276.

Katsaros, C. and Galatis, B. (1988) Thallus development in *Dictyopteris membranacea* (Phaeophyta, Dictyotales). *Br. Phycol. J.*, **23**, 71-88.

Katsaros, C. and Galatis, B. (1992) Immunofluorescence and electron microscope studies of microtubule organization during the cell cycle of *Dictyota dichotoma* (Phaeophyta, Dictyotales). *Protoplasma*, **169**, 75-84.

Katsaros, C., Karyophyllis, D. and Galatis, B. (2002) Cortical F-actin underlies cellulose microfibril patterning in brown algal cells. *Phycologia*, **41** (2), 178-183.

Katsaros, C., Karyophyllis, D. and Galatis, B. (2006) Cytoskeleton and morphogenesis in brown algae. *Annals of Botany*, **97**, 679-693.

Katsaros, C., Motomura, T., Nagasato, C. and Galatis, B. (2009) Diaphragm development in cytokinetic vegetative cells of brown algae. *Bot. Mar.*, **52**, 150-161.

Kawai, H., Maeba, S., Sasaki, H., Okuda, K. and Henry, E.C. (2003) *Schizocladia ischiensis*: A new filamentous marine chromophyte belonging to a new class, Schizocladiophyceae. *Protist*, **154**, 211-228.

Kim, I., Cho, E., Crawford, K., Hempel, F.D. and Zambryski, P.C. (2004) Cell-to-cell movement of GFP during embryogenesis and early seedling development in *Arabidopsis*. *Proc. Natl. Acad. Sci. U S A*, **102**, 2227-2231.

Kim, J.Y. (2005) Regulation of short-distance transport of RNA and protein. *Curr. Opin. Plant Biol.,* **8**, 45-52.

Kimura, S., Laosinchai, W., Itoh, T., Cui, X., Linder, C.R. and Brown, R.M. Jr. (1999) Immunogold labeling of rosette terminal cellulose-synthesizing complexes in the vascular plant *Vigna angularis*. *Plant Cell*, **11**, 2075-2085.

Kloareg, B. and Quatrano, R.S. (1988) Structure of the cell walls of marine algae and ecophysiological functions of the matrix of polysaccharides. *Oceanogr Mar. Biol. Annu. Rev.*, **26**, 259-315.

Knox, J.P. (2008) Revealing the structural and functional diversity of plant cell walls. *Curr. Opin. Plant Biol.*, **11**, 308-313.

Knox, J.P., Linstead, P.J., King, J., Cooper, C. and Roberts, K. (1990) Pectin esterification is spatially regulated both within cell walls and between developing tissues of root apices. *Planta*, **181**, 512-521.

Kremer, J.R., Mastronarde, D.N. and McIntosh, J.R. (1996) Computer visualization of three-dimensional image data using IMOD. *J. Struct. Biol.,* **116**, 71-76.

Kropf, D.L. (1994) Cytoskeletal control of cell polarity in a plant zygote. *Dev. Biol.*, **165**, 361-371.

Kumar, N.M. and Gilula, N.B. (1996) The gap junction review communication channel. *Cell*, **84**, 381-388.

Kusaykin, M., Bakunina, I., Sova, V., Ermakova, S., Kuznetsova, T., Besednova, N., Zaporozhets, T. and Zvyagintseva, T. (2008) Structure, biological activity, and enzymatic transformation of fucoidans from the brown seaweeds. *Biotechnol. J.*, **3**, 904-915.

La Barre, S., Potin, P., Leblanc, C. and Delage, L. (2010) The halogenated metabolism of brown algae (Phaeophyta), its biological importance and its environmental significance. *Mar. Drugs*, **8**, 988-1010.

La Claire, J.W. II (1981) Occurrence of plasmodesmata during infurrowing in a brown alga. *Biol. Cell*, **40**, 139-142.

Lamport, D.T.A., Kieliszewski, M.J., Chen, Y. and Cannon, M.C. (2011) Role of the extensin superfamily in primary cell wall architecture. *Plant Physiol.*, **156**, 11-19.

Le Bail, A., Billoud, B., Le Panse, S., Chenivesse, S. and Charrier, B. (2011) *ETOILE* regulates developmental patterning in the filamentous brown alga *Ectocarpus siliculosus*. *Plant Cell*, **23**, 1666-1678.

Le Bail, A., Billoud, B., Maisonneuve, C., Peters, A.F., Cock, J.M. and Charrier, B. (2008) Early development pattern of the brown alga *Ectocarpus siliculosus* (Ectocarpales, Phaeophyceae) sporophyte. *J. Phycol.*, **44**, 1269-1281.

Leblond, C. P., Glegg, R. E. and Eidinger, D. (1957) Presence of carbohydrates with free 1,2-glycol groups in sites stained by the periodic acid-Schiff technique. *J. Histochemistry and Cytochemistry*, **5**, 445-458.

Lee, JY. (2014) New and old roles of plasmodesmata in immunity and parallels to tunneling nanotubes. *Plant Sci.*, **221-222**, 13-20.

Lee, L.J.D., Marcus, S.E. and Knox, J.P. (2011) Cell wall biology: perspectives from cell wall imaging. *Mol. Plant*, **4** (2), 212-219.

Lee, K.Y. and Mooney, D.J. (2012) Alginate: properties and biomedical applications. *Progress in Polymer Science*, **37**, 106-126.

Lerouxel, O., Cavalier, D.M., Liepman, A.H. and Keegstra, K. (2006) Biosynthesis of plant cell wall polysaccharides-a complex process. *Curr. Opin. Plant Biol.*, **9**, 621-630.

Levy, A., Erlanger, M., Rosenthal, M. and Epel, B.L. (2007) A plasmodesmata-associated b-1, 3-glucanase in *Arabidopsis*. *Plant J.*, **49**, 669-682.

Li, S., Leia, L., Somervilleb, C.R. and Gu, Y. (2012) Cellulose synthase interactive protein 1 (CSI1) links microtubules and cellulose synthase complexes. *Proc. Natl. Acad. Sci., USA*, **109**, 185-190.

Lombard, V., Golaconda, R.H., Drula, E., Coutinho, P.M. and Henrissat, B. (2014) The carbohydrate-active enzymes database (CAZy) in 2013. *Nucleic Acids Res.*, **42**, 490-495.

Lucas, W.J. and Wolf, S. (1993) Plasmodesmata: the intercellular organelles of green plants. *Trends Cell Biol.*, **3**, 308-315.

Makowski, L., Caspar, D.L., Phillips, W.C., Baker, T.S. and Goodenough, D.A. (1984) Gap junction structures. VI. Variation and conservation in connexon conformation and packing. *Biophys. J.*, **45**, 208-218.

Marchant, H.J. (1976) Plasmodesmata in algae and fungi. In: Gunning, B.E.S., Robards T.A.W. (eds) Intercellular communication in plants: studies on plasmodesmata. Springer, Berlin, pp 59-80.

Mariani, P., C. Tolomio, C. and Braghetta, P. (1985) An ultrastructural approach to the adaptive role of the cell wall in the intertidal alga *Fucus virsoides*. *Protoplasma*, **128**, 208-217.

Mastronarde, D.N. (1997) Dual-axis tomography: an approach with alignment methods that preserve resolution. *J. Struct. Biol.*, **120**, 343-352.

Maule, A.J. (2008) Plasmodesmata: structure, function and biogenesis. *Curr. Opin. Plant Biol.*, **11**, 680-686.

Meslet-Cladière, L., Delage, L., Leroux, C.J.J., Goulitquer, S., Leblanc, C., Creis, E., Gall, E.A., Stiger-Pouvreau, V., Czjzek, M. and Potin, P. (2013) Structure/function analysis of a type III polyketide synthase in the brown Alga *Ectocarpus siliculosus* reveals a biochemical pathway in phlorotannin monomer biosynthesis. *Plant Cell*, **25**, 3089-3103.

Michel, G., Tonon, T., Scornet, D., Cock, J.M. and Kloareg, B. (2010a) The cell wall polysaccharide metabolism of the brown alga *Ectocarpus siliculosus*. Insights into the evolution of extracellular matrix polysaccharides in eukaryotes. *New phytol.*, **188**, 82-97.

Michel, G., Tonon, T., Scornet, D., Cock, J.M. and Kloareg, B. (2010b) Central and storage carbon metabolism of the brown alga *Ectocarpus siliculosus*: insights into the origin and evolution of the storage carbohydrates in eukaryotes. *New Phytol.*, **188**, 67-81.

Mizuno, M., Nishitani, Y., Tanoue, T., Matoba, Y., Ojima, T., Hashimoto T. and Kanazawa, K. (2009) Quantification and localization of fucoidan in *Laminaria japonica* using a novel antibody. *Biosci. Biotechnol. Biochem.*, **73** (2), 335-338.

Morris, V.J., Gromer A. and Kirby, A.R. (2009) Architecture of intracellular networks in plant matrices. *Struct. Chem.*, **20**, 255-261.

Motomura, T. (1994) Electron and immunofluorescence microscopy on the fertilization of *Fucus distichus* (Fucales, Phaeophyceae). *Protoplasma*, **178**, 97-110.

Motomura, T. and Sakai, Y. (1984) Ultrastructural studies of gametogenesis in *Laminaria angustata* (Laminariales, Phaeophyta) regulated by iron concentration in the medium. *Phycologia*, **23** (3), 331-343.

Müller, W.H., Koster, A.J., Humbel, B.M., Ziese, U., Verkleij, A.J., van Aelst, A.C., van der Krift, T.P., Montijn, R.C. and Boekhout, T. (2000) Automated electron tomography of the septal pore cap in *Rhizoctonia solani*. *J. Struct. Biol.*, **131**, 10-18.

Nagasato, C., Inoue, A., Mizuno, M., Kanazawa, K., Ojima, T., Okuda, K. and Motomura, T. (2010) Membrane fusion process and assembly of cell wall during cytokinesis in the brown alga, *Silvetia babingtonii* (Fucales, Phaeophyceae). *Planta*, **232**, 287-298.

Nagasato, C. and Motomura, T. (2002a) Influence of the centrosome in cytokinesis of brown algae: polyspermic zygotes of *Scytosiphon lomentaria* (Scytosiphonales, Phaeophyceae). *J. Cell Sci.*, **115**, 2541-2548.

Nagasato, C. and Motomura, T. (2002b) Ultrastructural study on mitosis and cytokinesis in *Scytosiphon lomentaria* zygotes (Scytosiphonales, Phaeophyceae) by freeze-substitution. *Protoplasma*, **219**, 140-149.

Nagasato, C. and Motomura, T. (2009) Effect of latrunculin B and brefeldin A on cytokinesis in the brown alga *Scytosiphon lomentaria* zygotes (Scytosiphonales, Phaeophyceae). *J. Phycol.*, **45**, 404-412.

Nagasato, C., Kajimura, N., Terauchi, M., Mineyuki, Y. and Motomura, T. (2014) Electron tomographic analysis of cytokinesis in the brown alga *Silvetia babingtonii* (Fucales, Phaeophyceae). *Protoplasma*, DOI 10.1007/s00709-014-0635-y.

Nakashima, J., Mizuno, T., Takabe, K., Fujita, M. and Saiki, H. (1997) Direct visualization of lignifying secondary wall thickenings in *Zinnia elegans* cells in culture. *Plant Cell Physiol.*, **38** (7), 818-827.

Novotny, A.M. and Forman, M. (1974) The Relationship between changes in cell wall composition and the establishment of polarity in *Fucus* embryos. *Dev. Biol.*, **40**, 162-173.

Novotny, A.M. and Forman, M. (1975) The Composition and development of cell walls of *Fucus* embryos. *Planta*, **122**, 67-78.

Nyvall P., Corre, E., Boisset, C., Barbeyron, T., Rousvoal, S., Scornet, D., Kloareg, B. and Boyen, C. (2003) Characterization of mannuronan C-5-epimerase genes from the brown alga *Laminaria digitata*. *Plant Physiol.*, **133**, 727-735.

Okazaki, M. and Tazawa, K. (1989) Alginic acid in Corallinaceae (Cryptonemiales,

Rhodophyta). *Korean J. Phycol.*, **4**, 213-219.

Oparka, K.J., Roberts, A.G., Boevink, P., Santa Cruz, S., Roberts, I., Pradel, K.S., Imlau, A., Kotlizky, G., Sauer, N., and Epel, B. (1999). Simple, but not branched, plasmodesmata allow the nonspecific trafficking of proteins in developing tobacco leaves. *Cell*, **97**, 743-754.

Osborn, M. and Weber, K. (1982) Immunofluorescence and immunocytochemical procedures with affinity purified antibodies: tubulin-containing structures. *In* Wilson, L. (Ed.) Methods in Cell Biology. Academic Press, New York, **24**, 97-132.

Peng, H.B. and Jaffe, L.F. (1976) Cell-wall formation in *Pelvetia* embryos. A freeze-fracture study. *Planta*, **133**, 57-7l.

Pickett-Heaps, J.D. (1967) Ultrastructure and differentiation in *Chara* sp. II. Mitosis. *Aust. J. Biol. Sci.*, **20**, 883-894.

Ponce, N.M., Pujol, C.A., Damonte, E.B., Flores, M.L. and Stortz, C.A. (2003) Fucoidans from the brown seaweed *Adenocystis utricularis*: extraction methods, antiviral activity and structural studies. *Carbohydrate Res.*, **338**, 153-165.

Popper, Z.A., Michel, G., Hervé, C., Domozych, D.S., Willats, W.G.T., Tuohy, M.G., Kloareg, B. and Stengel, D.B. (2011) Evolution and diversity of plant cell walls: From algae to flowering plants. *Annu. Rev. Plant Biol.*, **62**, 567-590.

Prochnik, S.E., Umen, J., Nedelcu, A.M., Hallmann, A. and Miller, S.M. et al. (2010) Genomic analysis of organismal complexity in the multicellular green alga *Volvox carteri*. *Science*, **329**, 223-226.

Provasoli, L. (1968) Media and prospects for the cultivation of marine algae. In: Watanabe, A., Hattori, A. (eds) *Cultures and collections of algae. Japanese Society of Plant Physiologists, Hakone,* pp 63-75.

Pueschel, C.M. (1977) A freeze-etch study of the ultrastructure of red algal pit plugs. *Protoplasma*, **91**, 15-30.

Quatrano, R.S. and Stevens, P.T. (1976) Cell wall assembly in *Fucus* zygotes. *Plant Physiol.*, **58**, 224-231.

Ramsey, D.M. and Wozniak, D.J. (2005) Understanding the control of *Pseudomonas aeruginosa* alginate synthesis and the prospects for management of chronic infections in cystic fibrosis. *Molecular Microbiology*, **56** (2), 309-322.

Raven, J.A. (2008) Evolution of plasmodesmata, in Plasmodesmata (ed Oparka K.J.), Blackwell Publishing Ltd, Oxford, UK, pp 33-50.

Rees, D.A. (1972) Shapely polysaccharides. *Biochem. J.*, **126**, 257-273.

Reiss, H.D., Katsaros, C. and Galatis, B. (1996) Freeze-fracture studies in the brown alga *Asteronema rhodochortonoides*. *Protoplasma*, **193**, 46-57.

Reynolds, E.S. (1963) The use of lead citrate at high pH as an electron-opaque stain in electron microscopy. *J. Cell Biol.*, **17**, 208-212.

Richmond, T.A. and Somerville, C.R. (2000) The cellulose synthase superfamily. *Plant Physiol.*, **124**, 495-498.

Robards, A.W. (1968) A new interpretation of plasmodesmatal ultrastructure. *Planta*, **82**, 200-210.

Robards, A.W. and Lucas, W.J. (1990) Plasmodesmata. *Annu. Rev. Plant Physiol. Plant Mol. Biol.*, **41**, 369-419.

Rose, J.K.C., Braam, J., Fry, S.C. and Nishitani, K. (2002) The XTH family of enzymes involved in xyloglucan endotransglucosylation and endohydrolysis: current perspectives and a new unifying nomenclature. *Plant Cell Physiol.*, **43** (12), 1421-1435.

Rozario, T. and DeSimone, D.W. (2010) The extracellular matrix in development and morphogenesis: A dynamic view. *Dev. Biol.*, **341**, 126-140.

Sakurai, N. (1998) Dynamic function and regulation of apoplast in the plant body. *J.*

Plant Res., **111** (1), 133-148.

Salmén, L. (2004) Micromechanical understanding of the cell-wall structure. *C. R. Biol.*, **327**, 873-880.

Salmon, M.S. and Bayer, E.M.F. (2012) Dissecting plasmodesmata molecular composition by mass spectrometry-based proteomics. *Front. Plant Sci.*, **3**, 307-315.

Samuels, A.L., Giddings, T.H. and Staehelin, L.A. (1995) Cytokinesis in tobacco BY-2 and root tip cells: a new model of cell plate formation in higher plants. *J. Cell Biol.*, **130**, 1345-1357.

Sarkar, P., Bosneaga, E. and Auer, M. (2009) Plant cell walls throughout evolution: towards a molecular understanding of their design principles. *J. Exp. Bot.*, **60**, 3615-3635.

Sato, T. (1968) Lead citrate stain in electron microscopy. *J. Electron Microsc.*, **17**, 158-159.

Scheller, H.B. and Ulvskov, P. (2010) Hemicelluloses. *Annu. Rev. Plant Biol.*, **61**, 263-289.

Schiel, D.R. and Foster, M.S. (2006) The population biology of large brown seaweeds: ecological consequences of multiphase life histories in dynamic coastal environments. *Annu. Rev. Ecology, Evolution, and Systematics*, **37**, 343-372.

Schmitz, K. (1981) Translocation. In: Lobban, C.S. and Wynne, M.J. (eds) The biology of seaweeds. Blackwell Scientific Publications, Oxford, pp 534-558.

Schmitz, K. (1990) Algae. In: Behnke, H.D. and Sjolund, R.D. (eds) Sieve elements. Comparative structure, induction and development. Springer, Berlin, pp 1-18.

Schmitz, K. and Kuhn, R. (1982) Fine structure, distribution and frequency of plasmodesmata and pits in the cortex of *Laminaria hyperborea* and *L. saccharina*. *Planta*, **154**, 385-392.

Schmitz, K. and Srivastava, L. (1974) Fine structure and development of sieve tubes in

Laminaria groenlandica Rosenv. *Cytobiologie*, **10**, 66-87.

Schmitz, K. and Srivastava, L. (1975) On the fine structure of sieve tubes and the physiology of assimilate transport in *Alaria marginata*. *Can. J. Bot.*, **53**, 861-876.

Schmitz, K. and Srivastava, L.M. (1976) The fine structure of sieve elements of *Nereocystis lutkeana*. *Am. J. Bot.*, **63**, 679-693.

Schmitz, K. and Srivastava, L.M. (1979) Long distance transport in *Macrocystis integrifolia*. I. Translocation of ^{14}C labelled assimilates. *Plant Physiol.*, **63**, 995-1002.

Schoenwaelder, M.E.A. and Clayton, M.N. (1999) The presence of phenolic compounds in isolated cell walls of brown algae. *Phycologia*, **38**, 161-166.

Schopfer, C.R. and Hepler, P.K. (1991) Distribution of membranes and the cytoskeleton during cell plate formation in pollen mother cells of *Tradescantia*. *J. Cell Sci.*, **100**, 717-728.

Schüβler, A., Hirn, S. and Katsaros, C. (2003) Cellulose synthesizing terminal complexs and morphogenesis in tip-growing cells of *Syringoderma phinneyi* (Phaeophyceae). *Phycol. Res.*, **51**, 35-44.

Schuster, E., Eckardt, J., Hermansson, AM., Larsson, A., Lorén, N., Altskär, A. and Ström, A. (2014) Microstructural, mechanical and mass transport properties of isotropic and capillary alginate gels. *Soft Matter*, **10**, 357-366.

Seagull, R.W. (1983) Differences in the frequency and disposition of plasmodesmata resulting from root cell elongation. *Planta*, **159**, 497-504.

Seguí-Simarro, J.M., Austin, J.R. II, White, E.A. and Staehelin, L.A. (2004) Electron tomographic analysis of somatic cell plate formation in meristematic cells of *Arabidopsis* preserved by high-pressure freezing. *Plant Cell*, **16**, 836-856.

Showalter, A.M., Keppler, B., Lichtenberg, J., Gu, D. and Welch, L.R. (2010) A bioinformatics approach to the identification, classification, and analysis of hydroxyproline-rich glycoproteins. *Plant Physiol.*, **153**, 485-513.

Simpson, C., Thomas, C., Findlay, K., Bayer, E. and Maule, A.J. (2009) An *Arabidopsis* GPI-anchor plasmodesmal neck protein with callose binding activity and potential to regulate cell-to-cell trafficking. *Plant Cell*, **21**, 581-594.

Smith, L.G. and Oppenheimer, D.G. (2005) Spatial control of cell expansion by the plant cytoskeleton. *Annu. Rev. Cell Dev. Biol.*, **21**, 271-295.

Staehelin, L.A. and Hepler, P.K. (1996) Cytokinesis in higher plants. *Cell*, **84**, 821-824.

Tamura, H., Mine I. and Okuda, K. (1996) Cellulose-synthesizing terminal complexes and microfibril structure in the brown alga *Sphacelaria rigidula* (Sphacelariales, Phaeophyceae). *Phycol. Res.*, **44**, 63-68.

Tenhaken, R., Voglas, E., Cock, J.M., Neu, V. and Huber, C.G. (2011) Characterization of GDP-mannose dehydrogenase from the brown alga *Ectocarpus siliculosus* providing the precursor for the alginate polymer. *J. Biological Chemistry,* **286**, 16707-16715.

Thomas, C.L., Bayer, E.M., Ritzenthaler, C., Fernandez-Calvino, L. and Maule, A.J. (2008) Specific targeting of a plasmodesmal protein affecting cell-to-cell communication. *PLoS Biol.*, **6**, 180-190.

Tonon, T., Rousvoal, S., Roeder, V. and Boyen, C. (2008) Expression profiling of the mannuronan C5–epimerase multigenic family in the brown alga *Laminaria digitata* (Phaeophyceae) under biotic stress conditions. *J. Phycol.*, **44**, 1250-1256.

Tsekos, I. (1999) The sites of cellulose synthesis in algae: diversity and evolution of cellulose-synthesizing enzyme complexes. *J. Phycol.*, **35**, 635-655.

Ueki, C., Nagasto, C., Motomura, T. and Saga, N. (2008) Reexamination of the pit plugs and the characteristic membranous structures in *Porphyra yezoensis* (Bangiales, Rhodophyta). *Phycologia,* **47**, 5-11.

Urban, E., Jacob, S., Nemethova, M., Resch, G.P. and Small, J.V. (2010) Electron tomography reveals unbranched networks of actin filaments in lamellipodia. *Nature Cell Biol.*, **12**, 429-435.

Vreeland, V., Slomich, M. and Laetsch W.M. (1984) Monoclonal antibodies as molecular probes for cell wall antigens of the brown alga, *Fucus. Planta*, **162**, 506-551.

Vreugdenhil, D., Dijkstra, M.L. and Libbenga, K.R. (1976) The ultrastructure of the cell wall of polar and apolar embryos of *Fucus vesiculosus*. *Protoplasma*, **88**, 305-313.

Wargacki, A.J., Leonard, E., Win, M.N., Regitsky, D.D., Santos, C.N.S., Kim, P.B., Cooper, S.R., Raisner, R.M., Herman, A., Sivitz, A.B., Lakshmanaswamy, A., Kashiyama, Y., Baker, D. and Yoshikuni, Y. (2012) An engineered microbial platform for direct biofuel production from brown macroalgae. *Science*, **335**, 308-313.

Wells, B., McCann, M.C., Shedletzky, E., Delmer, D. and Roberts, K. (1994) Structural features of cell walls from tomato cells adapted to grow on the herbicide 2,6-dichlorobenzonitrile. *J. Microscopy*, **173**, 155-164.

White, R.G. and Barton, D.A. (2011) The cytoskeleton in plasmodesmata: a role in intercellular transport? *J. Exp. Bot.*, **62**, 5249-5266.

Wille, A.C. and Lucas, W.J. (1984) Ultrastructural and histochemical studies on guard-cells. *Planta*, **160**, 129-142.

Wood, P.J. (1980) Specificity in the interaction of direct dyes with polysaccharides. *Carbohydrate Res.*, **85**, 271-287.

Wynne, M.J. and Loiseaux, S. (1976) Recent advances in life history studies of the Phaeophyta. *Phycologia*, **15**, 435-452.

Xu, P., Donaldson, L.A., Gergely, Z.R. and Staehelin, L.A. (2007) Dual-axis electron tomography: a new approach for investigating the spatial organization of wood cellulose microfibrils. *Wood Sci. Technol.*, **41**, 101-116.

Yoon, H.S., Hackett, J.D., Ciniglia, C., Pinto, G. and Bhattacharya, D. (2004) A molecular timeline for the origin of photosynthetic eukaryotes. *Mol. Biol. Evol.*, **21**, 809-818.

Yoshikawa, T., Eiguchi, M., Hibara, KI., Ito, JI. and Nagato, Y. (2013) Rice SLENDER

LEAF 1 gene encodes cellulose synthase-like D4 and is specifically expressed in M-phase cells to regulate cell proliferation. *J. Exp. Bot.*, **64**, 2049-2061.

Zambryski, P. (2004) Cell-to-cell transport of proteins and fluorescent tracers via plasmodesmata during plant development. *J. Cell Biol.*, **162**, 165-168.

Zavaliev, R., Ueki, S., Epel, B.L. and Citovsky, V. (2011) Biology of callose (β-1, 3-glucan) turnover at plasmodesmata. *Protoplasma*, **248**, 117-130.

Zhong, R. and Ye, ZH. (2007) Regulation of cell wall biosynthesis. *Curr. Opin. Plant Biol.*, **10**, 564-572.

Zuo, J., Niu, QW., Nishizawa, N., Wu, Y., Kost, B. and Chua, NH. (2000) KORRIGAN, an *Arabidopsis* endo-1,4-b-glucanase, localizes to the cell plate by polarized targeting and is essential for cytokinesis. *Plant Cell*, **12**, 1137-1152.

Table 1 Comparison of plasmodesmata distribution in cell walls among several species of brown algae.

Organism	Presence of pit field	Area of pit field (μm^2, mean ± SD)	n	Number of pit field per wall	Plasmodesmata frequency (μm^{-2}, mean ± SD)	n	Number of plasmodesmata per pit field	Distance between plasmodesmata (nm, mean ± SD)	n
Sphacelaria rigidula, male gametophyte	–, *1							265 ± 151	5
Ectocarpus siliculosus, male sporophyte	–				13 ± 5	6		251 ± 131	132
Scytosiphon lomentaria, gametophyte	+	1.1 ± 0.6	4	Unkown	73 ± 5, *2	4	80, *5	97 ± 16	15
Saccharina japonica, sporophyte	+	0.3 ± 0.2	3	Multiple	226 ± 41, *3	3	68	71 ± 13	112
Desmarestia ligulata, sporophyte	+	4.4 ± 1.5	2	Unkown	51 ± 3	3	224	118 ± 32	87
Fucus distichus, sporophyte	+	9.8 ± 5.8	3	1	90 ± 10	7	882	81 ± 12	72
Dictyota dichotoma, sporophyte	+	0.6 ± 0.1	3	Multiple	332 ± 38, *4	3	199	62 ± 16	226
PPD bofore initial cell wall development								81 ± 17	265
PPD after initial cell wall development								74 ± 11	62

*1 +: the pit field was observed, –: the pit field was not observed.

*2 The measured areas were smaller than 1 μm^2.
The absolute frequency was expressed as the number of plasmodesmata per 0.5 µm x 0.5 µm.
Plasmodesmata frequency per 1 μm^2 was calculated based on the absolute frequency.

*3 The measured areas were smaller than 1 μm^2.
The absolute frequency was expressed as the number of plasmodesmata per 0.4 µm x 0.4 µm or 0.25 µm x 0.25 µm.
Plasmodesmata frequency per 1 μm^2 was calculated based on the absolute frequency.

*4 The measured areas were smaller than 1 μm^2.
The absolute frequency was expressed as the number of plasmodesmata per 0.5 µm x 0.5 µm or 0.25 µm x 0.25 µm.
Plasmodesmata frequency per 1 μm^2 was calculated based on the absolute frequency.

*5 Calculated using mean area of pit field (μm^2) and mean plasmodesmata frequency (No. plasmodesmata / μm^2).

Table 2 Labeling frequency by anti-alginate antibody and colloidal gold-conjugated alginate lyase probe at the inner (L1) and outer (L2) layers in lateral cell walls.

Probe	No. gold particles per 1 μm² (0.4 μm x 2.5 μm)
Anti-alginate antibody (n=3)	
Inner layer (L1)	136 ± 3*
Outer layer (L2)	8 ± 6
Alginate lyase-gold (n=8)	
Inner layer (L1)	101 ± 17
Outer layer (L2)	89 ± 11

The results are based on thin section labeling experiments as shown in Plate 21. The labeling frequency is expressed as number of gold particles per 1 μm² (0.4 μm x 2.5 μm) in the inner (L1) and outer (L2) layers of the lateral cell wall (mean ± SD, n=3 for anti-alginate antibody, 8 for alginate lyase-gold). A Student's t-test was performed for each probe. The labeling frequency of L1 of the lateral cell wall was compared with that of L2 (*$P < 0.05$).

Legends of Plates

Plate 1

Light microscopic observation of the thallus of *Dictyota dichotoma*. (a) Overview of the multiseriate thallus indicating the observed positions. (b) Meristematic cells in the apical region of the thallus indicated in (a). An inset shows the dome-shaped tip cell (arrowhead). (c) Epidermal cells in the middle part of the thallus indicated in (a). Note that the cells are larger than those in the apical part (b). (d) Schematic illustration of the representative epidermal cell arrangement. Black lines are cell walls. Arrowheads point at three way junctions of the cell walls. Each cell shares cell wall interfaces with more than five cells (e.g. cell 1: 7 cells, cell 2: 5 cells, cell 3: 6 cells). (e) Initial stage of the hair cell formation. Some epidermal cells differentiate into hair cells (asterisks). (f) Hair cells. Inset shows initial hair cells. Arrowheads: septums of one hair cell.

Plate 2

Ultrastructure of plasmodesmata of *D. dichotoma*. (a) Overview of an epidermal cell. Plasma membranes and cell organelles are well preserved by the rapid freezing/freeze substitution. Arrow indicates a cell wall region containing many plasmodesmata (pit field). chl, Chloroplast; g, Golgi body; n, Nucleus; nu, Nucleolus; v, Vacuole. (b) and (c) Enlargement of the region indicated by the arrow in (a). Plasmodesmata traverse thin cell wall that is ~100 nm thick. Membranous structures are present in the vicinity of the plasmodesmata (arrow). cw, Cell wall; cp, Cytoplasm. (d) and (e) Numerous plasmodesmata are present in the cell wall and form a pit field. There is an electron-lucent sleeve between the plasmodesmata and the surrounding cell wall. (f) Longitudinal view of a plasmodesma showing the direct connection between the cytoplasm (cp) of adjacent cells. No desmotubular structure can be discerned in the lumen of the plasmodesma. cw, Cell wall; pm, Plasma membrane. (g) Transverse view of plasmodesmata. The inner diameter of the canal is generally 10-20 nm. Electron-dense structures (internal bridges, ib) are observed to extend from the plasma membrane within the plasmodesmata. Note that a "spoke" stretches from the plasma membrane of the sleeve to the cell wall (arrowhead). pm, plasma membrane.

Plate 3

Quantitative analysis of the occurrence of membranous structures in pit field. (a) A 1.54-nm-thick tomographic slice. A longitudinal section of a pit field is used. Single-axis tomogram. Thin (*I, III, V*) and thicker (*II, IV, VI*) cell wall regions were used for the

quantitative analysis (e). chl, Chloroplast; pm, Plasma membrane; pt, Pit field. (b) Three-dimensional tomographic model from the image in (a). Pit fields (pt) are located in the thin cell wall regions. pm, Plasma membrane; pt, Pit field. (c) and (d) Tilted view of the model shown in (b) illustrating the upper side (c) and the lower side (d) of the model. Note that tubular membranous structures are seen close to pit fields. These structures display branches (arrowheads). pm, Plasma membrane. (e) Quantification of the frequencies of membranous structures in pit fields and non-pit field regions. The volumes of the modeled membranous structures and the cross wall were calculated using 0.028 μm^3 boxes extracted from (a): thin (I, III, V) and thicker (II, IV, VI) cell wall regions. Each graph indicates mean ± SD of three measurements (n=3) for cross walls and membranous structures. The results were compared each other (line). $*P < 0.01$ (Student's t-test).

Plate 4

Tomographic analysis of pit fields. Two sets of single-axis tomograms (a-b, c-i). (a) A 2.23-nm-thick tomographic slice. A longitudinal section of the pit field is used. chl, Chloroplast; g, Golgi body; m, Mitochondria; n, Nucleus; pm, Plasma membrane; pt, Pit field. (b) Longitudinal SLICER view of the pit field enclosed by the dotted rectangle in (a). Note that the membranous structures are in part continuous from pm (arrow). Arrowheads indicate plasmodesmata. pm, Plasma membrane. (c) A 1.54-nm-thick tomographic slice. A glancing section of the pit field is used. pt, Pit field. (d) Transverse SLICER view of the pit field. Plasmodesmata canals are visible within the cell wall. (e) Transverse SLICER view of cytoplasmic region over the pit field. Well-developed membranous structures can be seen. (f) Three-dimensional tomographic model of the membranous structures in (e). These structures possess an intricate network. (g)-(i) Transverse SLICER views of serial slices of plasmodesmata. Internal bridges are recognizable (arrowheads).

Plate 5

Structure of PPD. (a) Overview of a cytokinetic plane during an early stage of cytokinesis. Formation of the cytokinetic plane proceeds perpendicularly to the longitudinal axis of the cell. Flat cisternae are arranged on the cytokinetic plane (arrowheads). Several membranous sacs have formed (arrows). n, Nucleus. (b) An enlarged membranous sac (ms) indicated by the arrow on the right in (a). Note that tubular pre-plasmodesmata (PPD) are present in the membranous sac (arrows). fc, Flat cisternae; gv, Golgi-derived vesicle. (c)-(g) Consecutive serial sections. Membrane protrusions can be seen in the membranous sacs (arrowheads). (h) A 2.23-nm-thick tomographic slice. A dual axis

tomogram. An expanded membranous sac (ms) with a gap (arrow). The inset shows a 2.23-nm-thick longitudinal slicer view of PPD. Note that electron-dense material is deposited on the outer surface of the PPD (arrowhead). pm, Plasma membrane. (i) Transverse SLICER view of the membranous sac enclosed in the dotted rectangle in (h). A gap (arrow in h) can be observed in the center of the membranous sac (arrow). Note that the PPD are unevenly distributed in the membranous sac (arrowheads), resulting in PPD-rich (pr) and PPD-free regions (pf).

Plate 6

Position of pit field in epidermal cells. (a) Schematic illustration indicating the cross view of the thallus. The thallus of *D. dichotoma* consists of three-layers of cell: outer epidermal cells and central medullar cells. (b) Position of pit fields. Transverse section of the thallus. Pit fields are located in the part of the cell walls of epidermal cells corresponding to the inner side of the thallus (arrows). ocw, Outer cell wall of the thallus; md, Medullar cell; n, Nucleus. (c) Position of PPD. The right side of the image is the outer side of the epidermal cell as (b). PPD are formed in the restricted region of the nascent cell partition membrane (arrowhead) as the mature pit field (arrow). ocw, Outer cell wall of the thallus. (d) Schematic illustration indicating the position of pit field and PPD. In epidermal cells, pit fields (plasmodesmata) are always present in the certain area of the cell walls of epidermal cells corresponding to the inner side of the thallus. PPD have the same distribution as the mature pit field in the newly formed cell partition membrane.

Plate 7

PPD in a nascent cell partition membrane. Two sets of dual-axis tomograms (a-d, e-i). (a) A 2.23-nm-thick tomographic slice. A number of PPD are present in the nascent cell partition membrane. chl, Chloroplast; m, Mitochondria; n, Nucleus; v, Vacuole. (b) Longitudinal views of PPD in the 2.23-nm-thick tomographic slice. Note that electron-dense material is present on the outer surface of the central portion of PPD and that electron-dense thin-layered structures extend from it to the middle space of the cell partition membrane (arrows). Arrowheads indicate PPD. fc, Flat cisterna. (c) Transverse SLICER view of the cell partition membrane enclosed in the dotted rectangle in (a). Distinct PPD-rich (pr) and PPD-free (pf) regions are present. (d) Enlarged transverse SLICER view of the cell partition membrane. Note the extension of electron-dense structure from the PPD (arrows). Arrowheads indicate PPD. (e) An advanced stage of cell partition membrane formation. A 1.54-nm-thick tomographic slice. A PPD-free region (pf) is located between two PPD-rich regions (pr). m, Mitochondria; v, Vacuole. (f)

Magnified image of the PPD-rich region shown in the upper left of (e). fc, Flat cisterna. (g) Magnified image of the PPD-free region shown in the center of (e). fc, Flat cisterna. (h) Three-dimensional tomographic model from (f) using ISOSURFACE. The cell wall materials (arrow) are well developed in the PPD-rich region. fc, Flat cisterna; pm, Plasma membrane. (i) Three-dimensional tomographic model drawn from (g) using ISOSURFACE. Development of cell wall materials (arrow) is delayed in the PPD-free region. fc, Flat cisterna; pm, Plasma membrane.

Plate 8

Immunogold localization of alginate and cellulose. (a) Alginate is present in the mature cell wall (cw) but not in the Golgi body (g). (b) Control section with pre-incubation of the anti-alginate antibody with alginate. Note that there are only a few gold particles. (c) Alginate can be detected in membranous sacs (ms). (d) Cell wall material is being deposited in a future pit field near the PPD where alginate can be detected. mcw, Mother cell wall. (e) Enlargement of (d) showing gold particles near the PPD (arrows). (f) Cellulose can be detected in mature thick cell walls. cw, Cell wall; g, Golgi body. (g) Immediately after the completion of formation of the cell partition membrane, cellulose cannot be detected. (h) Cellulose is localized in the mother cell wall (mcw), but not in the nascent cell partition membrane. (i) Cellulose can be detected in developing cell partition membrane. mcw, Mother cell wall.

Plate 9

Plasmodesmata of *Saccharina japonica*. (a) Overview of sporophyte thallus. Samples were prepared by chemical fixation. Small epidermal cells are seen in the upper side. Cortex cells in the central part are large and highly vacuolated cells. Medulla with expanded extracellular matrix is visible in the lower part. (b) Longitudinal view of plasmodesmata between cortex cells showing the similar structure to ones of *D. dichotoma*. No desmotubular structure can be discerned in the lumen of the plasmodesma. Membranous structures are present in the vicinity of the plasmodesmata (arrowheads). cw, Cell wall. (c) and (d) Transverse view of plasmodesmata between cortex cells. These images are from serial sections through the cell wall of a cortex cell. Note that three pit fields are present in the central part of the cell wall (arrowheads). (e) Transverse view of one pit field. Note that the distance between plasmodesmata is almost constant. (f) Overview of male gametophyte thallus. Sample was prepared by rapid freezing/freeze substitution. Gametophyte has uniseriate filamentous body. (g) Transverse view of plasmodesmata. Plasmodesmata frequency is much lower than that

of sporophyte and do not gather as pit field. Plasmodesmata are often located near to each other (arrowheads).

Plate 10

Plasmodesmata of *Fucus distichus.* Samples were prepared by chemical fixation. (a) Overview of outer cortex cells of thallus. Electron-dense intercellular spaces are visible (arrowheads). n, Nucleus. (b) Transverse view of plasmodesmata between cortex cells. One large pit field is present in the central part of the cell wall (arrowhead). (c) Longitudinal view of plasmodesmata. Plasmodesmata penetrate into the thick cell wall (arrowhead). (d) Transverse view of plasmodesmata. Note that the distance between plasmodesmata is almost constant. Inset shows the magnified image of the cross view of plasmodesmata. Some plasmodesmata are electron-dense in their lumen (arrowheads).

Plate 11

Plasmodesmata of Sphacelariales species. Samples were prepared by the rapid freezing/freeze substitution. (a) Overview of thallus of *Sphacelaria rigidula* male gametophyte. The long axis of the thallus corresponds to the vertical direction of the image. chl, Chloroplast; n, Nucleus. (b) Longitudinal view of plasmodesmata. The quite long plasmodesmata penetrate into the thick cell wall (arrowheads). pm, Plasma membrane. (c) Transverse view of two adjacent plasmodesmata. (d) Distribution of plasmodesmata in *S. rigidula.* Plasmodesmata are dispersed in the cell wall and their frequency is quite low (arrowheads). cp, Cytoplasm. (e) Distribution of plasmodesmata in *Halopteris paniculata* sporophyte. Plasmodesmata are dispersed in the cell wall and their frequency is quite low (arrowheads).

Plate 12

Plasmodesmata of *Ectocarpus siliculosus.* Samples were prepared by the rapid freezing/freeze substitution. (a) Light micrograph of an erect thallus of male sporophyte (bright field). *E. siliculosus* has a branched (arrowheads) uniseriate filamentous body. The septum is indicated by arrow. chl, Chloroplast. (b) Longitudinal view of plasmodesmata. Simple plasmodesmata are present in the cell wall (arrowheads). pm, Plasma membrane. (c) Transverse view of plasmodesmata. (d) and (e) Distribution of plasmodesmata in the central part of the septum (asterisk in (d)). Plasmodesmata are dispersed in the septum (arrowhead). chl, Chloroplast; cw, Cell wall. (f) and (g) Distribution of plasmodesmata in the peripheral part of the septum (asterisk in (f)). Plasmodesmata are dispersed in the septum (arrowhead) as the central part (e).

Plate 13

Observation of the lateral cell wall of vegetative cells of *Ectocarpus siliculosus*. (a) Light micrograph of an erect thallus (bright field). Upper and lower images are from the same erect thallus but on the different focus plane. chl, Chloroplast; py, Pyrenoid. (b) Schematic illustration depicting the plane of ultrathin sections. White arrowhead: the plane transverse to the cell. Black arrowhead: the plane longitudinal to the cell. (c) Electron micrograph of transverse section of the cylindrical cell. chl, Chloroplast; lw, Lateral cell wall; m, Mitochondria; v, Vacuole. (d) A vertical section of lateral cell wall. The cell wall is composed of electron staining-positive fibrils. Two layers can be detected in the wall: inner (solid line) and outer (dashed line) layers. An illustration in (d), (e), (g), (h) shows an angle of the section plane to the lateral cell wall (lw) and plasma membrane (pm) (indicated with a gray rectangle). chl, Chloroplast (e) An oblique section of lateral cell wall. The inner (solid line) and the outer layers (dashed line) both have a net arrangement. chl, Chloroplast. (f) Representative image of multilayered architecture of the lateral cell wall. The arrangements of fibrous structures in the innermost (L1), outer (L2) and outermost (L3) layers are different each other. L1 contains fibrous structures parallel or at an acute angle to plasma membrane (arrowhead) and rod- or wedge-shaped structure (white arrow). pm, Plasma membrane. (g) A tangential view through L1 and adjacent cytoplasm. The boundary of the cell wall (cw) and cytoplasm (cp) magnified from the area indicated with a dashed rectangle in the longitudinal section (inset). The net arrangement of L1 consists of about 4 nm-wide fibrous structures (arrowhead). The characteristic membranous structures are sometimes observed in the space between plasma membrane and cell wall (arrow). cp, Cytoplasm; sw, Septum cell wall. (h) Transverse view of L1 and L2. L2 appears to have a relatively irregular net arrangement compared with L1.

Plate 14

Electron staining-negative fibrils observed in ultrathin sections. (a) An oblique longitudinal section of the lateral cell wall. The electron-dense material is positioned in L2 (white arrow). Electron staining-positive fibrils are in L3 (black arrow). An illustration in (a) and (b) shows an angle of the section plane to the lateral cell wall (lw) and plasma membrane (pm) (indicated with a gray rectangle). cp, Cytoplasm. (b) A tangential section of the lateral cell wall showing the overview. The electron-dense material was widely distributed in L2 (white arrow) and electron staining-positive fibrils in the L3 (black arrow). (c) A magnified image of the rectangle indicated in (b). Electron

staining-negative fibrils are visible (arrow). (d) The boundary between the electron-dense region and L3. The left side of the image corresponds to the electron-dense region and right side to L3. In the boundary, the fibril in (c) is recognized (arrow). In L3, electron staining-positive fibrils are seen (arrowhead). (e) Overview of cellulase-gold labeling against the tangential section of the lateral cell wall. The lower left of the image corresponds to the inner side of the cell and the upper right to the region as (c). (f) A magnified image of the rectangle indicated in (e). The region containing the electron staining-negative fibrils was labeled. (g) Negative staining image of isolated cell wall-rich fraction. The linear fibrils similar to those in (c) were observed (arrow). (h) Cellulase-gold labeling of the cell wall-rich fraction (g).

Plate 15

Relationship between projection image and tomographic slice (Tomogram-5). (a) A projection image of tilt series at an angle of 0°. The unit membrane structure of plasma membrane is recognizable indicating that the section plane is almost vertical to the plasma membrane and the cell wall. L1 (solid line) and L2 (dashed line) each corresponds to one indicated in Plate 13f. Black dots (arrowhead) are gold particles as fiducial markers. pm, Plasma membrane. (b), (c) A projection image of tilt series at an angle of -40° (b) and +40° (c). pm, Plasma membrane. (d) A 0.78 nm-thick tomographic slice reconstructed from the tilt series (-60° - +60°) containing (a)-(c). The slice shows the internal structure of the network of fibrils seen in conventional TEM image. pm, Plasma membrane.

Plate 16

Overview of tomograms. (a) A tomographic slice in z-axis direction (Tomogram-1).The section vertical to the plasma membrane and the cell wall is used in the tomogram. An illustration in (a)-(d) shows an angle of the section plane to the lateral cell wall (lw) and plasma membrane (pm) (indicated with a gray rectangle). The dashed rectangle shows the observed area. The cell wall consists of L1, L2 and L3 composed of electron staining-positive fibrils as observed in Plate 13. (b) A tomographic slice in z-axis direction (Tomogram-2). The magnification is higher than (a), focusing on L1. It shows fibrils parallel or at an acute angle to plasma membrane (arrow) and electron-dense rod- or wedge-shaped and lump-like structures (arrowheads). (c) A tomographic slice in z-axis direction (Tomogram-3). The oblique section of the cell wall is used in the tomogram, focusing on L2 and L3. L3 contains the fibrils arranged parallel to the vertical direction of the panel (arrow). (d) A tomographic slice in z-axis direction (Tomogram-4). The

tangential section of the cell wall corresponding to Plate 14b is used in the tomogram. It contains electron staining-positive fibrils (arrow) and electron-dense amorphous materials in the space between the fibrils (asterisk). In the accumulation of the amorphous materials, white linear lines are seen (arrowheads).

Plate 17

Detail tomographic analysis of L1 in Tomogram-2. (a) Illustrations of slicing. In both left and right illustration, cell wall (cw, indicated by box) and plasma membrane (pm, indicated by darkest rectangle) corresponds to the whole Tomogram-2. When the slicing center (indicated by diamond mark in (b)-(j)) is defined as point zero, the slicing plane was defined based on the rotation degree about x-axis (horizontal direction), y-axis (vertical direction), and z-axis (depth direction). The left illustration shows slice planes tilted about the x-axis (four gray rectangles) (b)-(e). Although not shown here, the slice planes in (g)-(i) are also tilted about x-axis. The right illustration shows slice planes tilted about y-axis (two gray rectangles) (f) and (j). (b) A vertical slice of the cell wall (0° x-axis tilt). Fibrous structures parallel to plasma membrane are seen (arrowhead). The rod- or wedge-shaped and lump-like structures are connected to the fibrous structures (arrows). (c) An oblique slice of the cell wall (45° x-axis tilt). The net arrangement of fibrils is present in the oblique direction of the cell wall. (d) A horizontal slice of the cell wall (90° x-axis tilt). The fibrils are arranged in the horizontal direction of the cell wall. They were frequently branched, creating junctions (arrowheads). (e) A horizontal slice of the space between the cell wall and plasma membrane in (b) (90° x-axis tilt). The net arrangement of fibrils like L1 is absent. (f)-(j) Slicing of the lump-like structure (diamond mark). It is connected to the surrounding network in multiple directions (arrowheads). The arrowhead marked by asterisk in (f) and (j) indicates the same branch. (f) 0° x-axis tilt and 0° y-axis tilt. (g) 40° x-axis tilt. (h) 70° x-axis tilt. (i) 90° x-axis tilt. (j) 0° x-axis tilt and 90° y-axis tilt.

Plate 18

Quantitative analysis of the amount of fibrils. (a) A tomographic slice showing overview of Tomogram-1. The tomogram contains the whole thickness of the lateral cell wall. (b) A tomographic slice vertical to plasma membrane (vertical direction of the lateral cell wall) showing overview of analysed areas. The lower side corresponds to L1 and the upper side to L2. The lower two rectangles indicate the analysed areas for L1 and the upper two ones for L2. (c) A magnified image of the analysed area of L1 from (b). Many electron staining-positive fibrils are present. (d) A magnified image of the analysed area

of L2 from (b). It seems that less fibrils are present in L2 than in L1 (c). (e) A tomographic slice horizontal to plasma membrane (horizontal direction of the lateral cell wall) of L1. (f) A tomographic slice horizontal to plasma membrane (horizontal direction of the lateral cell wall) of L2. It seems that less fibrils are present in L2 than in L1 (f). (g) Preliminary measurement of gray values of fibrils and non-fibrous regions. Note that the gray value range is quite different between fibrous structures and non-fibrous regions and slightly different between vertical and horizontal direction of the cell wall. (h) Quantification of fibrous structures. Each graph indicates mean of results of 20 areas (n=20) of two different tomograms (Tomogram-1 and 5, ten areas each) with standard deviation (bar). The results were compared each other (lines). *P< 0.01, **P< 0.001 (Student's t-test).

Plate 19

Quantitative analysis of the number of junctions. (a) A tomographic slice showing overview of Tomogram-5. The tomogram contains the layer L1 and L2. (b) A tomographic slice vertical to plasma membrane (vertical direction of the lateral cell wall) showing overview of analysed areas. The lower side corresponds to L1 and the upper side to L2. The lower rectangles indicate the analysed areas for L1 and the upper ones for L2. pm, Plasma membrane. (c) and (d) A magnified image of the analysed area of L1 (c) and L2 (d) from (b). (e) and (f) A tomographic slice horizontal to plasma membrane (horizontal direction of the lateral cell wall) of L1 (e) and L2 (f). (g) and (h) Tracing of fibrils and counting of the number of junctions. Original image (g) and traced image (h). (i) Quantification of the number of junctions. Each graph indicates mean of six measurements (n=6) for vertical direction of the cell wall and 13 measurements (n=13) for horizontal direction of two different tomograms (Tomogram-1 and 5) with standard deviation (bar). The results were compared each other (lines). *P< 0.05, **P< 0.01, ***P < 0.001 (Student's t-test).

Plate 20

Distribution of cellulose and alginate in cells of erect filament by indirect immunofluorescence microscopy. (a)-(d): the same area. (a) Cellulose detected by CBM3a. Arrow: septum cell wall. Arrowhead: lateral cell wall. (b) No CBM3a control. (c) Alginate detected by anti-alginate antibody. Arrow: septum cell wall. Arrowhead: boundary of the lateral and septum cell walls. (d) No anti-alginate antibody control.

Plate 21

Localization of alginate in the lateral cell wall. (a) Labeling using anti-alginate antibody.

L1 is strongly labeled while few in L2. (b) Anti-alginate antibody preincubated with alginate before the labeling step as a control. The labeling is greatly reduced. (c) Labeling using alginate lyase-gold. Both L1 and L2 are evenly labeled. (d) Alginate lyase-gold boiled before the labeling step as a control. The labeling is substantially reduced. pm, Plasma membrane.

Plate 22

Dot blot assay using anti-alginate antibody against several alginate polymers. Each alginate solution (5 mg mL^{-1}, rows on the left of the plate) is diluted with TBS (x10 to x10000, lanes on the top of the plate) and 10 µl of each is spotted on the membrane. Lane 1: 5 mg mL^{-1} (x1), Lane 2: 500 µg mL^{-1} (x10), Lane 3: 50 µg mL^{-1} (x100), Lane 4: 5 µg mL^{-1} (x1000), Lane 5: 0.5 µg mL^{-1} (x10000). For the control, TBS was spotted instead of the alginate solution (the lower left of the plate).

Plate 23

TEM observation of septum cell walls. (a) A longitudinal section of the septum cell wall. The highly electron-dense cell wall is laid down between adjacent cells. Note that the layer with relatively lower density is recognizable in the middle of the septum cell wall (marked by asterisk). chl, Chloroplast; pd, Plasmodesmata; pm, Plasma membrane. (b) A transverse section of the septum cell wall. It is evident that the septum cell wall contains numerous electron staining-positive fibrils (arrowhead in inset). pd, Plasmodesmata. (c) A longitudinal section of the boundary between lateral and septum cell walls. L1 is continuous to the septum cell wall (arrowhead and arrow). chl, Chloroplast; pd, Plasmodesmata; pm, Plasma membrane. (d) Immunolabeling of the septum cell wall using anti-alginate antibody. The septum cell wall is strongly labeled (arrowhead). (e) Anti-alginate antibody preincubated with alginate before the labeling step as a control. (f) Labeling of the septum cell wall using alginate lyase-gold. (g) Alginate lyase-gold boiled before the labeling step as a control.

Plate 24

TEM observation of alginate-calcium gel. (a) A thin section of resin embedded-alginate-calcium gel. The section is stained by lead citrate (8 min). The net arrangement of electron staining-positive fibrils is evident. (b) The alginate-calcium gel at different position of the section from (a). The net arrangement seems to be different from (a). (c) The alginate-calcium gel at different position of the section from (a) and (b). The net arrangement of the fibrils appears to have smaller pores than (a) and (b). (d) A thin

section stained by TI blue (1h). The electron staining-positive fibrils are seen with much lower contrast.

Plate 25

In vitro test of gelation ability of alginates having different MG blocks in the presence of calcium. Each alginate solution (poly M, poly MG and poly G) was mixed with $CaCl_2$. The wet weight of the gel was measured. The graph indicates the mean weight of the gel with standard deviation (mean ± SD) of three independent experiments. * The mean weight is higher than that of poly M ($P < 0.05$, Student's t-test).

Plate 1

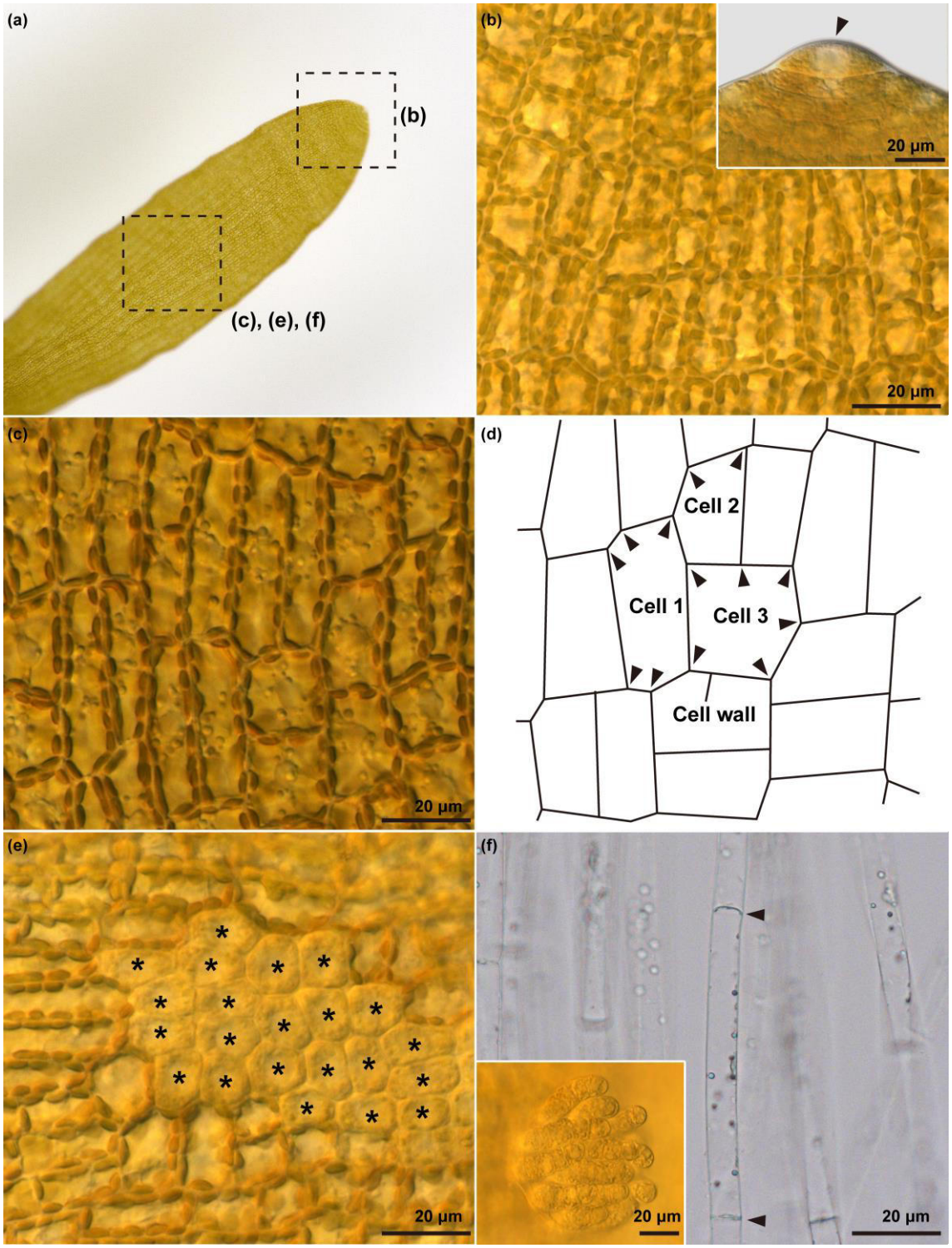
(a)
(b)
(c), (e), (f)
(b)
20 µm
20 µm
(c)
20 µm
(d)
Cell 2
Cell 1
Cell 3
Cell wall
(e)
20 µm
(f)
20 µm
20 µm

Plate 2

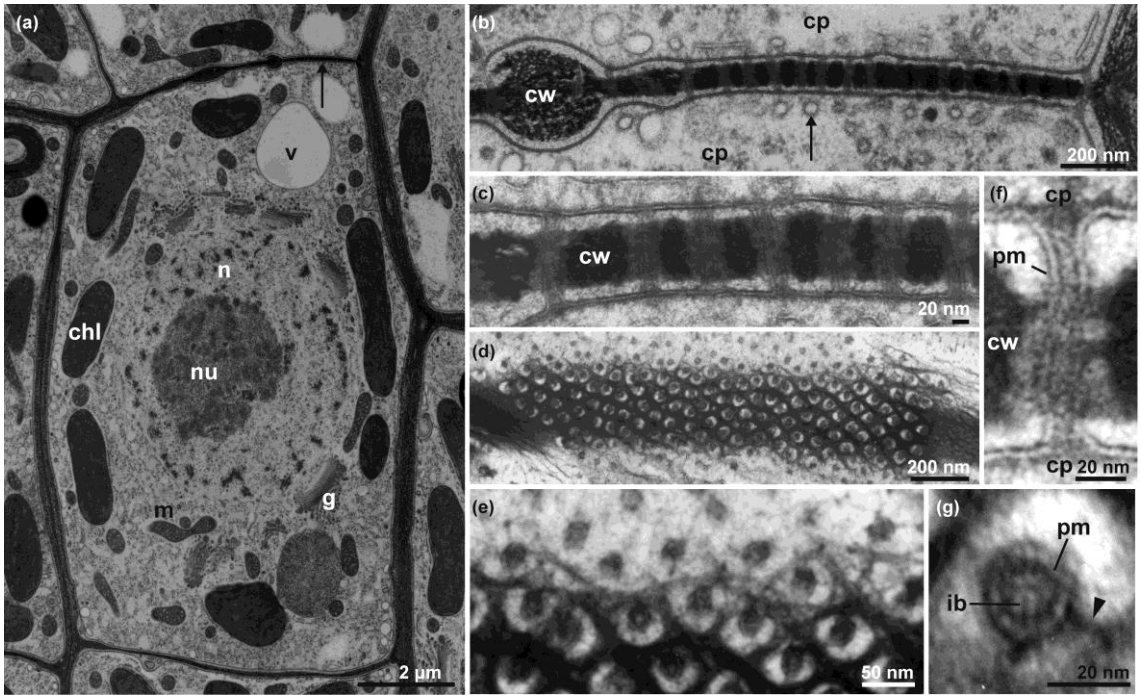
(a)
v
n
chl
nu
m
g
2 µm
(b)
cp
cw
cp
200 nm
(c)
cw
20 nm
(d)
200 nm
(f)
cp
pm
cw
cp
20 nm
(e)
50 nm
(g)
pm
ib
20 nm

Plate 3

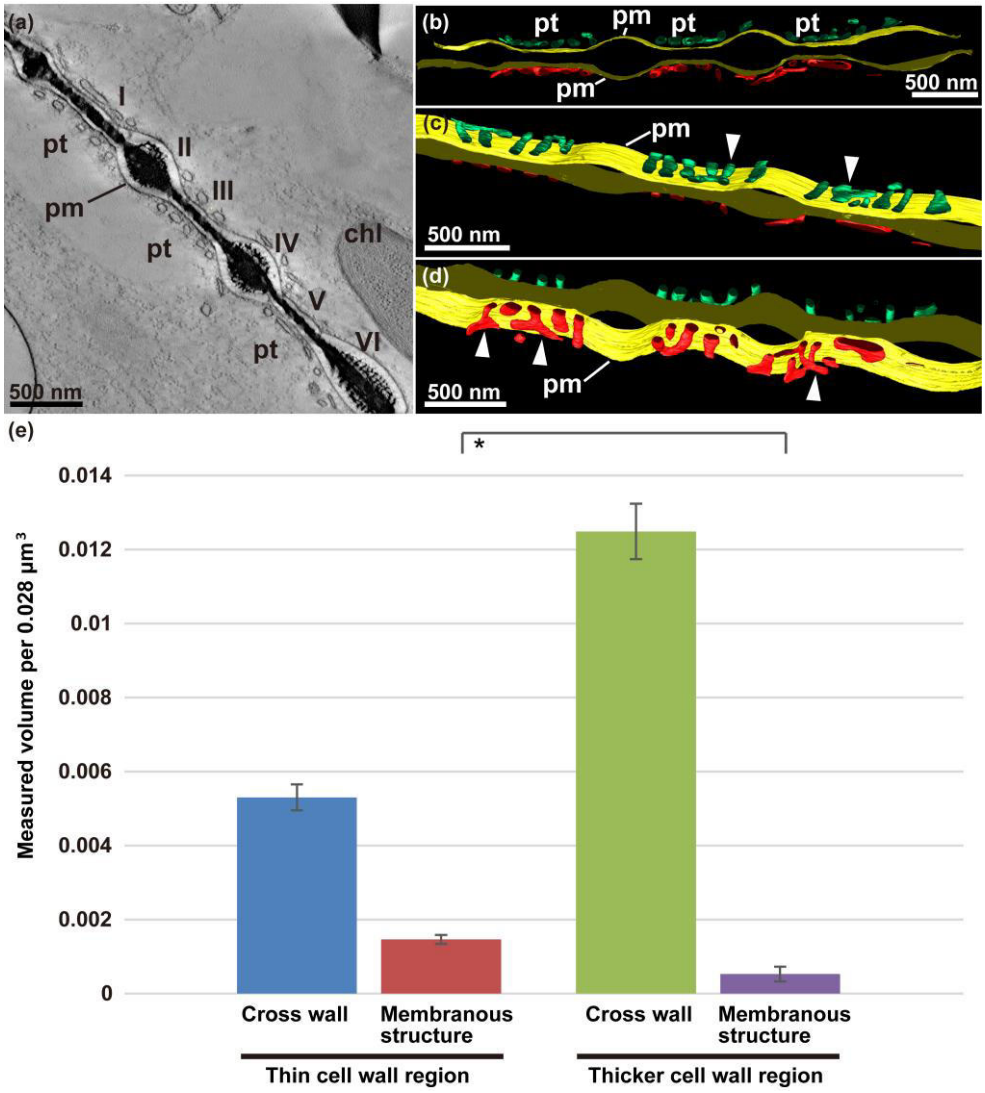
(a)
I
II
III
IV
V
VI
pt
pm
pt
pt
chl
500 nm
(b)
pt
pm
pt
pt
pm
500 nm
(c)
pm
500 nm
(d)
500 nm
pm
(e)
*
0.014
0.012
0.01
0.008
0.006
0.004
0.002
0
Measured volume per 0.028 µm³
Cross wall
Membranous structure
Cross wall
Membranous structure
Thin cell wall region
Thicker cell wall region

Plate 4

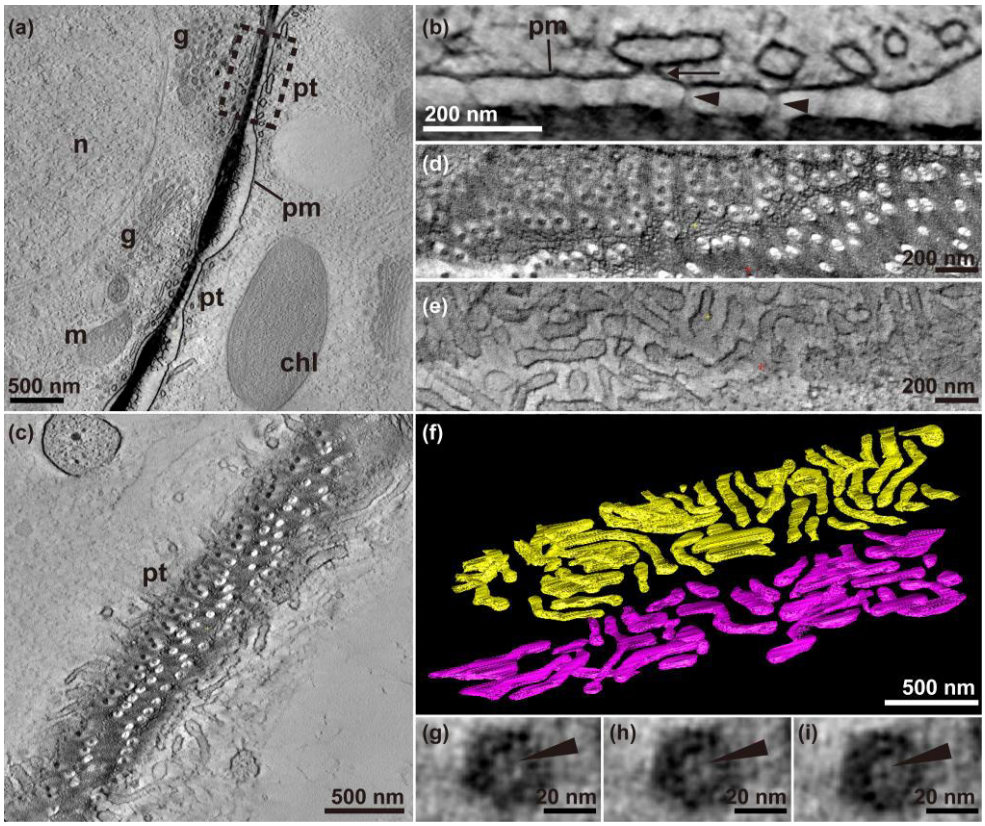
(a)
g
pt
n
pm
g
pt
m
chl
500 nm
(b)
pm
200 nm
(d)
200 nm
(e)
200 nm
(c)
pt
500 nm
(f)
500 nm
(g)
20 nm
(h)
20 nm
(i)
20 nm

Plate 5

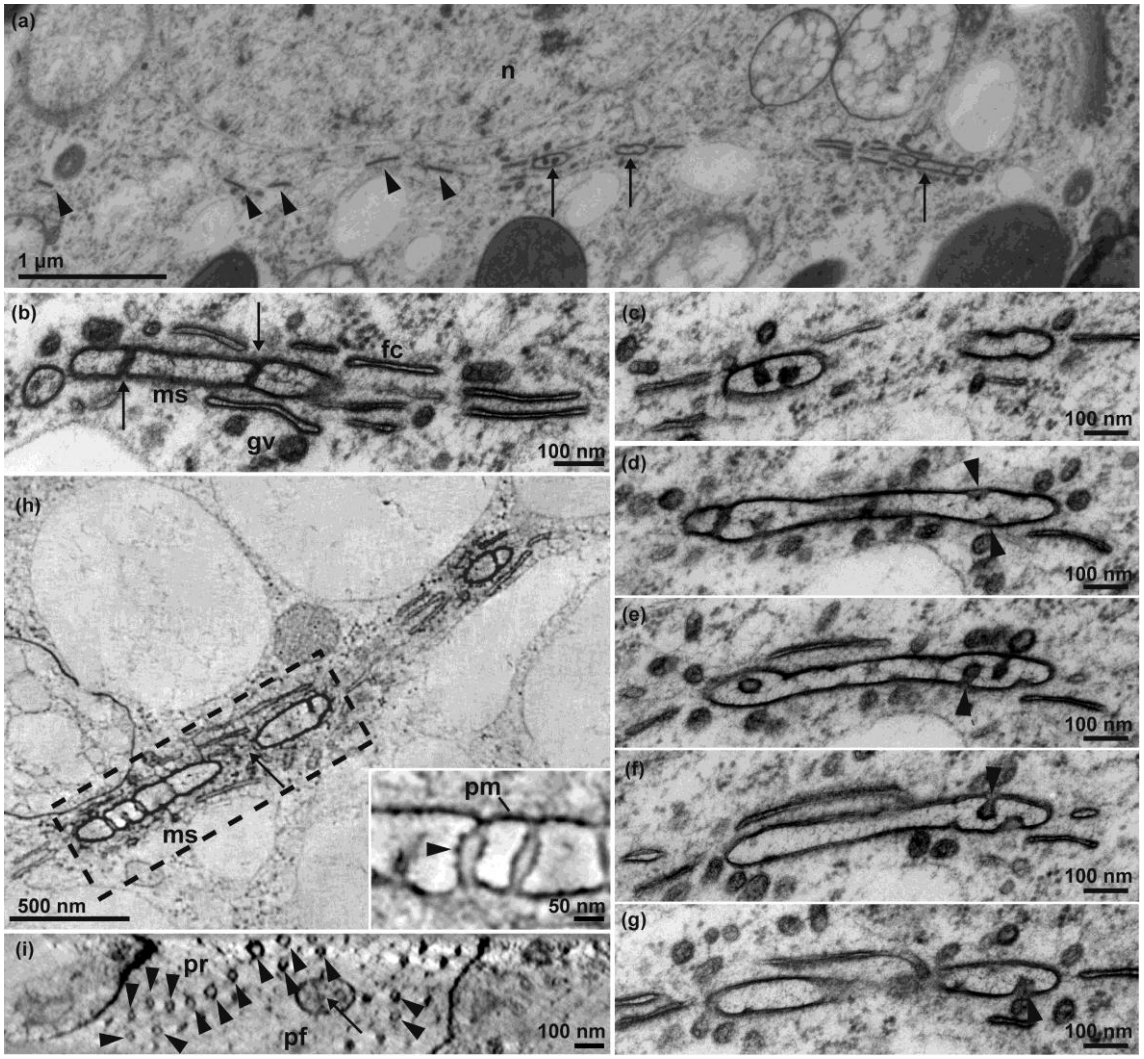
(a)
n
1 µm
(b)
fc
ms
gv
100 nm
(c)
100 nm
(d)
100 nm
(e)
100 nm
(f)
100 nm
(g)
100 nm
(h)
ms
500 nm
pm
50 nm
(i)
pr
pf
100 nm

Plate 6

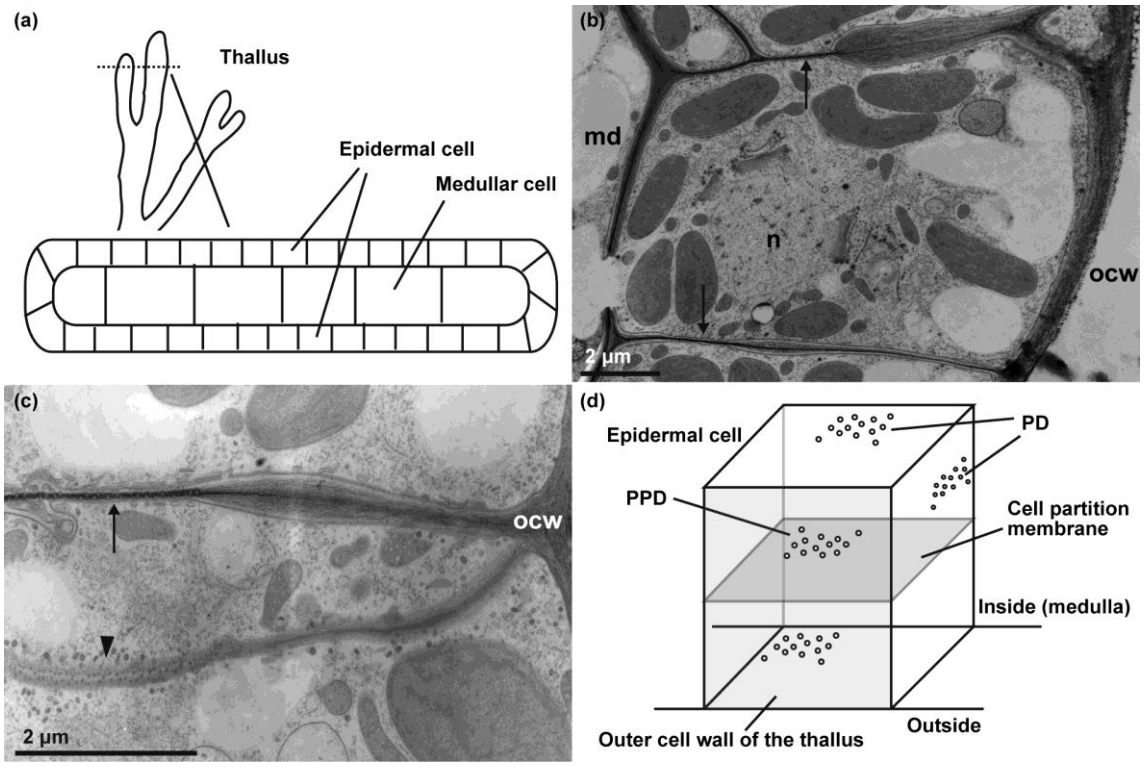
(a)
Thallus
Epidermal cell
Medullar cell
(b)
md
n
OCW
2 μm
(c)
OCW
2 μm
(d)
Epidermal cell
PD
PPD
Cell partition membrane
Inside (medulla)
Outside
Outer cell wall of the thallus

Plate 7

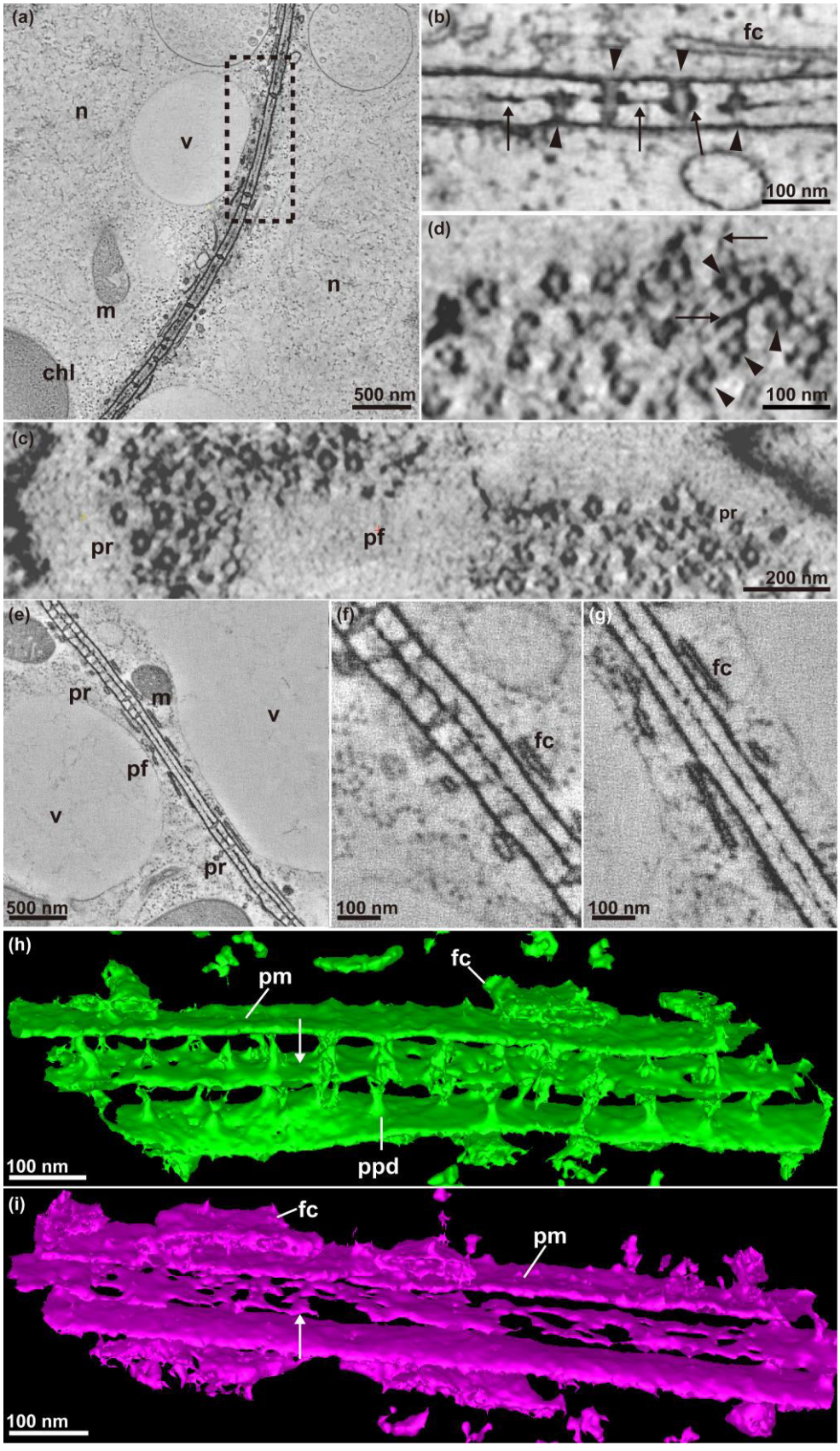
(a)
n
v
n
m
chl
500 nm
(b)
fc
100 nm
(d)
100 nm
(c)
pr
pf
pr
200 nm
(e)
pr
m
v
pf
v
pr
500 nm
(f)
fc
100 nm
(g)
fc
100 nm
(h)
pm
fc
ppd
100 nm
(i)
fc
pm
100 nm

Plate 8

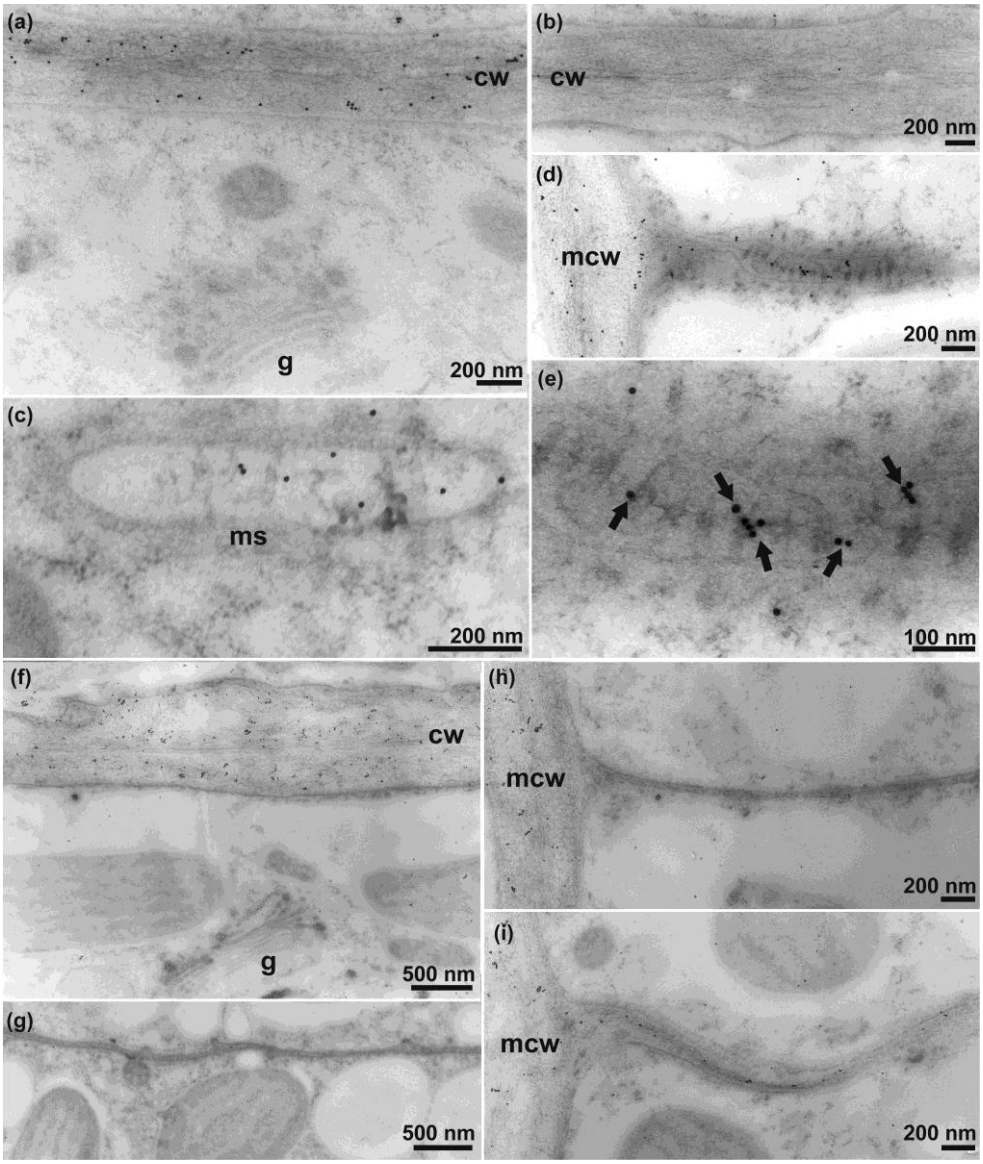
(a)
cw
g
200 nm
(b)
cw
200 nm
(d)
mcw
200 nm
(c)
ms
200 nm
(e)
100 nm
(f)
cw
g
500 nm
(h)
mcw
200 nm
(g)
500 nm
(i)
mcw
200 nm

Plate 9

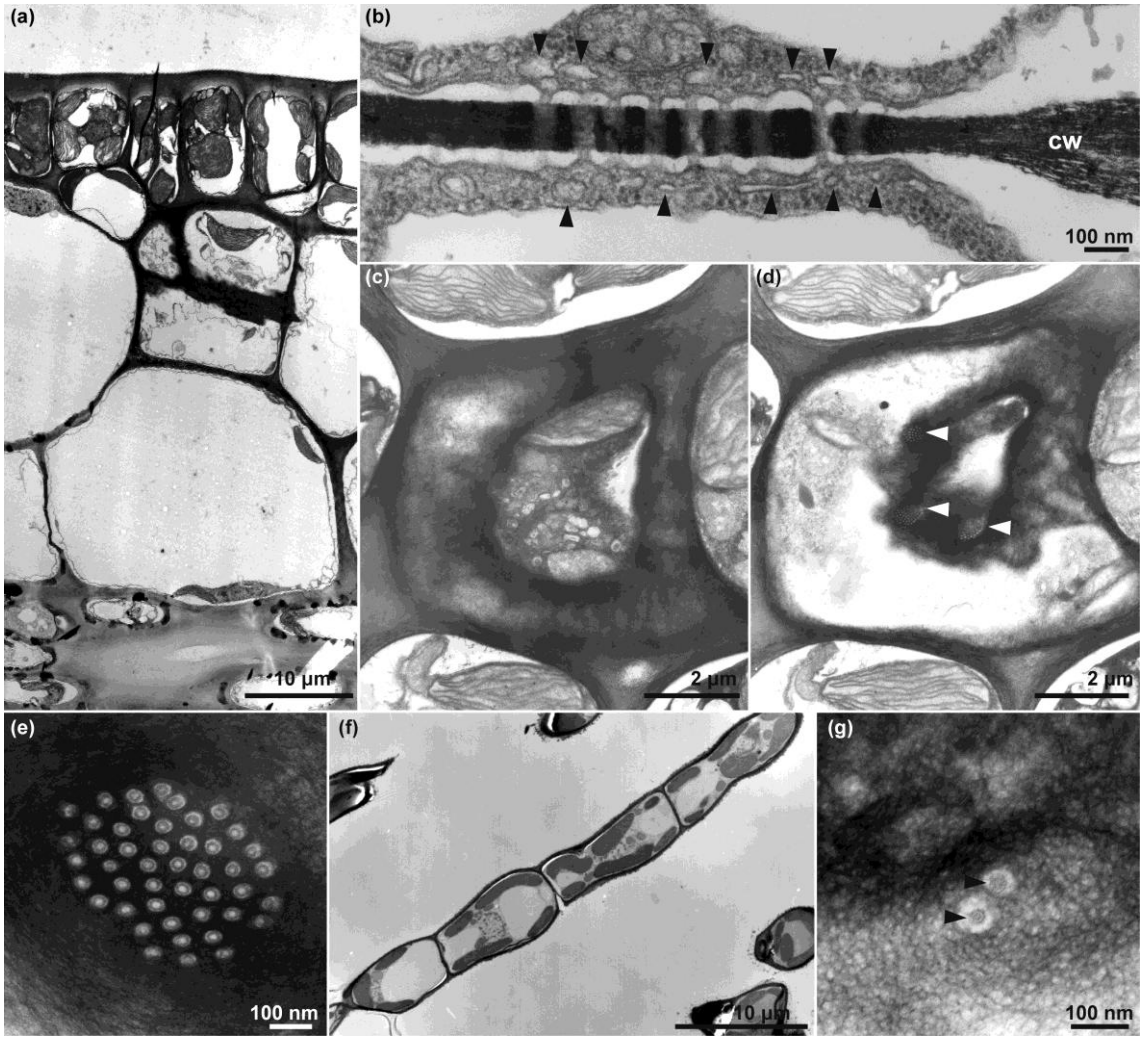

Plate 10

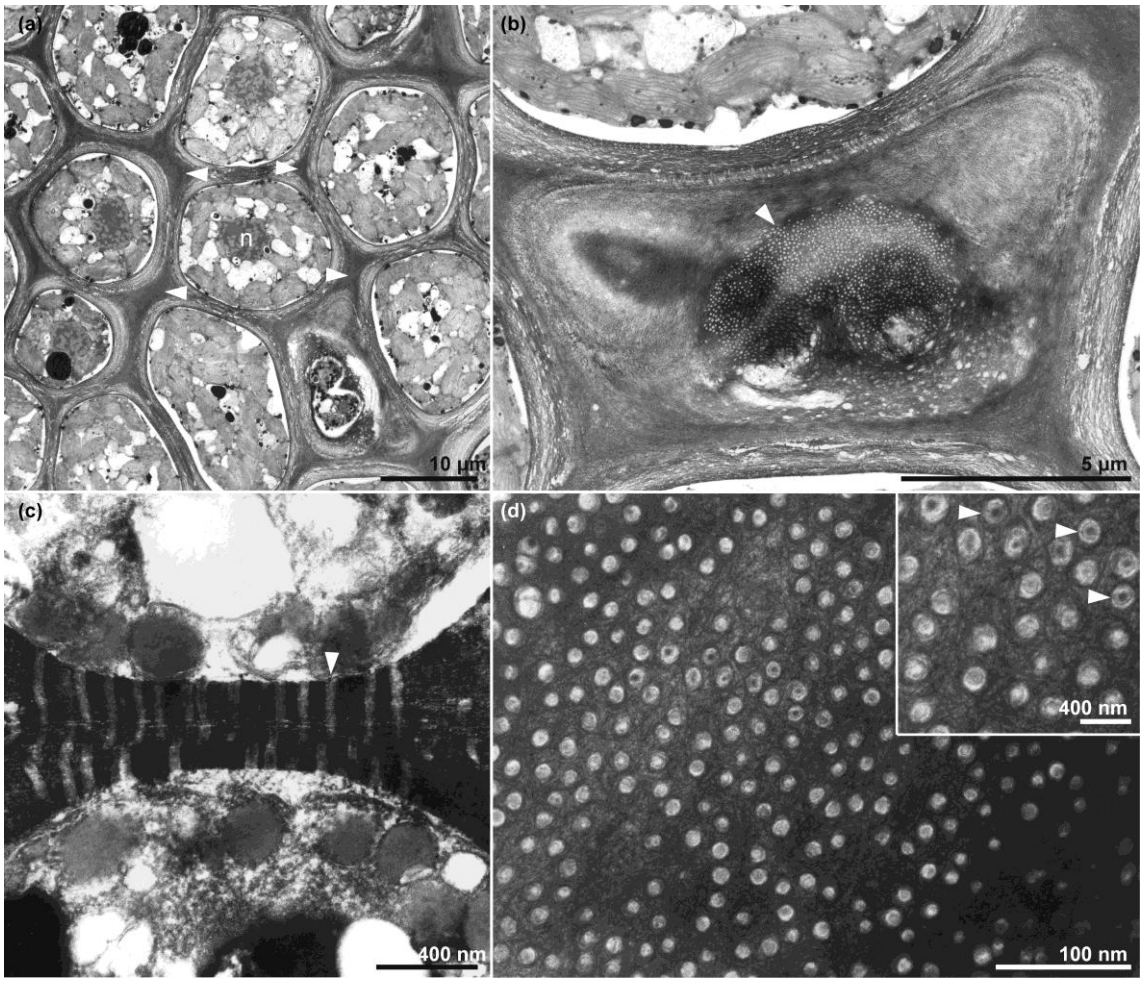

Plate 11

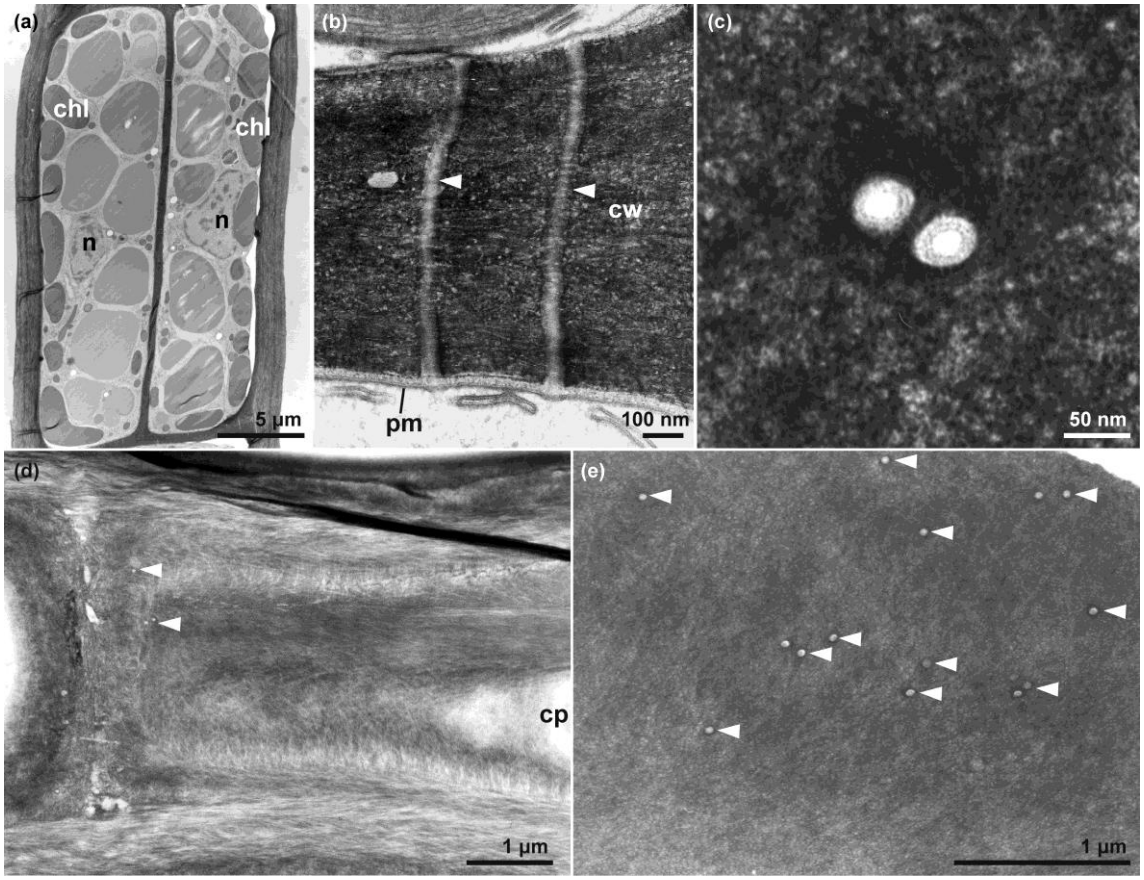

Plate 12

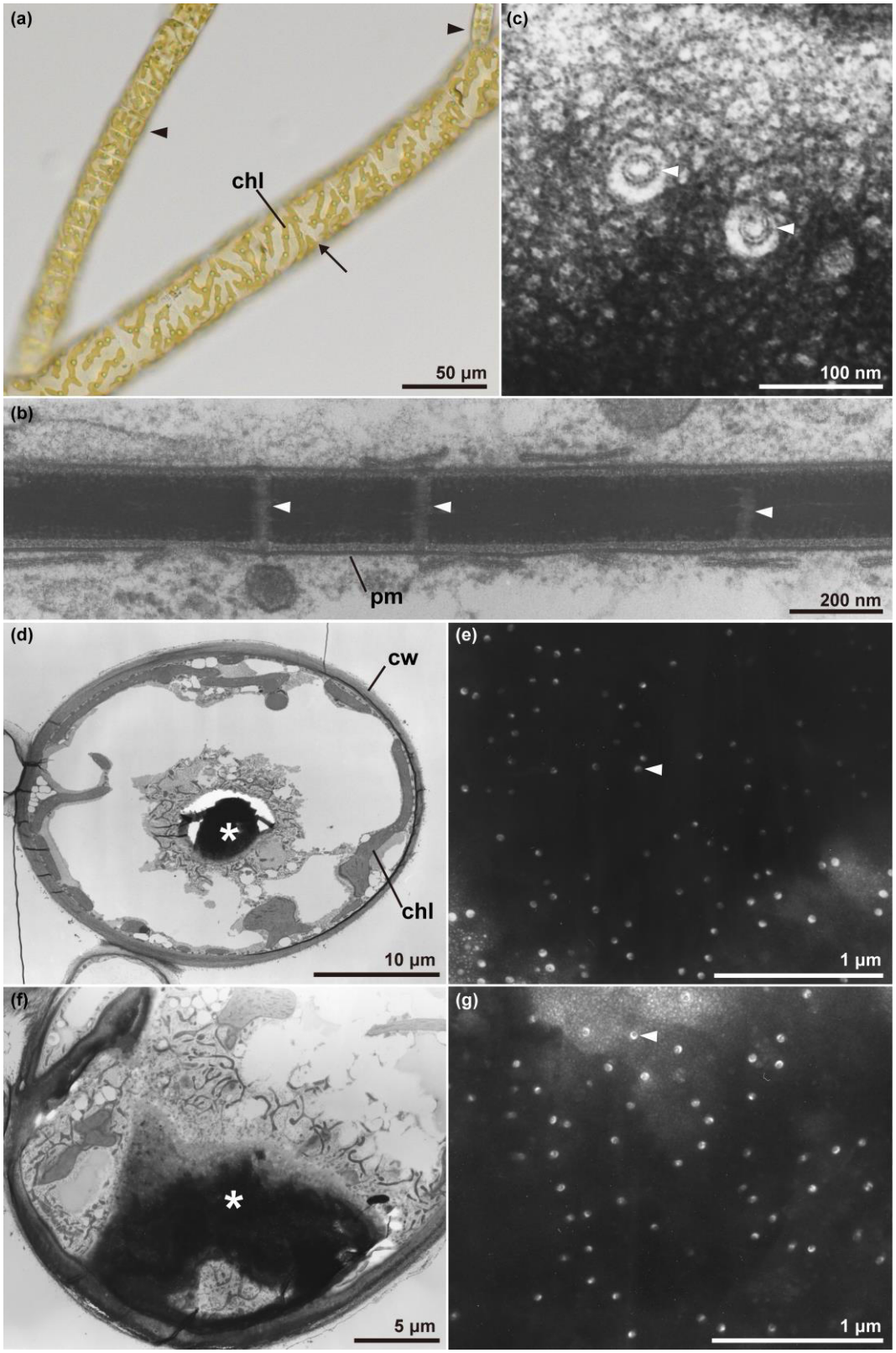

Plate 13

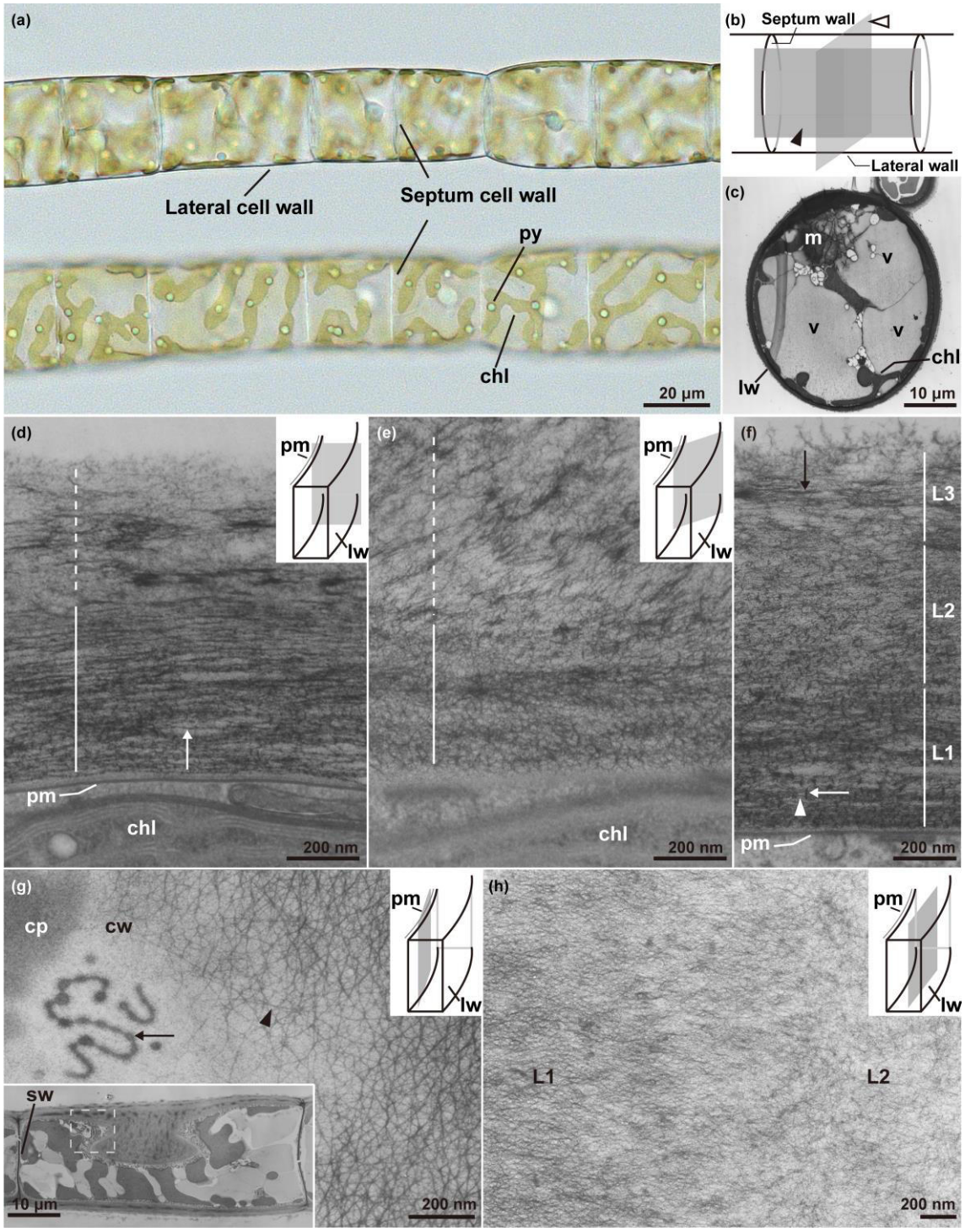
(a)
Lateral cell wall
Septum cell wall
py
chl
20 µm
(b) Septum wall
Lateral wall
(c)
m
v
v
v
chl
lw
10 µm
(d)
pm
lw
pm
chl
200 nm
(e)
pm
lw
chl
200 nm
(f)
L3
L2
L1
pm
200 nm
(g)
cp
cw
pm
lw
sw
10 µm
200 nm
(h)
pm
lw
L1
L2
200 nm

Plate 14

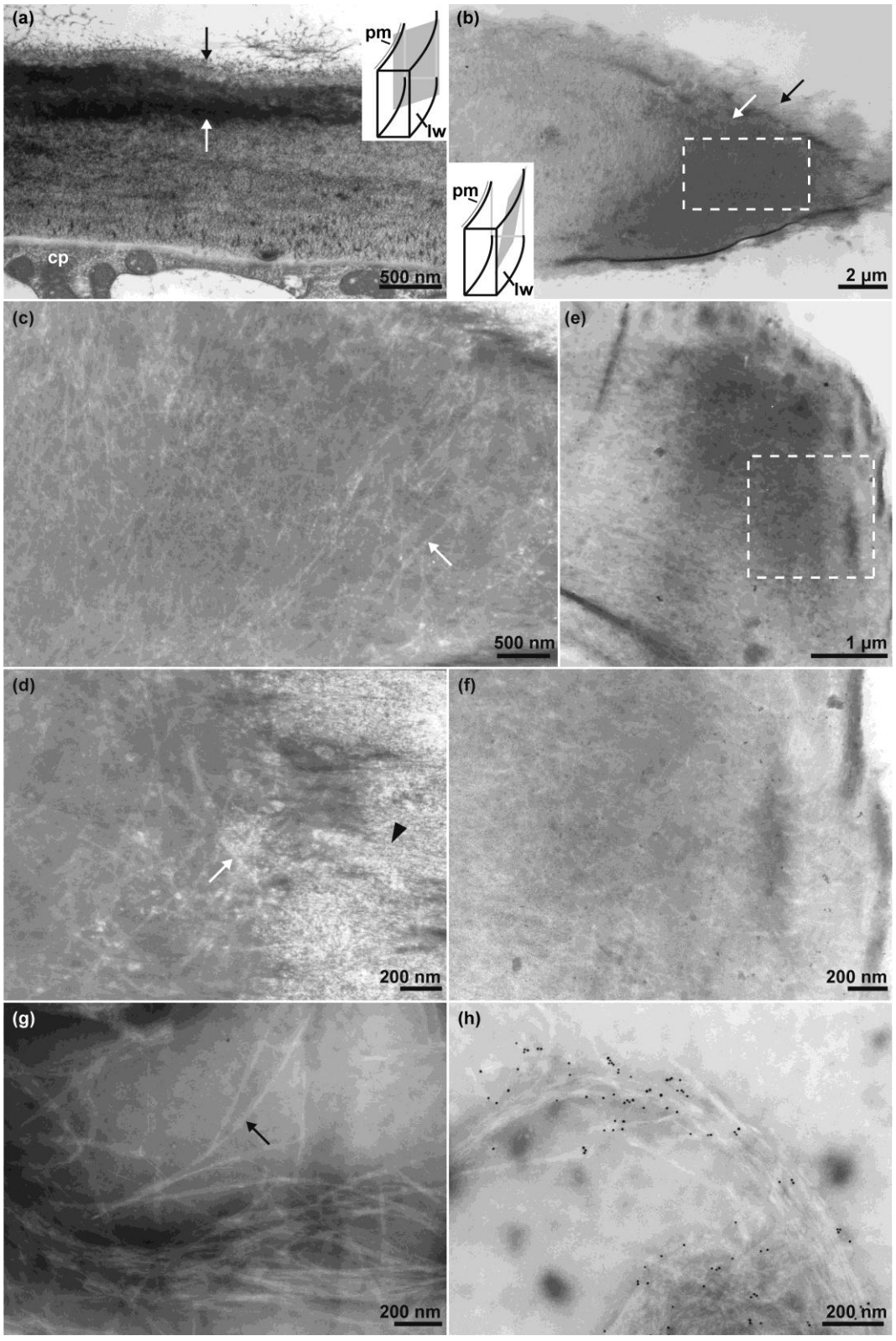
(a)
pm
lw
cp
500 nm
(b)
pm
lw
2 µm
(c)
500 nm
(e)
1 µm
(d)
200 nm
(f)
200 nm
(g)
200 nm
(h)
200 nm

Plate 15

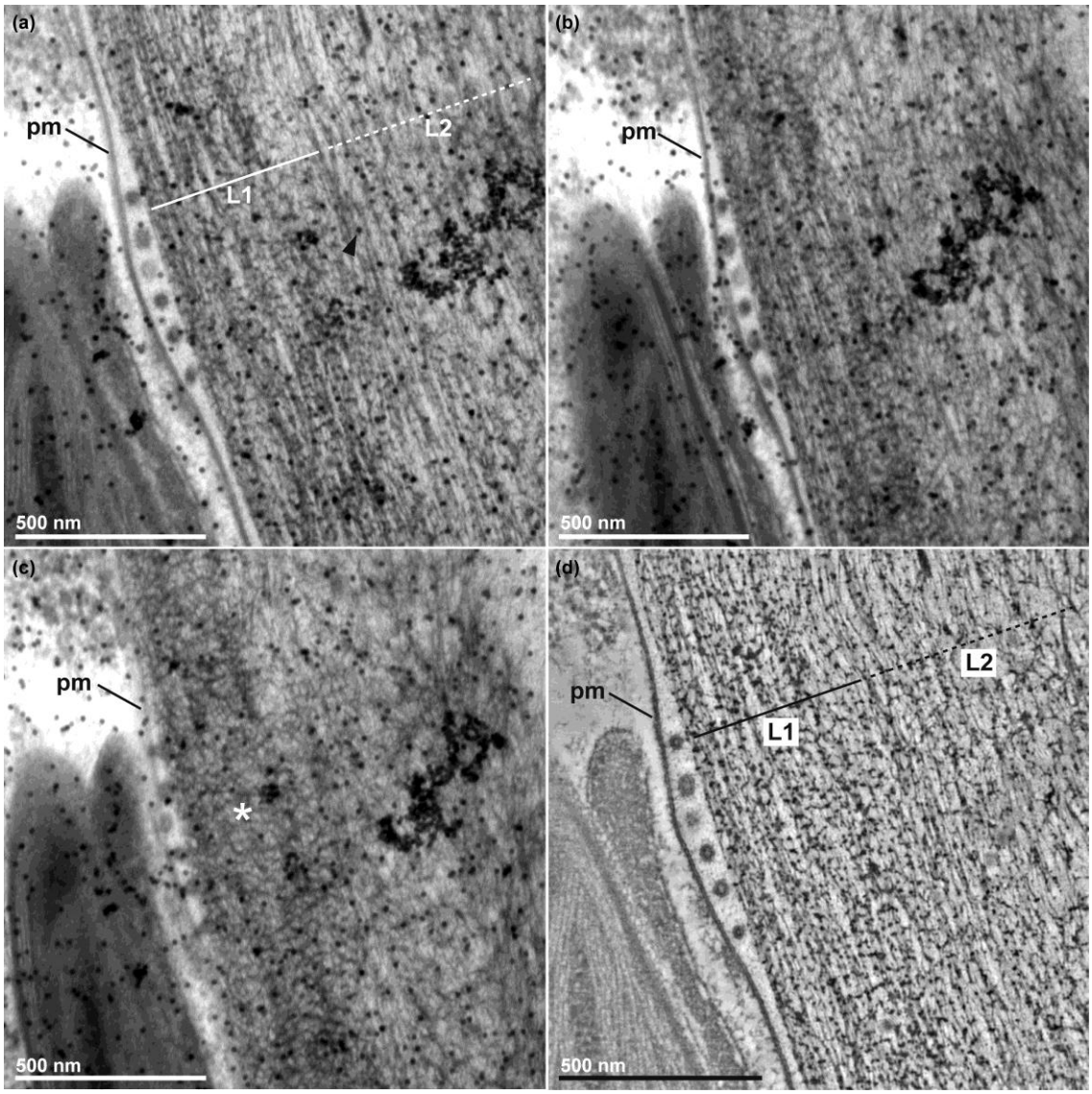

Plate 16

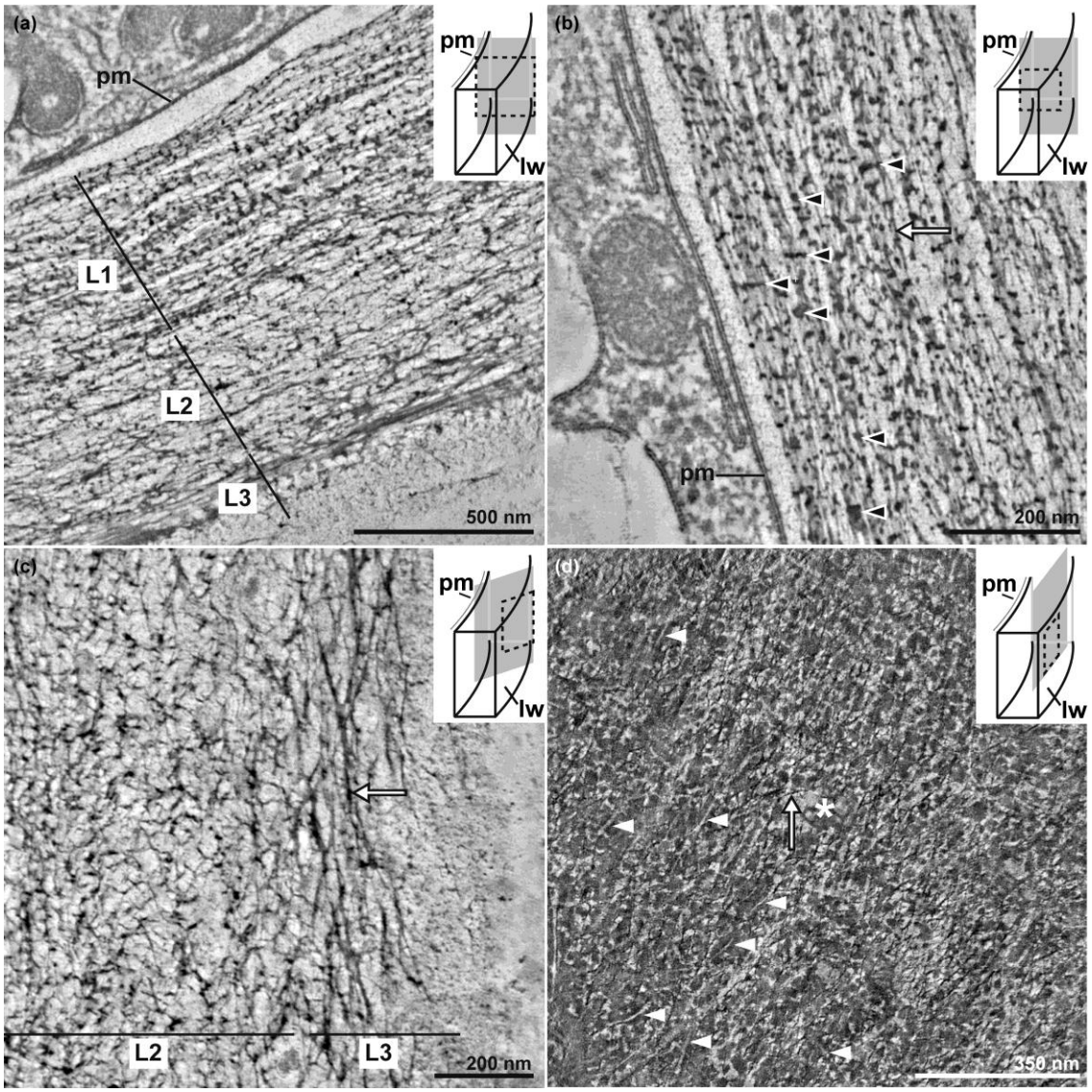
(a)
pm
lw
L1
L2
L3
500 nm
(b)
pm
lw
pm
200 nm
(c)
pm
lw
L2
L3
200 nm
(d)
pm
lw
*
350 nm

Plate 17

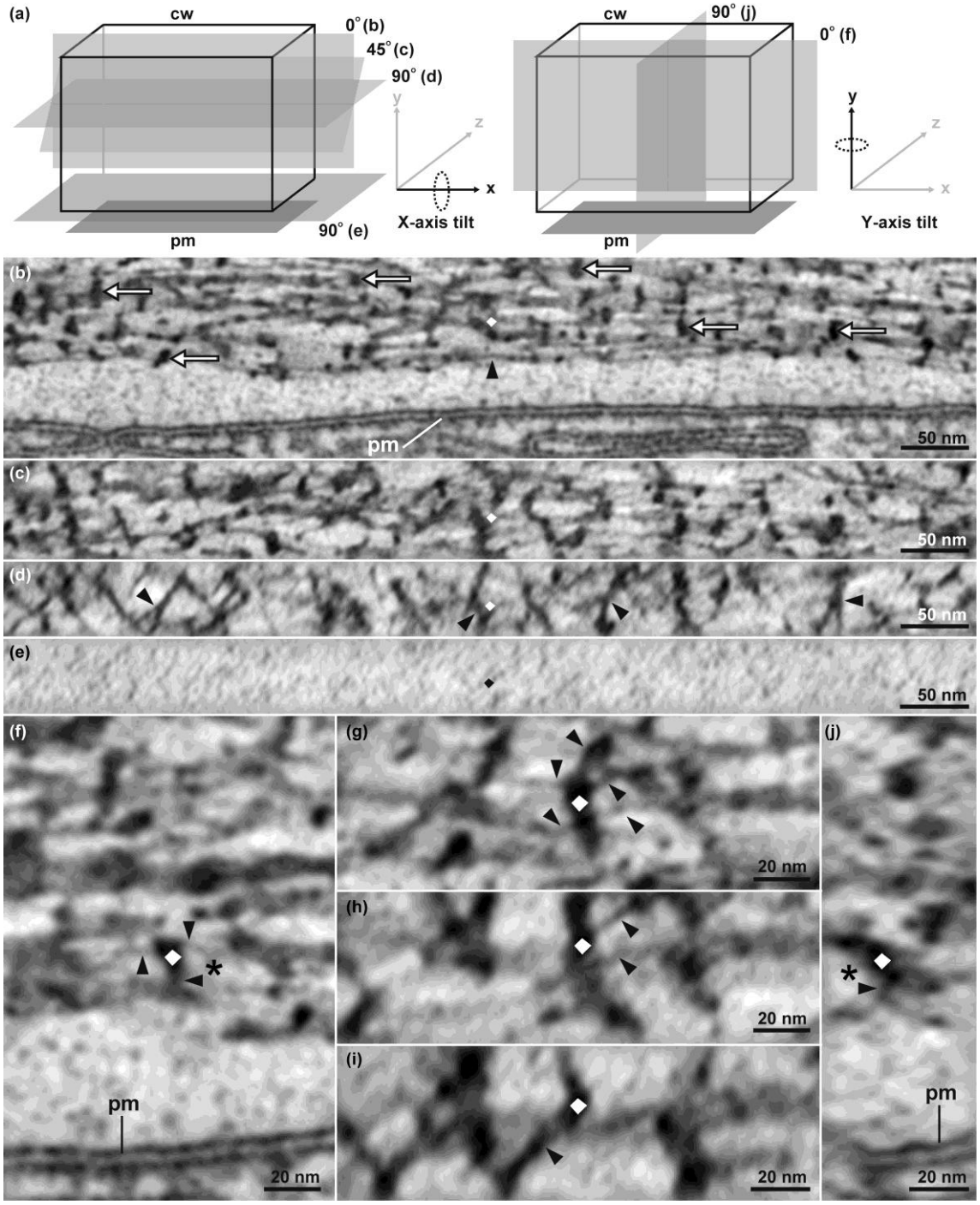
(a)
cw
0° (b)
45° (c)
90° (d)
90° (e)
pm
y
z
x
X-axis tilt
cw
90° (j)
0° (f)
pm
y
z
x
Y-axis tilt
(b)
pm
50 nm
(c)
50 nm
(d)
50 nm
(e)
50 nm
(f)
pm
20 nm
(g)
20 nm
(h)
20 nm
(i)
20 nm
(j)
pm
20 nm

Plate 18

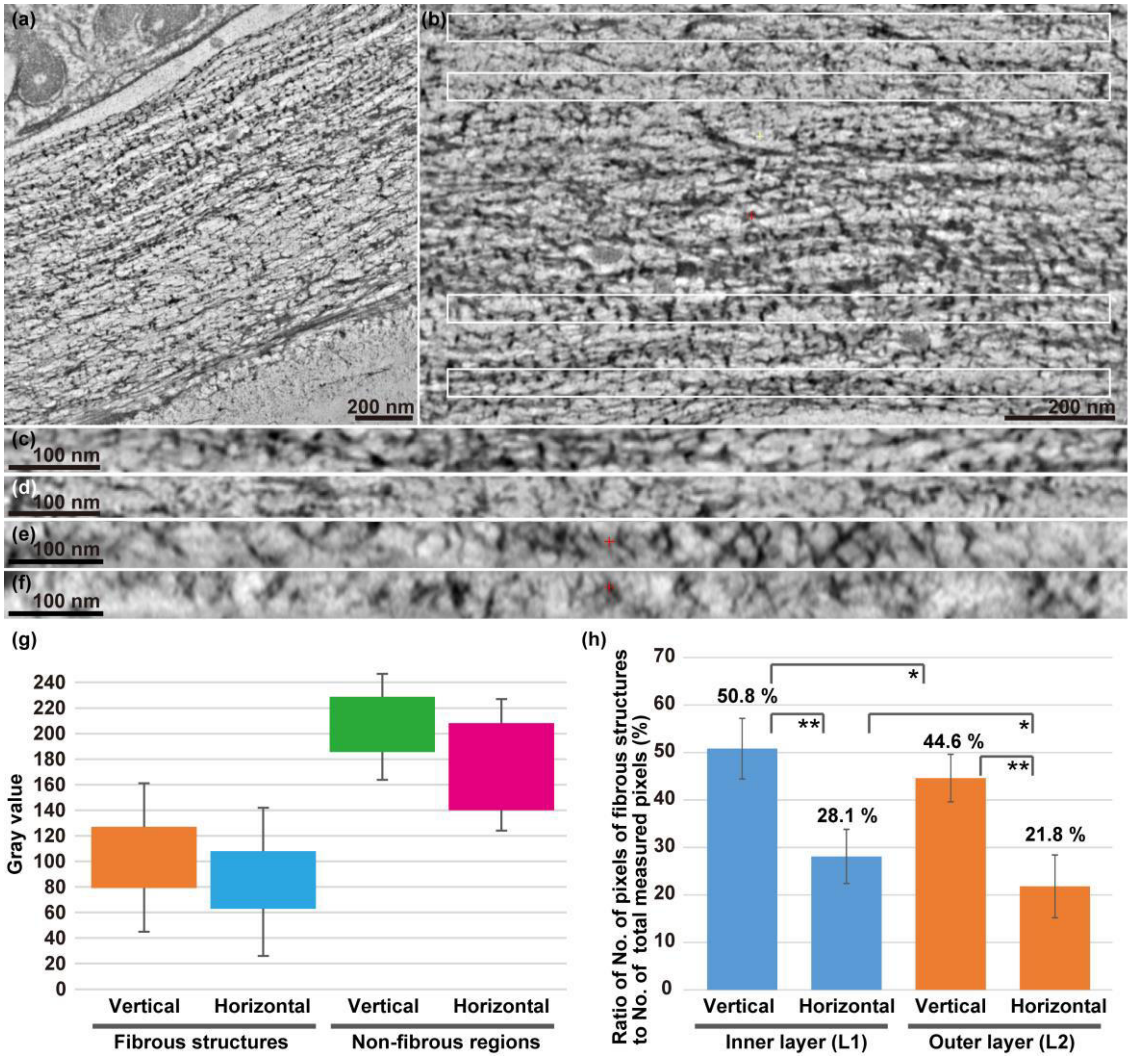
(a)
200 nm
(b)
200 nm
(c)
100 nm
(d)
100 nm
(e)
100 nm
(f)
100 nm
(g)
Gray value
240
220
200
180
160
140
120
100
80
60
40
20
0
Vertical
Horizontal
Vertical
Horizontal
Fibrous structures
Non-fibrous regions
(h)
Ratio of No. of pixels of fibrous structures to No. of total measured pixels (%)
70
60
50
40
30
20
10
0
50.8 %
28.1 %
44.6 %
21.8 %
*
**
*
**
Vertical
Horizontal
Vertical
Horizontal
Inner layer (L1)
Outer layer (L2)

Plate 19

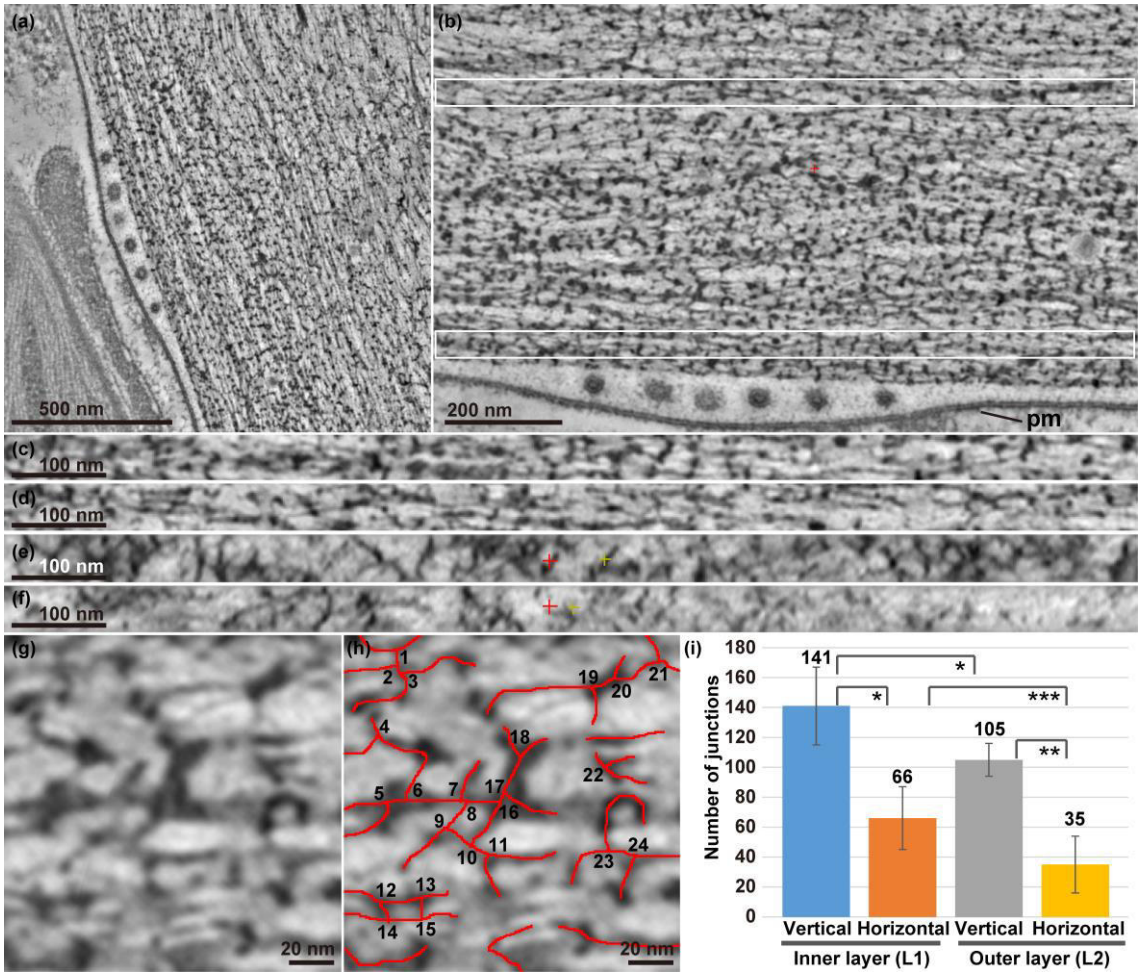
(a)
500 nm
(b)
200 nm
pm
(c)
100 nm
(d)
100 nm
(e)
100 nm
(f)
100 nm
(g)
20 nm
(h)
1
2
3
4
5
6
7
8
9
10
11
12
13
14
15
16
17
18
19
20
21
22
23
24
20 nm
(i)
Number of junctions
180
160
140
120
100
80
60
40
20
0
141
66
105
35
*
*
***
**
Vertical
Horizontal
Vertical
Horizontal
Inner layer (L1)
Outer layer (L2)

Plate 20

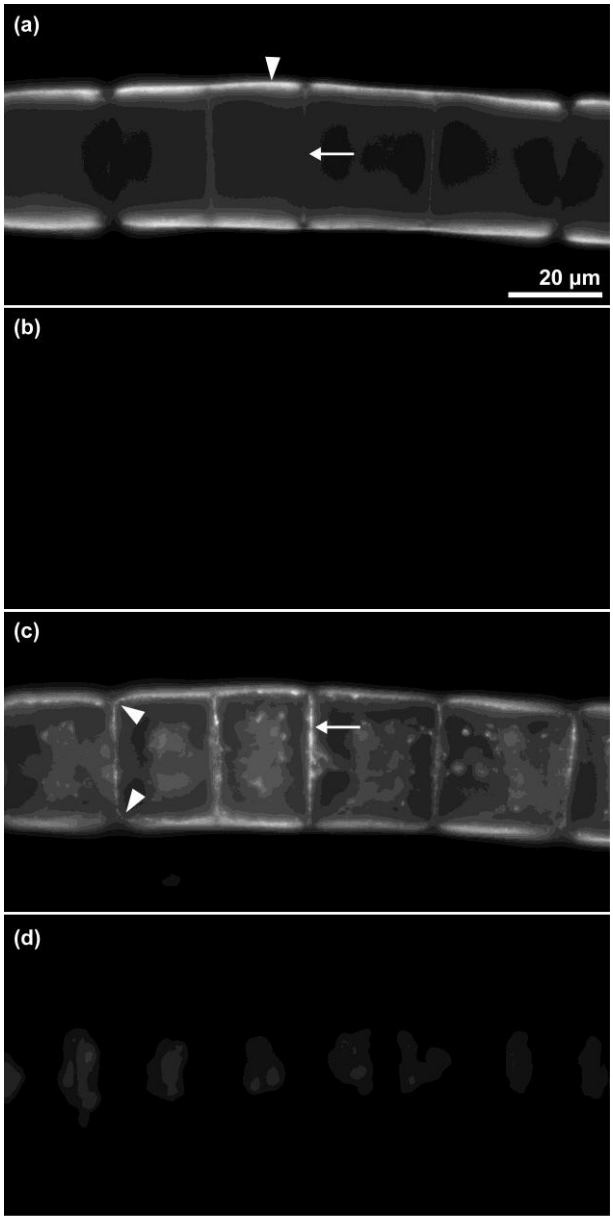

Plate 21

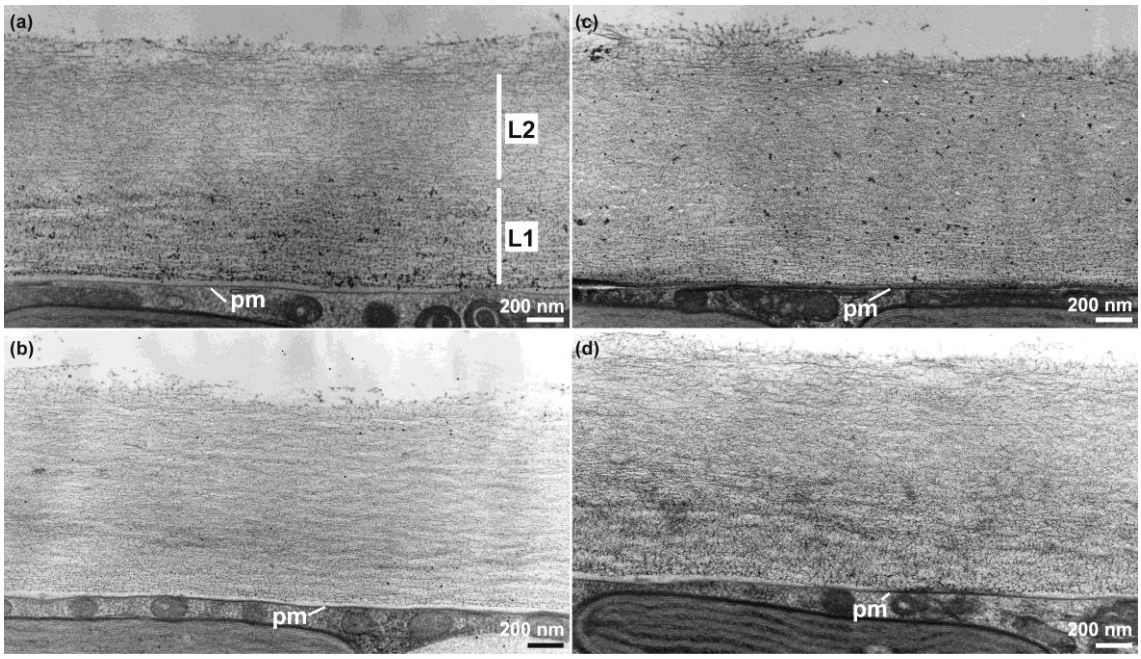

Plate 22

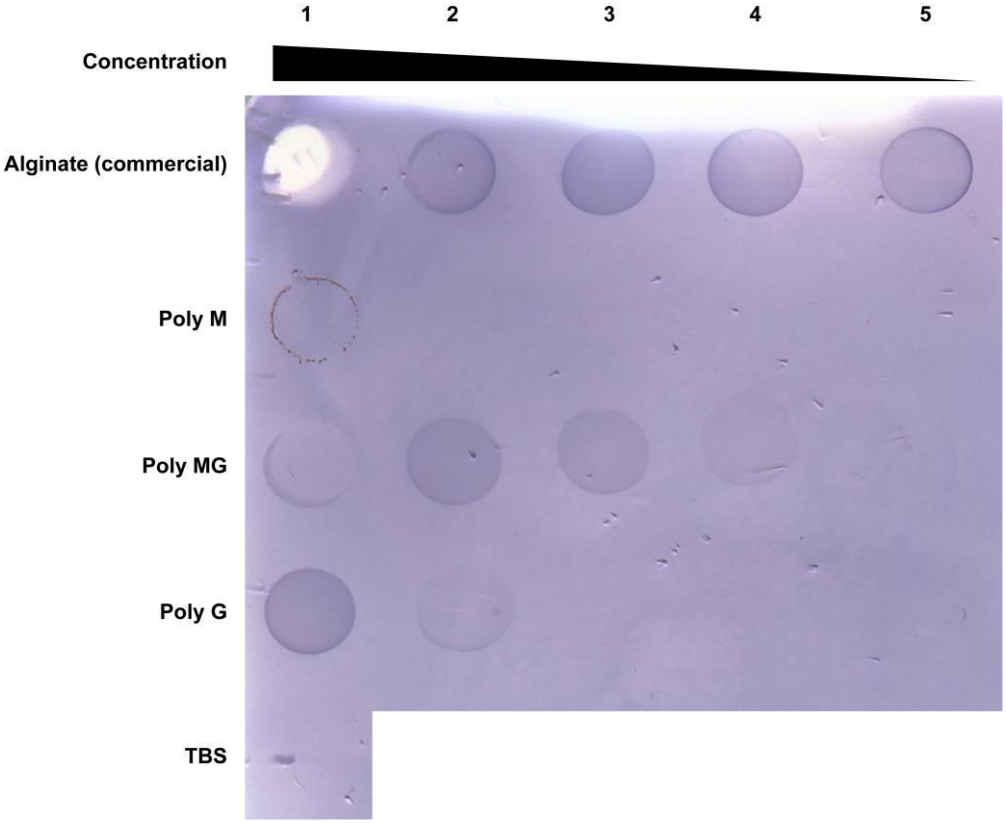
1
2
3
4
5
Concentration
Alginate (commercial)
Poly M
Poly MG
Poly G
TBS

Plate 23

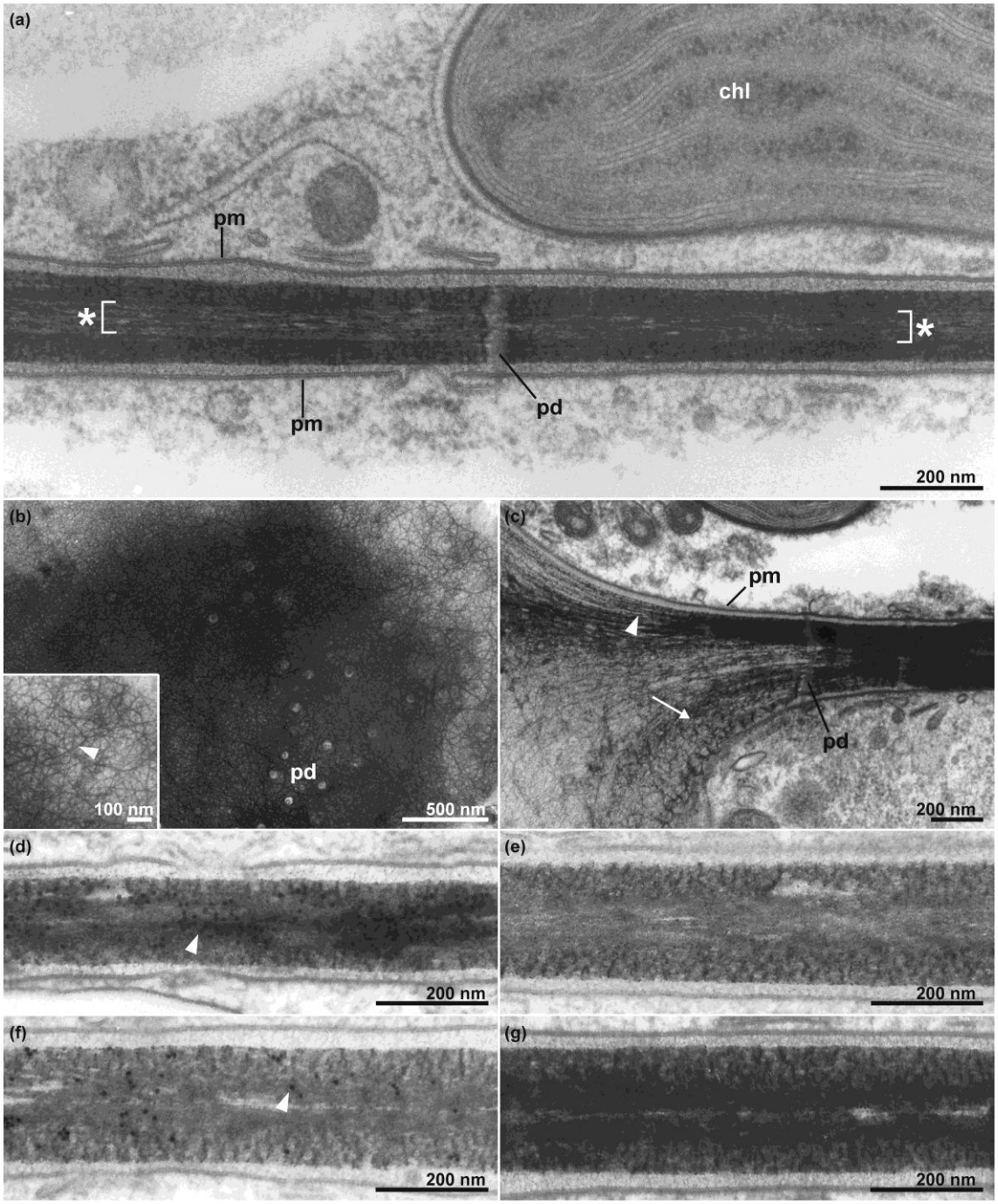
(a)
chl
pm
*
*
pm
pd
200 nm
(b)
100 nm
pd
500 nm
(c)
pm
pd
200 nm
(d)
200 nm
(e)
200 nm
(f)
200 nm
(g)
200 nm

Plate 24

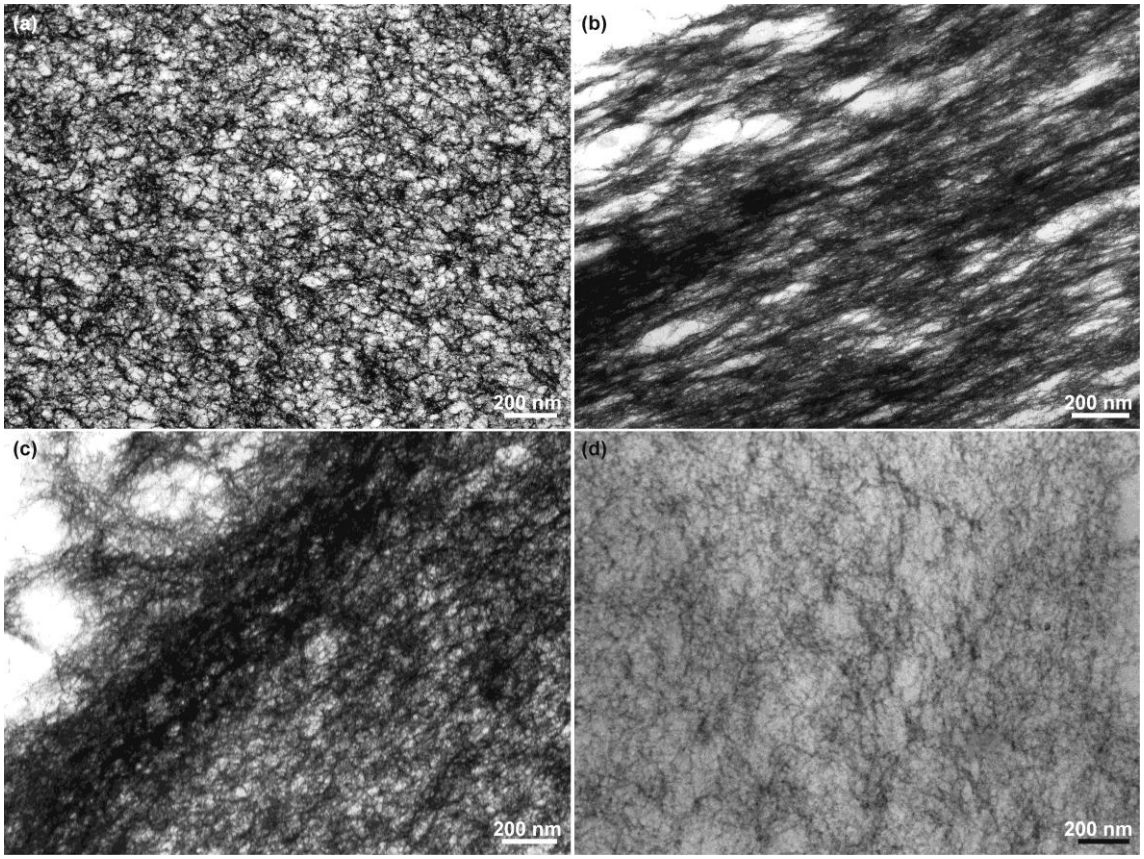

Plate 25

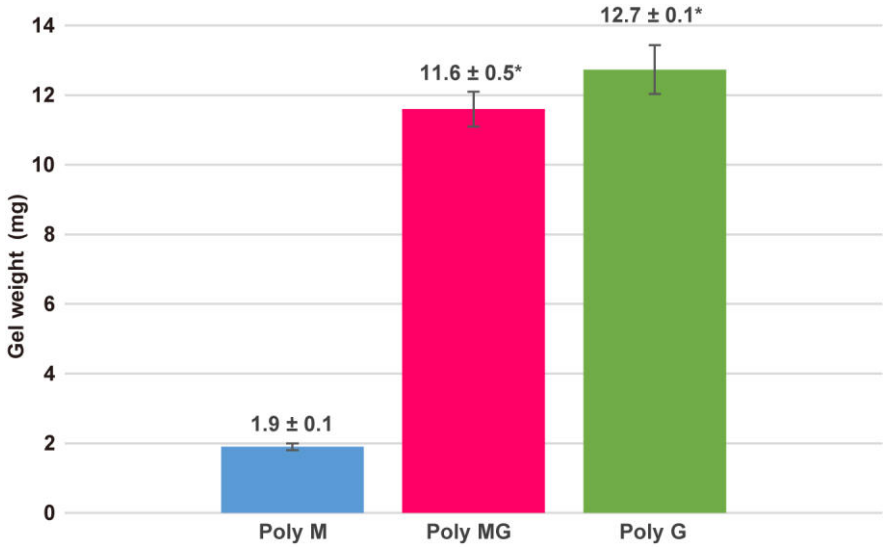
14
12
10
8
6
4
2
0
Gel weight (mg)
1.9 ± 0.1
11.6 ± 0.5*
12.7 ± 0.1*
Poly M
Poly MG
Poly G

Abbreviations

AFM	Atomic force microscopy
CBM	Carbohydrate-binding module
CE	Carbohydrate esterase
CES	Cellulose synthesizing enzyme
DCB	2,6-dichlorobenzonitrile
ECM	Extracellular matrix
ER	Endoplasmic reticulum
GDP	Guanosine diphosphate
GFP	Green fluorescent protein
GH	Glycoside hydrolase
GPI	Glycosylphosphatidylinositol
GT	Glycosyl transferase
HRGP	Hydoxyproline-rich glycoprotein
MEP	Mannuronan C5-epimerase
NMR	Nuclear magnetic resonance
PAS	Periodic acid/Schiff
PBS	Phosphate buffered saline
PDCB	Plasmodesmata callose binding protein
PDLP	Plasmodesmata located protein
PEG	Polyethylene glycol
PL	Polysaccharide lyase
PPD	Pre-plasmodesmata
SEL	Size exclusion limit
TBS	Tris-buffered saline
TEM	Transmission electron microscopy